Evaluation of Resilient Modulus of Unbound Coarse Materials in Idaho

A Thesis
Presented in Partial Fulfillment of the Requirements for the
Degree of Master of Science
with a
Major in Civil Engineering
in the
College of Graduate Studies
University of Idaho
by

S M Robinur Mohshin Chowdhury

Major Professor: Emad Kassem, Ph.D., P.E.
Committee Members: Fouad Bayomy, Ph.D., P.E.; Sunil Sharma, Ph.D., P.E.;
Debakanta Mishra, Ph.D., P.E.
Department Chair: Patricia J. S. Colberg, Ph.D., P.E.

May 2019

Authorization to Submit Thesis

This Thesis of S M Robinur Mohshin Chowdhury submitted for the degree of Master of Science with a Major in Civil Engineering and titled "EVALUATION OF RESILIENT MODULUS OF UNBOUND COARSE MATERIALS IN IDAHO" has been reviewed in final form. Permission, as indicated by the signatures and dates below, is now granted to submit final copies to the College of Graduate Studies for approval.

Major Professor: _____ Date: _____
Emad Kassem, Ph.D., P.E.

Committee Members: _____ Date: _____
Fouad Bayomy, Ph.D., P.E.

_____ Date: _____
Sunil Sharma, Ph.D., P.E.

_____ Date: _____
Debakanta Mishra, Ph.D., P.E.

Department Chair: _____ Date: _____
Patricia J. S. Colberg, Ph.D., P.E.

Abstract

Many transportation agencies are moving towards the implementation of the AASHTOWare Pavement Mechanistic-Empirical Design (PMED) software to design and analyze pavement structures. The PMED software requires accurate characterization of material properties. The resilient modulus is a primary input parameter for granular base and subbase layers. The main objective of this study was to develop a material database for typical unbound materials in Idaho. The material database, while it was focused on the resilient modulus as being the main property required for PMED, also includes other material parameters that are useful for pavement design and construction. For this research, eighteen base and subbase materials were collected from all six districts designated by Idaho Transportation Department (ITD). Preliminary characterization tests including particle size distribution, Atterberg limits, soil classification, moisture-density relationships were carried out to obtain the inherent material properties. The resilient modulus test was conducted in accordance to the AASHTO T 307. The test procedure is quite complex and requires high level of training and expensive testing machines that are capable of applying dynamic loads.

In this study, the resilient modulus was determined using deformations measured by external Linear Variable Differential Transducers (LVDTs) as well as internal LVDTs. Although AASHTO T 307 specifications call only for external LVDTs, this research also used internal LVDTs to investigate the effect of the testing setup. The results showed that the resilient modulus based on the internal LVDT deformation was about 24% higher in comparison to values based on external LVDT deformation. The same materials were also tested to determine their CBR values and elastic modulus (E) using the Light Weight Deflectometer (LWD).

One of the main objectives of this research was to develop predictive models of the resilient modulus as a function of other material parameters that are more common and are easier to measure. The prediction models developed in this study provided good correlations ($R^2 > 0.9$) with the laboratory measured resilient modulus values. Results of the resilient modulus were also correlated to the CBR values and to the LWD elastic modulus. The LWD elastic modulus values showed a better correlation ($R^2 = 0.82$) with the resilient modulus, while the CBR correlation was just “fair” ($R^2 = 0.56$). Although, these correlations can be

used to estimate the resilient modulus, the prediction model of the resilient modulus is recommended over these correlations. Additionally, the prediction model provides estimates for the resilient modulus at all stress states provided in the AASHTO standard. The proposed models will allow transportation agencies to estimate the resilient modulus values for base and subbase materials from basic properties that are easy to measure.

***Keywords*:** Unbound aggregates, resilient modulus, internal LVDT, prediction model, correlation

Acknowledgements

I would like to express my sincere appreciation to my supervisor Dr. Emad Kassem for showing me the limitless support and patience and believing on me. I am grateful to my supervisor who dedicated his time and effort to achieve my research goals, and who promptly responded to my difficulties and queries. Working under his supervision paved my way to achieve my goals. Needless to say, none of this would have been possible without his help and direction.

I would like to thank Dr. Fouad Bayomy, Dr. Sunil Sharma and Dr. Debakanta Mishra (Boise State University) for being my committee members and guiding me towards the MS degree. My sincere thanks to Mr. Don Parks for being there always in the lab with his helping attitude.

Additional thanks go to all of my awesome lab mates Assi, Wahid, Hamza, Hasnat, Simpson, Ebenezer, Charles and Md. Jibon (Boise State University). Thank you, Hamza, for being there with me as my friend and helping me in my research work. I appreciate those times, both day night, we spent together with laughter and joy even on your birthday and vacation. I am also grateful to Md. Jibon (Boise State University) for his all supports.

This study is part of a research project (RP 263) funded by the Idaho Transportation Department (ITD). I greatly appreciate all the support provided by the ITD personnel in collecting materials and related information essential for this research. I am also grateful to the Department of Civil and Environmental Engineering and the National Institute for Advanced Transportation Technology (NIATT) at the University of Idaho for providing all the necessary resources for completing this research.

Dedication

In the memory of my father and my loving mother who always supported me and inspired me to be a good human being

Table of Contents

List of Tables

List of Figures

CHAPTER 1 INTRODUCTION

1.1 Overview and Problem Statement

The performance of highway pavements is influenced by the structure and properties of its supporting layers. The pavements structure consists of several layers including subgrade, subbase, base, and surface course (or wearing course). The materials placed between the subgrade and wearing course are unbound materials, which typically consist of compacted, granular aggregates. The main role of the base and subbase layers is to transmit the traffic loading to the subgrade. To avoid pavement failure, the applied stresses on subgrade should not to exceed its bearing capacity.

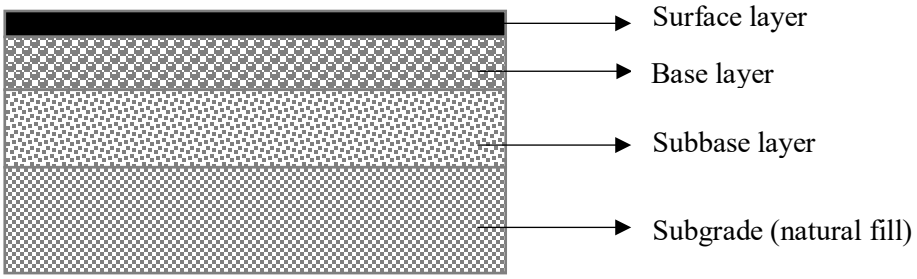

Figure 1.1 Typical pavement cross-section

Good pavement design requires proper characterization of all layers. Many transportation agencies are moving towards the implementation of the mechanical-empirical approaches for the design and analysis of pavement structures. One of these mechanical-empirical approaches is the Mechanistic-Empirical Pavement Design Guide (MEPDG). The AASHTOWare Pavement Mechanistic-Empirical Design (PMED) is the latest software that uses the MEPDG to analyze and design flexible and rigid pavements. MEPDG requires the properties of materials used in the various layers of the pavement structure. The resilient modulus (M_R) and Poisson's ratio (υ) of the granular base and subbase layers are the two primary input parameters for design. AASHTO T 307 (AASHTO, 1999) and NCHRP 1-28A, also known as Harmonized Protocol (Witczak, 2003) are standard test procedures that are commonly used to evaluate the resilient properties of unbound materials in the laboratory. AASHTOWare Pavement ME classifies the input of resilient modulus for unbound materials into three different levels. Level-1design requires laboratory testing or field evaluation of resilient modulus. Level-2 design uses resilient modulus values derived from correlations

between resilient modulus and other index properties of materials such as California bearing ratio (CBR) and resistance value (R–value). Level-3 design input is a set of default values embedded in the program. These default values were estimated based on limited information about material characteristics such as gradation and material classification (AASHTO, 2015).

The test procedure for determining the resilient modulus for pavement materials is quite complex and requires sophisticated equipment. Also, the required test setup for resilient modulus testing is not generally available in many material testing laboratories due its high cost. The test requires the preparation of a compacted cylindrical sample with 152.4 mm (6 in) diameter and 304.8 mm (12 in) height, provided that the maximum aggregate size is 25.4 mm (1 in). To replicate the actual situation of the unbound materials under wheel loading, the sample is subjected to repeated compressive loads. The whole process of sample preparation, loading, and measurement of sample deformation is very complex and requires trained and experienced operators. The complete test from the preliminary characterization to completion of the actual resilient modulus test, takes almost five days to complete for two replicates of a single material. The measurement of the deformations is really a sensitive issue within the test procedure.

Due to the complexity and time requirements for resilient modulus testing, many state department of transportations (DOTs) are seeking alternative procedures for determining resilient modulus. One popular approach is to estimate the resilient modulus value based on other parameters which are more readily determined in the laboratory. Another approach classifies aggregates into unique groups according to their anticipated behavior, and then assigns an estimated resilient modulus value to the groupings (e.g., recommended resilient modulus according to their soil classification in ASSHTO [2015]). Either approach will then assign a resilient modulus value to the aggregate without actually performing a resilient modulus test.

The first approach which links other simpler parameters to the resilient modulus was used in this study. The resilient modulus was determined for the most commonly used aggregates for highway construction in Idaho. Additionally, simpler material parameters such as grain size distribution, Atterberg limits test, moisture-density relationship test and index parameters such as California bearing ratio (CBR), modulus obtained by light weight

deflectometer (LWD) were determined for same aggregates. The results were analyzed for potential correlations. Such correlations would allow the designers to estimate the required resilient modulus values based on more readily determined material parameters.

1.2 Research Goals and Objectives

The resilient modulus of the unbound materials is a required input for AASHTOWare Pavement ME. Thus, accurate values for the resilient modulus are needed for proper design. In order to meet this goal, the following objectives were achieved.

- Measure the resilient modulus of unbound coarse materials commonly used for pavement construction in Idaho.
- Conduct a comparative study of resilient modulus measurements using internal and external deformations and assess the relationship between internally- and externally-measured resilient modulus.
- Evaluate existing constitutive models which describe the behavior of unbound materials at different stress conditions and determine the regression parameters of studied models.
- Develop predictive models for the resilient modulus of base and subbase granular materials. These models are based on basic material parameters which are readily determined from routine laboratory tests.
- Explore the correlation between the resilient modulus and other simple monotonic tests such as the California bearing ratio (CBR) and elastic modulus values obtained from the light weight deflectometer (LWD).

1.3 Thesis Organization

The thesis consists of five chapters. Chapter 1 includes the problem statements, goals and objective, and thesis organization. Chapter 2 provides the main findings of a comprehensive literature review conducted by the author on the behavior of unbound granular materials, test methods used to measure various properties of granular materials, factors that affect the resilient properties of unbound granular materials. Chapter 2 also presents the available prediction models and the constitutive relationships that describe the behavior of unbound materials, and correlation between resilient modulus and index parameters of unbound materials. Chapter 3 describes the test materials used for this research

and various tests conducted including preliminary characterization (e.g., particle size distribution, Atterberg limits, and material classification), moisture-density relationships, resilient modulus test, California bearing ratio, and light weight deflectometer.

Chapter 4 discusses the results of various tests conducted for this research, evaluation of existing constitutive models to explain the behavior of unbound materials, development of predictive models of resilient modulus of unbound materials, correlation between resilient modulus and other tests methods. Chapter 5 summarizes the main findings and conclusions of this research and provides recommendations for future studies.

CHAPTER 2 LITERATURE REVIEW

2.1 Overview

This chapter presents of the main findings of the literature review on evaluation and behavior of unbound granular materials used as base and subbase layers in pavements. The literature review included laboratory tests used to evaluate various properties of unbound granular materials including material classification, particle size distribution, moisture-density relationship, resilient modulus California bearing ratio, and Light weight deflectometer. In addition, existing correlations among these properties and prediction models for resilient modulus were also reviewed.

2.2 Unbound Granular Materials and Their Deformation Behavior

Unbound granular materials used to construct the base and subbase layers in pavements play a vital role in governing the structural behavior of pavements (e.g., resisting deformation). To develop and implement a rational pavement design method, the responses of these unbound materials under loading should be accurately evaluated. The mechanistic – empirical (ME) pavement design method determines the structural behavior (e.g., stress, strain, deformation) of pavements due to the applied loads. It uses empirical relationships to estimate the life of pavements using its structural behavior. Due to traffic loading (e.g. wheel loading), an element in pavement structure system experiences various stresses (i.e., vertical, horizontal and shear) (Lekarp et al., 2000). The horizontal and vertical stress components are positive while the shear stresses turn to negative from positive as the wheel load passes through the element (Figure 2.1). The transition in shear stress from positive to negative leads to complex behavior of the unbound materials (Lekarp et al., 2000).

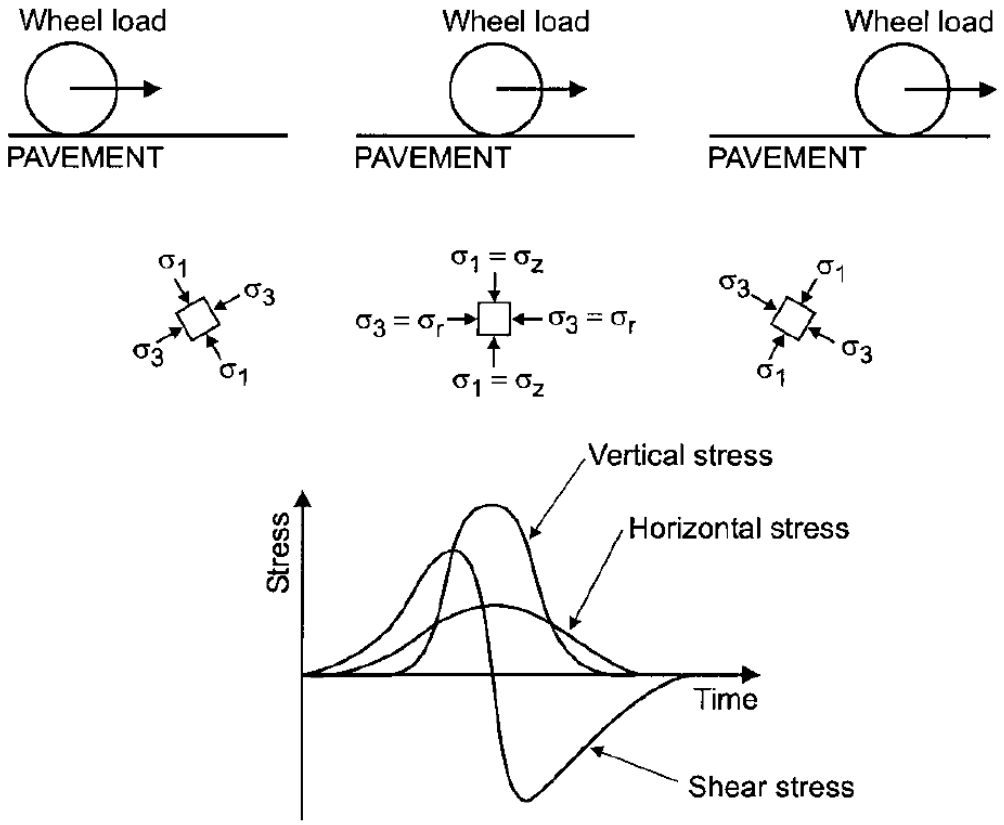

Figure 2.1 Stress state of a pavement element induced by moving wheel load; reproduced with permission after Lekarp et al. (2000)

Granular materials experience recoverable (resilient or elastic) and non-recoverable (permanent or inelastic) deformation under repeated traffic loading. Figure 2.2 shows a typical stress-strain diagram of granular materials under loading. The relative magnitude of the elastic and plastic portions of the total strain is dependent on several factors including traffic loading and speed, thickness and strength of the unbound layer, quality of granular material, etc. The accumulation of permanent deformation decreases gradually with load repetitions as the base layer approaches "stable" compacted conditions. The subsequent loading ideally yields deformations that are elastic in nature. A well-constructed unbound layer should not experience any permanent deformation during the service life of the pavement. Consequently, the mechanistic-based pavement design protocols have traditionally focused on the elastic response of the unbound layers (Tutumluer, 2013).

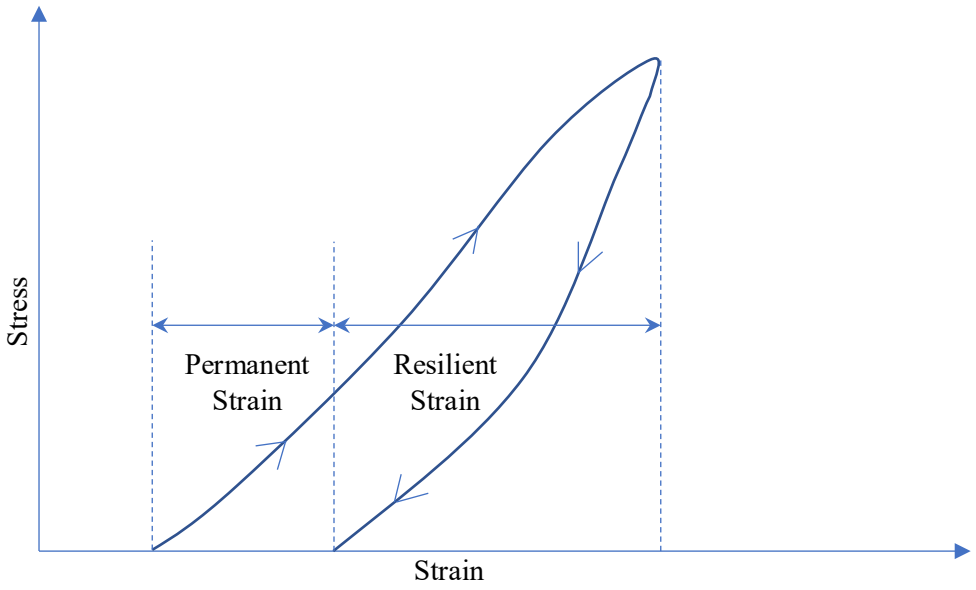

Figure 2.2 Strains of unbound materials induced by one cycle of loading; reproduced based on the drawing by Tutumluer (2013)

2.3 Repeated Load Triaxial Testing (RLT)

In order to study and characterize the mechanical properties of unbound materials, the material should be tested under state of stresses similar to the field. In the triaxial testing (Figure 2.3), the intermediate principal stress (σ_2) and minor principal stress (σ_3) are equal to the confining stress to simulate the field conditions (Adu-Osei, 2000).

In this test, a constant confining stress along with an axially applied deviatoric stress are applied to a cylindrical test specimen for a certain number of cycles. Usually, the confining stress is produced by air which simulates the confinement of the materials in the field. The stress conditions (confining stress and deviatoric axial stress) are selected to simulate the stress conditions that are experienced by the materials in the field (Adu-Osei, 2000). Barksdale (1971) proposed a chart that can be used to select the applied loads. A typical loading cycle consists of 0.1 sec. of loading followed by a rest period of 0.9 sec. This loading cycle was developed to simulate traffic loading on pavements (Barksdale, 1971).

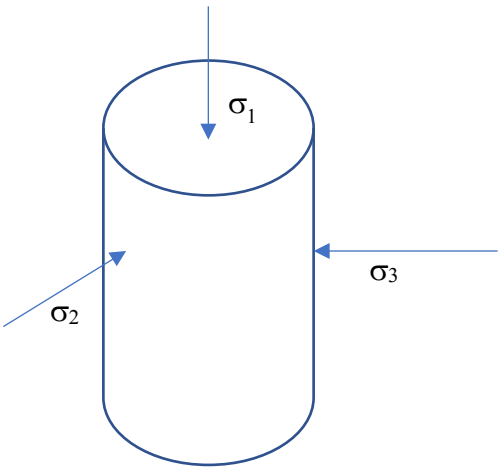

Figure 2.3 Cylindrical specimen in triaxial test; reproduced based on the drawing by Adu-Osei (2000)

2.4 Resilient Modulus

The resilient modulus (M_R) is a basic material property used to characterize unbound pavement materials. According to AASHTO T 307, the resilient modulus is defined as the ratio of the amplitude of the axial repeated (cyclic) stress to the amplitude of resultant recoverable axial strain under repeated triaxial loading (AASHTO, 1999). The resilient modulus is a measure of material's stiffness. It provides a means to quantify pavement construction material's stiffness under different compaction conditions and applied stress states (AASHTO, 1999). Proper resilient modulus characterization is needed to model the performance and predict the service life of pavements (Taylor, 2008). The resilient modulus is calculated as presented in Equation 2.1.

$$M_R = \sigma_{cyclic} / \varepsilon_r \quad (2.1)$$

where,

M_R = resilient modulus

σ_{cyclic} = axial deviator stress in cyclic order

ε_r = axial recoverable strain

The first official resilient modulus testing protocol adopted by the American Association of State Highway and Transportation Officials (AASHTO) was AASHTO T

274-82, “Standard Method of Testing for Resilient Modulus of Subgrade Soils”. Over time, the test protocols experienced several modifications and changes. The evolution of the resilient modulus test procedure is discussed by Puppala (2008). After many modifications, AASHTO adopted T 307 as a universal testing procedure for unbound materials in 1999. In this protocol, fifteen different load sequences along with a preconditioning sequence are recommended for both base/subbase and subgrade materials. AASHOT T 307-99 follows the recommendation of NCHRP 1-28A of maintaining the minimum ratio of sample size to maximum aggregate size but requires measuring the axial deformations externally since it simplifies the testing procedure. Figure 2.4 shows the equipment setup required for AASHTO T 307.

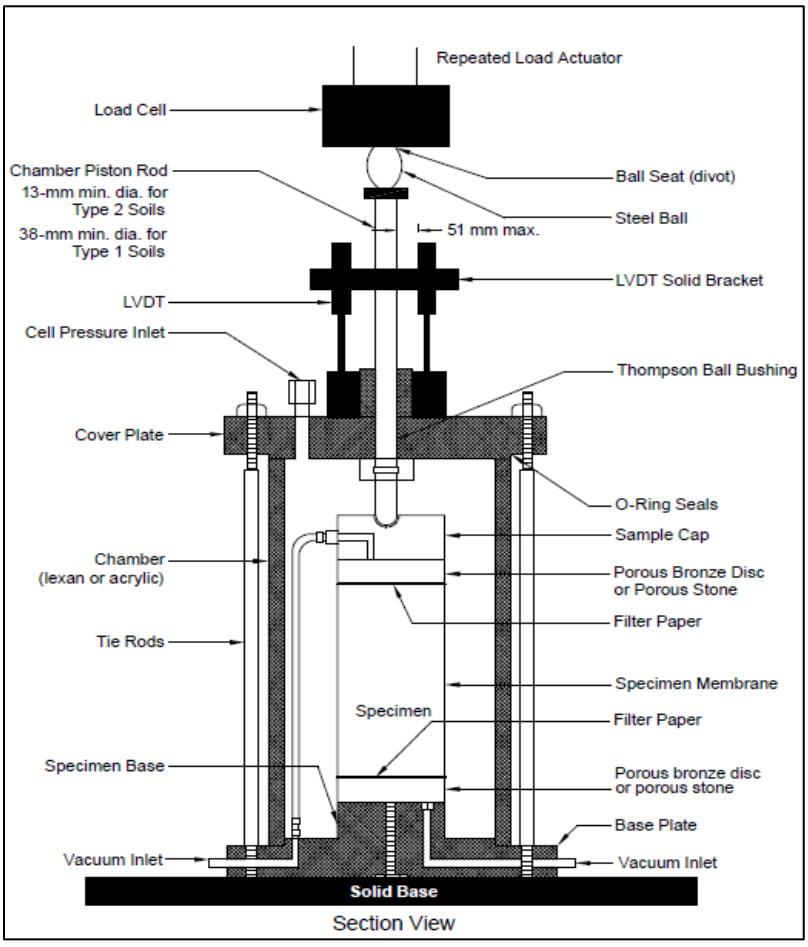

Figure 2.4 Instrumental setup of resilient modulus test according to AASHTO T 307; reproduced with permission after AASHTO (1999)

Ping et al. (2003) measured the resilient modulus using LVDTs that are mounted on the test sample (internal measurements at half length of the sample) at different heights and using LVDTs mounted at the loading plate (external measurements considering full length of the specimen) as shown in Figure 2.5 and Figure 2.6, on subgrade materials.

Ping et al. (2003) reported that, the resilient modulus measured at middle half of the specimen yielded the highest resilient modulus value while the externally measured (e.g. LVDT mounted on the top platen, outside the triaxial chamber) provided the lowest resilient modulus values. The external deformation measurements are affected by the end plate effects. (Ping at al., 2003). Although, the internal LVDTs were hard to mount on the test specimens, Ping et al. (2003) concluded that the internally measured resilient modulus is the most reliable one. The findings on this study were consistent with the recommendations provided by Witczak (2003) for measuring deformation in the resilient modulus test. Witczak (2003) recommended LVDTs should be mounted at the middle half of the specimen where the end-friction effects are negligible.

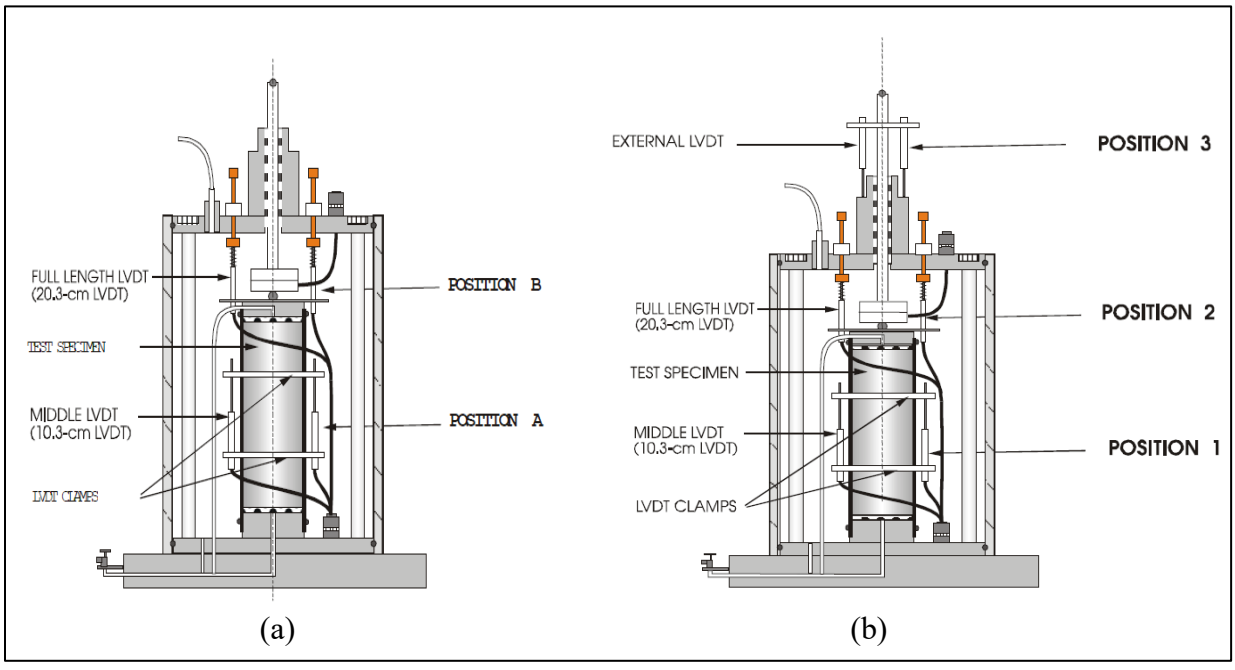

Figure 2.5 Different positions of LVDTs for methods (a) AASHTO T 292-91 and (b) AASHTO 294-92 (Ping et al., 2003)

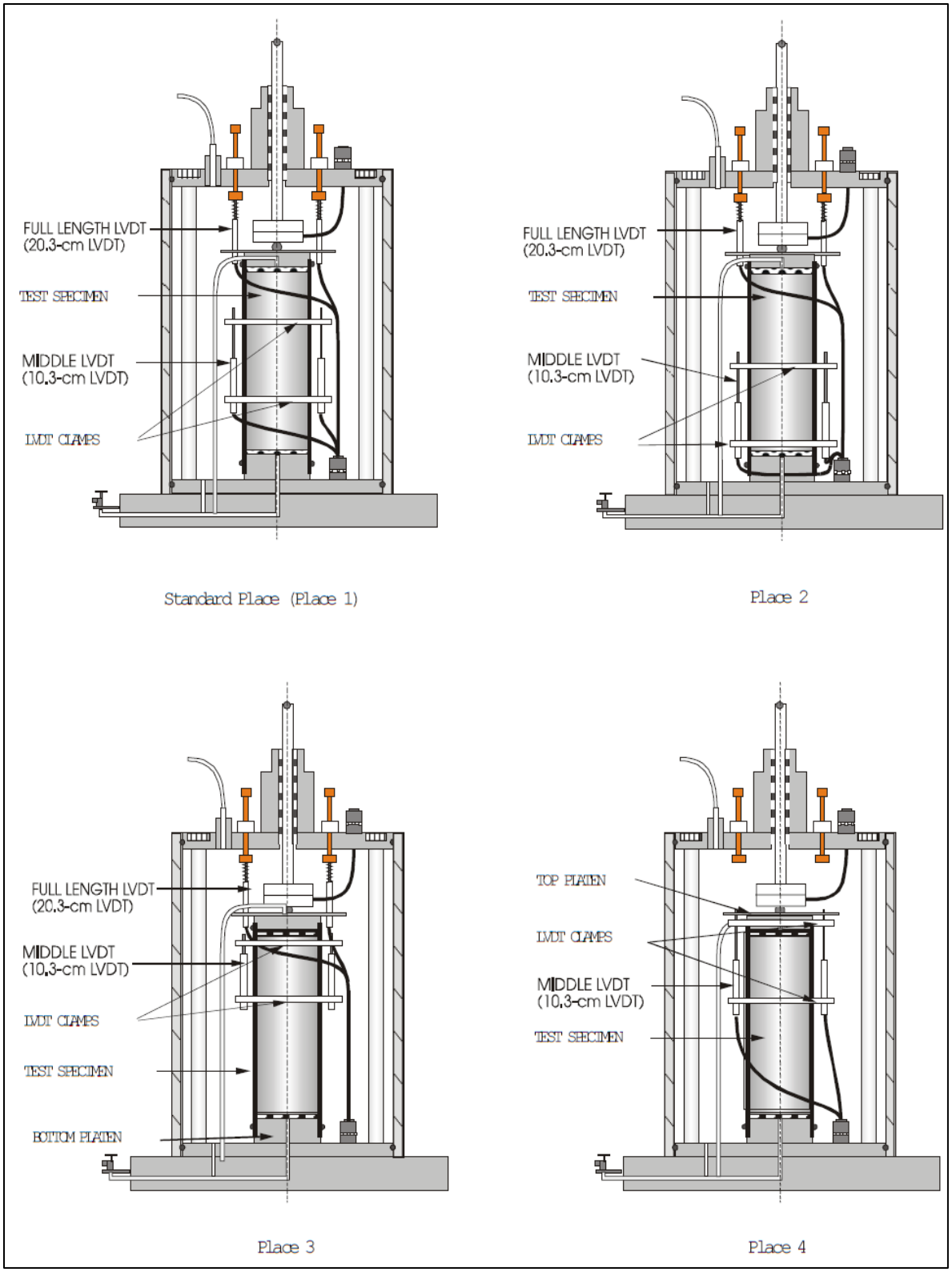

Figure 2.6 Different positions of middle-half LVDTs (Ping et al., 2003)

2.5 Factors Affecting Resilient Properties of the Unbound Granular Materials

There are several factors that affect the resilient modulus of unbound granular materials. These factors include density, aggregate type and shape, percent of fines, gradation and grain size, moisture content, stress state and history, specimen size, and load duration and frequency. This section discusses the effect of each of these factors.

Effect of Density

Density of unbound granular materials is used as an indicator for quality control. It is a measure of the degree of compaction. Generally, increased density leads to higher stiffness. Besides, it reduces the deformation (i.e., both recoverable and non-recoverable) to static and dynamic loads (Seyhan, 2001). There is no direct proportional relationship between density and resilient modulus. Some researchers found that density to have slight impact on the resilient modulus (Knutson and Thompson, 1977; Elliott and Thornton, 1988) while others observed that resilient modulus increases with density (Rowshanzamir, 1995; Tutumluer and Seyhan, 1998). Holubec (1969) observed increased resilient modulus with density for unbound materials with angular particles compared to rounded particles.

Effect of Aggregate Type and Shape

The resilient modulus increases with angularity and roughness of aggregates while it decreases with the Poisson's ratio (Hicks and Monismith, 1971; Allen and Thompson, 1974; Thom, 1988; Thom and Brown, 1988; Barksdale and Itani, 1989). Crushed aggregates increase the number of contact points, create more friction between particles leading to increased stiffness (Lekarp et al., 2000). This mechanism is referred to as aggregate interlock. Allen (1973) and Barksdale and Itani (1989) evaluated the effect of surface characteristics of granular materials on resilient modulus. They concluded that angular particles can provide better resistant to permanent deformation compared to rounded particles. Angular particles provide better particle-to-particle contact leading to higher shear resistance. More recently, Rao et al. (2002) investigated the effect of aggregate surface characteristics with image processing and concluded that surface characteristics are directly related to the resistance to the permeant deformation.

Effect of Percent of Fines

Fines content, generally known as the percent passing of 0.075 mm (No. 200) sieve, is used to categorize aggregates in accordance with the AASHTO soil classification system, M 145 (AASHTO, 1991). Previous studies showed that resilient behavior of unbound granular materials can be affected by fines content (Hicks, 1970). Hicks and Monismith (1971) observed a drop in resilient modulus with the increase in fines content for partially crushed materials, but there was an opposite trend for fully crushed aggregates. Several researchers including Hicks (1970), Barksdale and Itani (1989) investigated the influence of fines content on resilient modulus but didn't come to a solid conclusion. For example, Hicks (1970) found a minor influence on resilient modulus by varying the fines content from 0 to 10% but Braksdale and Itani (1989) found a drastic drop in resilient modulus (60% reduction) with the same variation of fines. It is worthy to mention, aggregates with the same amount of fines and similar shape of grain size distribution, the resilient modulus increases with increasing maximum aggregate size (Gray, 1962; Thom, 1988; Kolisoja, 1997).

Effect of Gradation and Grain Size

Gradation and the fines content are interconnected, and both affect the stiffness of granular materials. Amount of fines more than optimum level may influence the strength, resilient, and permanent deformation characteristics of granular materials. Extra fines fill the voids between coarse particles and further reduce interparticle interactions by separating them apart (Xiao and Tutumluer, 2012). Gray (1962) found that maximum strength was achieved for a dense-graded crushed aggregate of 25 mm (1 in) maximum size at fines content of about 8%. Kolisoja reported that, the resilient modulus increased with the maximum particle size, provided that the aggregate has similar grain size distribution and same fines content. Generally, coarse-grained materials yield higher resilient modulus values (Kirkpatrick, 1965; Lekarp et al., 2000; Leslie, 1963; Tian et al., 1998; Zaman et al., 1994), whereas, fine-grained materials yield lower resilient modulus values (Hicks and Monismith, 1971; Lekarp et al., 2000; Tian et al., 1998). Coarse-grained materials exhibit higher resilient modulus compared to fine grained modulus due to improved aggregate interlock. (Cunningham et al., 2013). For many granular materials, the dry density is correlated with resilient modulus since the density is closely related to the particle-size distribution (Barksdale and Itani, 1989; Hicks and Monismith, 1971; Lekarp et al., 2000; Rada and

Witczak, 1982; Tian et al., 1998; Zeghal, 2000). Thom and Brown (1988) reported that, the impact of gradation varies with the compaction level. They found that uniformly graded materials are slightly stiffer than well-graded ones. Afterwards, Kamal et al. (1993) and Dawson et al. (1996) demonstrated that the impact of gradation was more significant than the level of compaction with respect to resistance to permeant deformation for dense-graded mix.

Effect of Moisture Content

The effect of moisture content on aggregate can be described in three different ways; (1) capillary suction, (2) lubrication and (3) access pore water pressure. The capillary suction makes the aggregate matrix stronger whereas lubrication makes the matrix weaker. Further lubrication leads to access pore water pressure which decreases the strength of the aggregate matrix (Tutumluer, 2013). The moisture content of the aggregates was found to affect the resilient response of the material but the effect of moisture is dependent on the analysis process (Kancherla, 2004).

Mitry (1964), Seed et al. (1964) and Hicks (1970) demonstrated that the resilient modulus decreases due to the saturation if the analysis of resilient modulus is based on the total stress. While, resilient modulus remains approximately unchanged if the analysis is based on the effective stress (Hicks and Monismith, 1971; Pappin, 1979). Dawson et al. (1996) found that stiffness tends to increase with increasing moisture level if below optimum moisture content. While, stiffness decreases rapidly with moisture content beyond the optimum moisture content. Hicks and Monismith (1971) also observed that the resilient modulus decreases when the moisture content exceeds an optimum value.

Effect of Stress State and History

The stress level or stress state is one of the most important factors affecting the resilient behavior of unbound granular materials. Previous studies demonstrated that the resilient modulus of untreated granular materials is dependent on confining pressure and bulk stress (Mitry, 1964; Monismith et al., 1967; Hicks, 1970; Smith and Nair, 1973; Uzan, 1985; Sweere, 1990). Monismith et al. (1967) found an increase of 500% in resilient modulus when the confining pressure increased from 20 to 200 kPa. Smith and Nair (1973) found 50% increased resilient modulus when the bulk stress was doubled (i.e., increased from 70 kPa to 140 kPa).

The deviatoric stress was found to have less effect on the stiffness when compared to confining stress (Kancherla, 2004). Morgan (1966) showed that the resilient modulus decreased slightly with repeated deviatoric stress under constant confining stress. Hicks (1970) reported that there is no impact of deviatoric stress on resilient modulus provided that there is no excessive plastic deformation. Meanwhile, Hicks and Monismith (1971) reported a slight decrease in stiffness at low deviatoric stress levels and minor increase in stiffness at higher stress levels.

Stress history may also have an impact on the resilient modulus of granular unbound materials. The effect of stress history is a result of progressive densification and rearrangement of particles under repeated triaxial loading (Dehlan, 1969). Therefore, several researchers suggested a sequence of specific load repetitions to eliminate the effects of stress history (Boyce et al., 1976; Hicks, 1970; Allen, 1973).

Effect of Load Duration and Frequency

Previous research found that the load duration and frequency have no significant effect on the resilient behavior of granular materials (Seed et al., 1965; Morgan, 1966; Hicks, 1970). Hicks (1970) conducted the resilient modulus test at various loading durations (e.g., 0.1, 0.15, and 0.25 sec) and found no change in the resilient modulus. When the moisture content approaches saturation, the resilient modulus exhibits a reduction with loading frequency. The developed transient pore pressure causes a reduction in effective stress. This phenomenon is significant when there is little opportunity for drainage (Lekarp et al., 2000).

Effect of Specimen Size

Effect of specimen size is closely related to end restraint condition of the specimen. Many researchers (Taylor, 1941; Lee and Frank, 1978; Rowe and Branden, 1964; Bishopand Green, 1965; Duncan and Dunlop, 1968) studied end restraint effects on the shear strength of soils. They demonstrated that if frictionless platens are used, sample slenderness can be reduced to one. Adu-Osei (2000) investigated the effect of specimen size. He changed the slenderness ratio of 2:1 to 1:1 and obtained reliable results when the end pates were lubricated. He also noticed that the specimen itself was more stable and practical.

Standard procedure of AASHTO for resilient modulus test specifies the diameter of the specimen as a function of the maximum aggregate size and requires the height to diameter ratio of 2.0 (AASHTO, 1999).

2.6 Prerequisite for Resilient Modulus Test

There are several factors related to aggregate properties, mentioned in previous section, affect the resilient modulus of an aggregate. It is better to have some knowledge of the properties of an aggregate prior to conduct resilient modulus test of that aggregate. The Standard test method, AASHTO T 307, also makes some preliminary characterization test, such as particle size distribution, Atterberg limit test, moisture-density relationship etc. as prerequisite for the resilient modulus testing (AASHTO, 1999). The preliminary characterization tests are discussed in the following sections.

2.6.1 Particle Size Distribution

Before starting the resilient modulus testing, the first preliminary characterization test is the "Particle Size Distribution". Also known as "Grain Size Distribution". The available standard for doing the test is AASHTO T 27 (AASHTO, 2011). The outcomes of the particle size distribution can be noted as co-efficient of uniformity, $C_{u,}$ co-efficient of curvature, $C_{c,}$ percent fines i.e. passing of 0.075 mm (No. 200) sieve, maximum aggregate size and nominal maximum size of the aggregate. The maximum size of the aggregate is required to prepare a specimen for resilient modulus test. Because, AASHTO T 307 specifies that the minimum diameter of the specimen should be at least five times larger than the maximum aggregate size (AASHTO, 1999).

As mentioned earlier, Particle size distribution or the gradation of the material has significant impact on the resilient modulus of the aggregate. Coarse grained particles exhibit more interlocking under the repeated loading, results higher resilient modulus. On the other hand, fine grained particles act as bonding or filler material to aggregate matrix, minimizes the movement of the coarse particles (Knight, 1935; Radjai et al., 1998; Voivret et al., 2009).

2.6.2 Soil Classification

The material classification is dependent on the outcome of the particle size distribution and the results of the consistency limits test. The consistency limits test is also known as Atterberg limits test. The Atterberg limits include liquid limit, plastic limit and

plasticity index. According to AASHTO T 90, the plasticity index (PI) is the difference between plastic limit and liquid limit (AASHTO, 2000). The consistency limits are sensitive to water content. The standards for measuring plasticity index are documented in AASHTO T 89 (AASHTO, 2010a) and AASHTO T 90 (AASHTO, 2000).

Soil classification is performed using either AASHTO M 145 (AASHTO, 1991) or Unified Soil Classification system (USCS). The AASHTO M 145 system has seven major categories (e.g. A – 1 to A – 7) for aggregate classification. Classification "A-1-a" indicate an excellent to good quality aggregate (AASHTO, 1991). According to USCS, a soil is classified as gravel (G), sand (S), silt (M), clay (C), or organic (O) with additional designations to indicate poorly-graded (P) or well-graded (W) materials. This classification also describes the plasticity of test materials as high (H) or Low (L).

Past research found that the resilient modulus of aggregate base materials to increase with the increase of plasticity index of fines (Drumm et al. 1990, Farrar and Turner 1991, George 2004). Meanwhile, other researchers (Carmichael and Stuart, 1978; Rahim, 2005) didn't find plasticity index as a significant issue to affect the resilient modulus of coarse-grained unbound materials.

2.6.3 Moisture-Density Relationship

Compaction of the test specimen is another prerequisite of resilient modulus testing. AASHTO T 307 (AASHTO, 1999) specifies that the specimen should be compacted to approximate the in-situ wet density and moisture condition. If the undisturbed sample is not available or the in-situ density and moisture data is not available, then a percentage of the maximum dry density (MDD) and corresponding optimum moisture content (OMC), obtained by standard compaction or modified compaction method, can be used to compact the specimen for resilient modulus test (AASHTO, 1999). The official standard for standard compaction method is AASHTO T 99 (AASHTO, 2010b) and AASHTO T 180 (AASHTO, 2010c) for modified compaction method.

The density of specimen reaches the MDD when the water content at the time of compaction is equal to OMC. The dry density of the specimen increases proportionally with water content up to OMC and the dry density decreases with increasing water content beyond OMC. These two parameters (e.g., MDD and OMC) are the outcomes of the moisture density

relationship test and they are needed prior to compact the test specimens for the resilient modulus test (Amber and Von Quintus, 2002).

2.7 California Bearing Ratio Test

The California Bearing Ratio (CBR) of subgrade or base/subbase materials represents the bearing capacity of the test materials relative to that of standard crushed rock (Huang, 2004). The CBR test is performed in accordance with ASTM D 1883 or AASHTO T 193 standards. The test is conducted by penetrating a 50.8 mm (2 in) diameter circular face piston into the surface of a compacted test specimen at constant rate of 1.27 mm/minute (0.05 in/minute). The applied load and resulting penetration are recorded during the test. The CBR value is obtained by calculating the bearing stress obtained by the recorded load for each penetration and dividing that bearing stresses by standard at 2.54 mm (0.1 in) and 5.08 mm (0.2 in) as provided in ASTM D 1883 or AASHTO T 193. The highest ratio is multiplied by 100 to report as the CBR for the tested material.

Most of the factors that affect the resilient modulus of granular unbound materials also affect the CBR. These factors include the degree of particle to particle contact within coarse aggregate matrix along with the particle size, fines content, plasticity characteristics etc. The materials with high CBR values may also have higher resilient modulus values (ARA 2004; Heukelom and Klomp, 1962; Webb and Campbell, 1986). However, good correlations between CBR and resilient modulus for some materials may be difficult to obtain due to differences in loading conditions and non-linear behavior of different material types (Figueroa and Thompson, 1980; Zaman et al., 1994). However, the correlation between CBR and resilient modulus can be further improved if other material properties such as shear strength are considered (Kyalham and Willis, 2001).

2.8 Light Weight Deflectometer Test

The Light Weight Deflectometer (LWD) is a newly introduced test in pavement industry. The LWD test is dynamic plate load test that determines the dynamic modulus (E_{LWD}) of the soils and unbound materials (Schwartz et al., 2017). In this test, an impulse (impact) load is applied and associated deflection is measured. The pulse load is applied by releasing standard load from a given height. Schwartz et al. (2017) documented the principle and the procedure of the LWD test in details.

Due to light weight of the instrument and its simplicity, the test is gaining popularity. In LWD test, the applied load and obtained deflection data is used in the calculation procedure of the modulus of the test material. The LWD can be used to measure the modulus of the soil/aggregate in the field as well as laboratory. The LWD is often used in the field to assess the quality of construction or compaction of the granular layers. The LWD test is proposed as a replacement to the Nuclear Density Gauge (NDG) (Schwartz et al., 2017). In the laboratory, the LWD test can be conducted in both standard and modified proctor mold. The test specimen can be tested using LWD at different levels of moisture content and density. An extensive study was carried out on the LWD test at University of Maryland and researchers proposed two test protocols; AASHTO TP 123-01 "Laboratory Determination of Target Modulus Using LWD Drops on Compacted Proctor Mold" and AASHTO TP 456-01 "Compaction Quality Control Using LWD" (Schwartz et al., 2017).

2.9 Existing Correlations of Resilient Modulus

The resilient modulus test is time consuming and required trained personnel. In addition, the related equipment is not readily available to all transportation agencies. Tutumluer (2013) documented that only 14 out of examined 46 agencies conduct resilient modulus testing on unbound materials. Recently, Hajj et al. (2018) reported that 28 state DOTs conduct the resilient modulus test to characterize unbound materials.

Many transportation agencies rely on the numerous correlation equations available in the literature to predict the resilient modulus based on other easy-to-measure properties. Most of these correlations were established using regression analysis in which test results of resilient modulus were correlated with results obtained from less expensive or more conventional test such as R-value, CBR, unconfined compression test, and index property tests (George, 2004). The following sections discuss different correlations available in the literature used to predict resilient modulus for soils and aggregates based on other material properties.

2.9.1 Prediction of Resilient Modulus

Several studies were conducted to estimate the resilient modulus of granular materials as function of inherent properties of aggregates (George, 2004). In this section, the equations

used to estimate the resilient modulus of coarse-grained materials were reviewed since it is the main interest of the study.

Carmichael and Stuart (1978) proposed two different models for predicting the resilient modulus of fine-grained and coarse-grained soils. These models were developed based on data collected from literature and some laboratory testing. Although the data had differences in the testing protocol, the models provide good estimate of the resilient modulus values ($R^2 = 0.836$). The resilient modulus equation for the coarse-grained soil is presented in Equation 2.2.

$$\log M_R = 0.523 - 0.025 \times w_c + 0.544 \times \log \theta + 0.173 \times SM + 0.197 \times GR \quad (2.2)$$

where,

M_R = resilient modulus (ksi)
w_c = gravimetric moisture content (%)
θ = stress invariant or bulk stress (psi)
SM = 1 for SM soils classified using USCS
= 0 otherwise
GR = 1 for GM, GW, GC, or GP soils classified using USCS
= 0 otherwise

Rahim (2005) conducted resilient modulus testing on various aggregate samples from Mississippi. The test materials had a wide range of classifications (i.e., A-1-a to A-7). He developed two correlation equations; one for fine-grained soils and other for coarse-grained soils. The equation for coarse-grained sandy soil is presented in Equation 2.3. The R^2 of the Equation 2.3 is 0.75.

$$M_R \text{ (MPa)} = 324.14 \times (\gamma_d / (w_c + 1))^{0.8998} \times (p\ \#200 / \log C_u)^{-0.4652} \quad (2.3)$$

where,

p #200 = percent Passing of #200 sieve (%),
γ_d = dry density (kN/m^3),
w_c = moisture content (%),
C_u = coefficient of uniformity

Jackson (2015) measured the resilient modulus for various base materials in Utah. The resilient modulus data were used to develop database needed for implementing the Mechanistic-Empirical Pavement Design Guide (MEPDG) by Utah Department of Transportation. Equation 2.4 presents the prediction model developed by Jackson (2015). The Equation 2.4 provided a good correlation between the measured and predicted resilient modulus values ($R^2 = 0.968$).

$$M_R = (- 200 - 1.51 \times P_{200} - 418 \times D_{30} - 3.09 \times OMC + 1.94 \times MDD) \times \gamma_{dr} \quad (2.4)$$

where,

M_R = resilient modulus (ksi)
P_{200} = percent passing of No. 200 sieve (%)
D_{30} = particle diameter corresponding to 30 percent finer (in.)
OMC = optimum moisture content (%)
MDD = maximum dry density (pcf)
γ_{dr} = ratio of dry density to MDD, expressed as fraction

In addition, Jackson (2015) investigated the correlation between the resilient modulus and CBR of the tested materials. He didn't find significant correlation between CBR and resilient modulus ($R^2 = 0.119$ and p-value of 0.402.)

Hajj et al. (2018) measured the resilient modulus for various base and subgrade materials to implement MEPDG in Nevada. The resilient modulus test was conducted in accordance with AASHTO T 307 (AASHTO, 1999). They developed a prediction model of resilient modulus of the unbound materials as a function of several factors including R-value, aggregate gradation, optimum moisture content and equivalent thickness of base layer as presented in Equation 2.5. This equation will be used for pavement rehabilitation purpose.

$$\ln (M_R) = 8.014 + 0.0261\, R - 0.0485\, P_{40} + 0.0161\, P_{3/8} - 0.0659\, OMC - 0.0089\, H_{eq} \quad (2.5)$$

where,

M_R = resilient modulus (psi)
R = R – value

P_{40} = percent passing the No. 40 sieve (%)

$P_{3/8}$ = percent passing the 3/8" sieve (%)

OMC = optimum moisture content (%)

H_{eq} = equivalent thickness of base layer (inch)

2.9.2 Correlation between Resilient Modulus and California Bearing Ratio (CBR)

Many studies explored the correlation between CBR and resilient modulus since the former is simpler to conduct compared to the latter. Heukelom and Foster (1960) developed a relationship between resilient modulus and CBR for soil samples as presented in Equation 2.6.

$$M_R \text{ (psi)} = 1565 \text{ x CBR} \tag{2.6}$$

In 1962, Heukelom and Klomp (1962) proposed a revised formula as presented in Equation 2.7. It should be noted that the resilient modulus in Equation 2.7 was measured using the vibratory wave propagation technique at low strain levels and this equation is applicable to materials with CBR values between 2 and 200. Dione et al. (2015) reported that the Heukelom and Klomp correlation is the most widely used one. This correlation seems to be more reasonable for fine grained soils and fine sands than the granular materials (Huang, 2004).

$$M_R \text{ (psi)} = 1500 \text{ x CBR} \tag{2.7}$$

Green and Hall (1975) found a relationship between in-situ CBR and dynamic modulus as presented in Equation 2.8. Similar to Heukelom and Klomp (1962), they measured the resilient modulus using vibratory wave propagation technique. In addition, Equation 2.8 is also applicable to materials with CBR values between 2 and 200.

$$M_R \text{ (psi)} = 5409 \text{ x CBR}^{0.711} \tag{2.8}$$

The South African Council on Scientific and Industrial Research (CSIR) uses a correlation of CBR and M_R given by Equation 2.9. But the problem associated with this equation is, it is dependent of the nature of the material of which the resilient modulus is predicted. This correlation was documented by Paterson and Maree (1978).

$$M_R \text{ (psi)} = 3000 \text{ x CBR}^{0.65} \tag{2.9}$$

Witczak et al. (1995) documented that Lister and Powell (1987) suggested the correlation between resilient modulus and CBR (Equation 2.10). Equation 2.10 was originally proposed by the Transportation and Road Research Laboratory (TRRL) in United Kingdom for flexible pavement design. Although, it is an old correlation, MEPDG uses this equation to convert CBR to resilient modulus as Level-2 input (AASHTO, 2015).

$$M_R \text{ (psi)} = 2555 \times CBR^{0.64} \quad (2.10)$$

Erlingsson (2007) proposed a correlation between resilient modulus and CBR presented in Equation 2.11. Erlingsson (2007) modified the correlation proposed by the CSIR (Equation 2.10) by incorporating a stress state as a variable. Since the resilient modulus is stress dependent value, Erlingsson (2007) used a bulk stress parameter in his model and proposed Equation 2.11.

$$M_R \text{ (MPa)} = 9.25 \times CBR^{0.65} (3P/P_a)^{0.4} \quad (2.11)$$

2.9.3 Correlation between Resilient Modulus and E_{LWD}

There are limited number of studies that were carried out to correlate the resilient modulus with the modulus obtained by the LWD, known as E_{LWD}, since the LWD is a relatively new test. The applied load and obtained deflection data are used to calculate the stiffness of the aggregate which further used to measure the $E_{LWD.}$

Schwartz et al. (2017) measured the LWD modulus of several subgrade and base materials using three different LWD equipment. The LWDs were Zorn, Dynatest and Olson. The researchers conducted the tests on the Proctor mold. To evaluate the stress dependency of the resilient modulus, Schwartz et al. (2017) conducted the LWD test with different heights and combination of six drops. They found strong correlations between the LWD modulus and resilient modulus measured in the laboratory. They found R^2 was 0.89 for Dynatest, 0.79 for Zorn, and 0.73 for Olson. Obtaining the E_{LWD} at different moisture content, density and Poisson's ratio was the main benefit of conducting LWD test on Proctor mold since the LWD test is considered as an add-on to the routine moisture-density relationship test (Schwartz et al., 2017).

White et al. (2007) developed a correlation between LWD and resilient modulus for subgrade materials as presented in Equation 2.12. In this equation, the resilient modulus

values were measured at 41.4 kPa (6 psi) confining pressure and a deviatoric stress of 69 kPa (10 psi). In addition, a Poisson's ratio of 0.35 and shape factor of $\pi/2$ for cohesive soil and 2 for cohesionless soil were used.

$$M_R\ (MPa) = \{E_{LWD}\ (MPa) + 45.3\} / 1.24 \quad (2.12)$$

Mohammad et al. (2008) proposed Equation 2.13 to correlate LWD to the resilient modulus. They selected a Poisson's ratio of 0.4 and shape factor of $\pi/2$ for cohesive soil and 2 for cohesionless soil similar to the values used by White et al. (2007).

$$M_R\ (MPa) = \{E_{LWD}\}^{0.18}\ (MPa) \quad (2.13)$$

Mousavi et al. (2017) examined the correlation between the MEPDG model coefficients for resilient modulus (i.e., k_1, k_2, and k_3) and the LWD applied stress and resulting deflection for subgrade materials. This correlation is very useful since the resilient modulus can be estimated at any stress state. Equation 2.14 presented the proposed model by Mousavi et al. (2017). This model provided a good between predicted and measured resilient modulus ($R^2 = 0.83$).

$$k_i = C_1 + C_2 \left(\frac{\sigma}{\delta}\right) \qquad i = 1,2,3 \quad (2.14)$$

where,

k_i = MEPDG model parameter

C_i = parameter estimates for equation

The coefficients of Equation 2.14 are reported elsewhere (Mousavi et al. 2017).

2.10 Resilient Modulus Predictive Models as Function of Stress State

Several constitutive models were developed over the years to predict the resilient modulus of unbound materials based on different stress state parameters. The author conducted comprehensive literature review and developed Table 2.1 that summarizes the models developed by various researchers over the years. However, the most commonly used models are:

- K-θ model (developed by Hicks and Monismith in 1971)

- Uzan Model (developed by Uzan in 1985)
- Modified Uzan Model (developed by Witczak and Uzan in 1988)
- MEPDG Model (developed by ARA inc. in 2004).

Table 2.1 Chronological list of different resilient modulus constitutive models

SL #	Model Proposed By	Model Formulation	Notes
1	Biarez (1961)	$E = K(\sigma_m)^n$	E = Secant modulus K, n are empirical constants
2	Dunlap (1963)	$M_R = k_1 p_a \left(\frac{\sigma_3}{p_a}\right)^{k_2}$	
3	Seed et al. (1967)	$M_R = k_1 p_a \left(\frac{\theta}{p_a}\right)^{k_2}$	Primarily for granular soils
4	Hicks and Monismith (1971)	$M_R = k_1(\theta)^n$	K – θ Model
5	Shackel (1973)	$M_R = k_1 \left\{\frac{(\tau_{oct})^{k_2}}{(\sigma_{oct})^{k_3}}\right\}$	
6	Boyce (1980)	$K = \frac{k_i p^{(1-n)}}{1-\beta\left(q/p\right)^2}$ $G = G_i p^{(1-n)}$	Bulk Shear Model
7	Moossazadeh and Witczak (1981)	$M_R = k_1 p_a \left(\frac{\sigma_d}{p_a}\right)^{k_2}$	Deviatory Model
8	Uzan (1985)	$M_R = k_1 p_a \left(\frac{\theta}{p_a}\right)^{k_2} \left(\frac{\sigma_d}{p_a}\right)^{k_3}$	Normalized Shackel (1973) model
9	Lade and Nelson (1987)	$E = M p_a \left[\left(\frac{I_1}{p_a}\right)^2 + R\frac{j_2}{p_a}\right]^{\lambda}$	Lade and Nelson Model
10	Witczak and Uzan (1988); Modified Uzan Model	$M_R = k_1 p_a \left(\frac{\sigma_\theta}{p_a}\right)^{k_2} \left(\frac{t_{oct}}{p_a}\right)^{k_3}$	Adopted in the 1993 AASHTO design guide

Table 2.1 Chronological list of different resilient modulus constitutive models (cont.)

11	Itani (1990)	$M_R = k_1 p_a \left(\frac{\sigma_\theta}{p_a}\right)^{k_2} (\sigma_d)^{k_3} (\sigma_3)^{k_4}$	Itani Model
12	Crockford et al. (1990)	$M_R = \beta_0 \left(\theta + 3\psi \frac{v_w}{v_t}\right)^{\beta_1} (\tau_{oct})^{\beta_2} \left(\frac{\gamma}{\gamma_w}\right)^{\beta_3}$	Crockford et al. Model
13	Pezo (1993)	$M_R = k_1 p_a \left(\frac{\sigma_3}{p_a}\right)^{k_2} \left(\frac{\sigma_d}{p_a}\right)^{k_3}$	UT-Austin Model
14	Lytton (1995)	$M_R = k_1 p_a \left(\frac{I_1 - 3\,\theta f\, h_m}{p_a}\right)^{k_2} \left(\frac{\tau_{oct}}{p_a}\right)^{k_3}$	Lytton Model
15	Kolisoja (1997)	$M_R = A\,(n_{max} - n) p_a \left(\frac{\theta}{p_a}\right)^{0.5}$	Effect of density included n = porosity of the aggregate
16	Ni et al. (2002)	$M_R = k_1 p_a \left(1 + \frac{\sigma_3}{p_a}\right)^{k_2} \left(1 + \frac{\sigma_d}{p_a}\right)^{k_3}$	UKTC Model
17	Ooi et al. (2004)	$M_R = k_1 p_a \left(1 + \frac{\theta}{p_a}\right)^{k_2} \left(1 + \frac{\sigma_d}{p_a}\right)^{k_3}$	
18	Ooi et al. (2004)	$M_R = k_1 p_a \left(1 + \frac{\sigma_3}{p_a}\right)^{k_2} \left(1 + \frac{\tau_{oct}}{p_a}\right)^{k_3}$	
19	ARA, Inc. (2004)	$M_R = k_1 p_a \left(\frac{\theta}{p_a}\right)^{k_2} \left(1 + \frac{\tau_{oct}}{p_a}\right)^{k_3}$	Adopted in the MEPDG (ARA Inc., 2004).
20	Gupta et al. (2007)	$M_R = k_1 p_a \left(\frac{\sigma_b - 3\,k_6}{p_a}\right)^{k_2} \left(k_7 + \frac{\tau_{oct}}{p_a}\right)^{k_3} + \alpha_1 (U_a - U_w)^{\beta_1}$	$(U_a - U_w)$ = Matric Suction Model

2.10.1 K-θ Model

The K-θ model is one of the most widely used models, established by Hicks and Monismith (1971) in 1971. This model is used for predicting resilient modulus for both subgrade and base/subbase materials. This model uses stress state, bulk stress or stress invariant, as function to predict resilient modulus as presented in Equation 2.15.

$$M_R = K\,(\theta)^n \qquad (2.15)$$

where,

θ is the bulk stress = ($\sigma_1 + \sigma_2 + \sigma_3$) or $\sigma_d + 3\sigma_3$,

σ_d is the deviatoric stress = (σ_1-σ_3) and

k, n are the regression constants obtained from experimental results

2.10.2 Uzan Model

The k-θ model does not consider the effect of shear behavior or the impact of deviatoric load. Uzan (1985) made a modification to the k-θ model. An additional variable of deviator stress was introduced to the model and the modified relationship yielded a better goodness of fit. Uzan's model is presented in Equation 2.16.

$$M_R = k_1 P_a \left(\frac{\theta}{P_a}\right)^{k_2} \left(\frac{\sigma_d}{P_a}\right)^{k_3} \quad (2.16)$$

where,

θ is the bulk stress = ($\sigma_1 + \sigma_2 + \sigma_3$) or $\sigma_d + 3\sigma_3$,

σ_d is the deviatoric stress = (σ_1-σ_3),

P_a is atmospheric pressure and

k_1, k_2, k_3 are the regression constants.

2.10.3 Modified Uzan Model

Modified Uzan model was proposed by Witczak and Uzan in 1988 (Witczak and Uzan 1988). Modified Uzan model is an improved version of Uzan model, where the deviator stress was replaced by the octahedral shear stress as presented in Equation 2.17.

$$M_R = k_1 P_a \left(\frac{I_1}{P_a}\right)^{k_2} \left(\frac{\tau_{oct}}{P_a}\right)^{k_3} \quad (2.17)$$

where,

I_1 is the first stress invariant = ($\sigma_1 + \sigma_2 + \sigma_3$) or $\sigma_1 + 2\sigma_3$.

τ_{oct} is the deviatoric stress = $\frac{1}{3}\{(\sigma_1 - \sigma_2)^2 + (\sigma_1 - \sigma_3)^2 + (\sigma_2 - \sigma_3)^2\}^{1/2} = \frac{\sqrt{2}}{3}\sigma_d$,

P_a is atmospheric pressure and k_1, k_2, k_3 are the regression constants.

2.10.4 MEPDG Model

The MEPDG model (Equation 2.18) is model generalized for the unbound materials (both unbound aggregates and fine-grained subgrade soil) and this model is adopted in the AASHTOWare Pavement ME software. This model provides a very high goodness of fit. This model is capable of capturing both the stiffening effect of bulk stress and the softening effect of shear stress. The goodness of fit must exceed 0.90 to properly find the values of the model constants according to Tutumluer (2013).

$$M_R = k_1 P_a \left(\frac{\theta}{P_a}\right)^{k_2} \left(\frac{\tau_{oct}}{P_a} + 1\right)^{k_3} \quad (2.18)$$

where,

θ is the bulk stress = $(\sigma_1 + \sigma_2 + \sigma_3)$ or $\sigma_1 + 2\sigma_3$.

τ_{oct} is the deviatoric stress = $\frac{1}{3}\{(\sigma_1 - \sigma_2)^2 + (\sigma_1 - \sigma_3)^2 + (\sigma_2 - \sigma_3)^2\}^{1/2} = \frac{\sqrt{2}}{3}\sigma_d$,

P_a is atmospheric pressure

k_1, k_2, k_3 are the regression constants.

The model parameters or regression coefficients (i.e., k_1, k_2, and k_3) are obtained through statistical analysis after resilient modulus test is carried out in the laboratory.

2.11 Resilient Modulus Model Parameters

Apart from the above-discussed efforts, several studies were carried out to determine typical values for resilient modulus model parameters such as k_1, k_2, and k_3 values needed for the MEPDG model. Not only MEPDG model, other models were also evaluated, based on the choice of the tensing agency. Each transportation agency tests their materials and determine the model parameters. Once these model parameters are determined, the values can be used in AASHTOWare Pavement ME to design pavements without requiring additional laboratory testing (Ceylan and Kim, 2009).

2.11.1 Maryland Department of Transportation

Wambura (2003), at University of Maryland, tested the resilient modulus and permanent deformation behavior for four coarse-grained, and four fine-grained soils for Maryland Department of Transportation. The testing protocol of NCHRP 1-28A was followed in this study. Upon the completion of the required laboratory testing, Wambura

(2003) determined the regression coefficients/model parameters (k_1, k_2, k_3) for the MEPDG model as explained in Section 2.10. The model parameters for the coarse-grained soils are presented in Table 2.2.

Table 2.2 Resilient modulus model parameters established for four coarse grained soils in Maryland (Wambura, 2003)

Base Aggregate	k_1	k_2	k_3	R^2
CRREL	803	0.931	-0.612	0.952
	537	1.10	-0.0561	0.997
	622	1.01	-0.585	0.954
GTX	685	1.124	-0.664	0.986
	866	1.034	-0.599	0.988
	672	1.128	-0.716	0.985
	741	1.091	-0.653	0.986
MSU-1	1043	0.813	-0.476	0.858
	871	1.008	-0.763	0.872
	957	0.906	-0.641	0.851
MSU-2	640	1.239	-0.651	0.976
	727	0.974	-0.481	0.933
	685	1.113	-0.581	0.971

2.11.2 Iowa Department of Transportation

Ceylan and Kim (2009) tested various unbound materials (soils and aggregates) used in pavement construction in Iowa. The resilient modulus testing was conducted in accordance with standard procedure of AASHTO T 307 (AASHTO, 1999) at 10% moisture content. The researchers used the results and determined the required parameters for two resilient modulus models; MEPDG Model and Uzan Model. Table 2.3 provides a summary of the model coefficients for the aggregate samples evaluated in this study.

Table 2.3 Resilient modulus model parameters for aggregate evaluated by Ceylan and Kim (2009)

Sample I.D.	MEPDG Model					Uzan Model				
	$M_R = k_1 p_a \left(\frac{\theta}{p_a}\right)^{k_2} \left(1+\frac{\tau_{oct}}{p_a}\right)^{k_3}$					$M_R = k_1 p_a \left(\frac{\theta}{p_a}\right)^{k_2} \left(\frac{\sigma_d}{p_a}\right)^{k_3}$				
	k_1	**k_2**	**k_3**	**R^2**	**SEE**	**k_1**	**k_2**	**k_3**	**R^2**	**SEE**
Aggregate/ MC=10%	1,080.55	0.585	-0.103	0.997	0.021	1,032.05	0.584	-0.028	0.997	0.01

2.11.3 Alabama Department of Transportation

Taylor and Timm (2009) characterized different unbound materials used in pavement construction at the National Center for Asphalt Technology (NCAT) test track. They followed the test procedure presented in NCHRP 1-28A (Harmonized Protocol) (Witczak, 2003). Parameters for four different models were determined in this study as summarized in Table 2.4.

Table 2.4 Resilient modulus model parameters determined by Taylor and Timm (2009)

Material Type	Bulk Stress-Sensitivity Model $M_R=k_1(\theta)^{k_2}$			Deviatoric Stress-Sensitivity Model $M_R=k_1 p_a \left(\frac{\sigma_d}{p_a}\right)^{k_2}$		
	k_1	k_2	R^2	k_1	k_2	R^2
Limerock Base	22966.7	0.4773	0.5618	39001.4	0.2174	0.2204
Granite Base	10862.1	0.6267	0.886	21350	0.3866	0.5765
Type 5 Base	14049.7	0.671	0.8721	29487.2	0.3876	0.5334
Track Soil	26833.28	0.0447	0.0179	28878.92	-0.0572	0.0478

Material Type	Universal Stress-Sensitivity Model $M_R = k_1 p_a \left(\frac{\theta}{p_a}\right)^{k_2} \left(\frac{\sigma_d}{p_a}\right)^{k_3}$				MEPDG Stress-Sensitivity Model $M_R=k_1 p_a \left(\frac{\theta}{p_a}\right)^{k_2} \left(1+\frac{\tau_{oct}}{p_a}\right)^{k_3}$			
	k_1	k_2	k_3	R^2	k_1	k_2	k_3	R^2
Limerock Base	717.04	1.2338	-0.5645	0.8562	1266.83	1.2081	-1.2332	0.9326
Granite Base	581.08	0.8529	-0.1870	0.9172	716.28	0.8468	-0.4632	0.9253
Type 5 Base	643.69	1.0318	-0.2833	0.9349	883.54	1.005	-0.6575	0.9478
Track Soil	1095.43	0.5930	-0.4727	0.6642	1878.97	0.4067	-0.7897	0.4202

2.11.4 Oklahoma Department of Transportation

Hossain et al. (2013) measured the resilient modulus (M_R) and other properties (i.e., gradation, Los Angeles abrasion loss, standard Proctor, and unconfined compressive strength) for commonly used limestone and sandstone aggregates in Oklahoma. A total of 105 samples were tested, and the regression constants for four different stress-based resilient modulus models were determined. They found that Uzan's model to outperform the other three models (i.e., K-θ, UT-Austin and MEPDG) in terms of "goodness of fit". Accordingly,

the following three equations were recommended to predict the k_1, k_2, and k_3 values for Uzan model.

$$k_1 = 259.44 \text{ x } P_{200} - 1.951\text{x UCS}; \qquad R^2 = 0.38 \qquad (2.19)$$

$$k_2 = 0.530 - 0.902 \text{ x } k_3; \qquad R^2 = 0.78 \qquad (2.20)$$

$$k_3 = -0.044 \text{ x OMC} + 0.087 \text{ x PI}; \qquad R^2 = 0.42 \qquad (2.21)$$

where,

k_i = model parameter

P200 = percent passing through No. 200 sieve

UCS = unconfined compressive strength

OMC = optimum moisture content

CHAPTER 3 MATERIALS AND METHODOLOGY

3.1 Overview

Chapter 3 provides a description of the test materials used in this study, in addition to the laboratory testing program. The researcher conducted several laboratory tests including resilient modulus, California bearing ratio (CBR), light weight deflectometer (LWD), in addition to the preliminary material characterization e.g. particle-size distribution, Atterberg limits, soil classification and moisture density relationship.

3.2 Material Collection

In this study, the researcher tested granular unbound coarse aggregates used in road construction in the state of Idaho. All six districts of Idaho identified the most commonly used base/subbase materials in each district. A total of 18 different granular unbound coarse aggregates were selected and sampled by ITD engineers and shipped to the laboratory at the University of Idaho. Table 3.1 lists the materials received from various districts and sample identification as provided by ITD engineers while Figure 3.1 depicts the distribution of the sampling sources across the state of Idaho.

Table 3.1 Aggregates samples collected from various districts in Idaho

District 1	**Base**	**Sub-Base**	**District 4**	**Base**	**Sub-Base**
	KT - 215	-		CS - 184	CS 184
	BR - 2	-		LN - 80	-
	-	-		-	-
District 2	**Base**	**Sub-Base**	**District 5**	**Base**	**Sub-Base**
	NP-82	-		BK - 181	-
	WCW	-		PW - 84	-
	-	-		BK - 100	-
District 3	**Base**	**Sub-Base**	**District 6**	**Base**	**Sub-Base**
	EL - 132			LE -160	-
	VY - 63	CN - 148		A	-
	IMC - 140	PY - 720		B	-

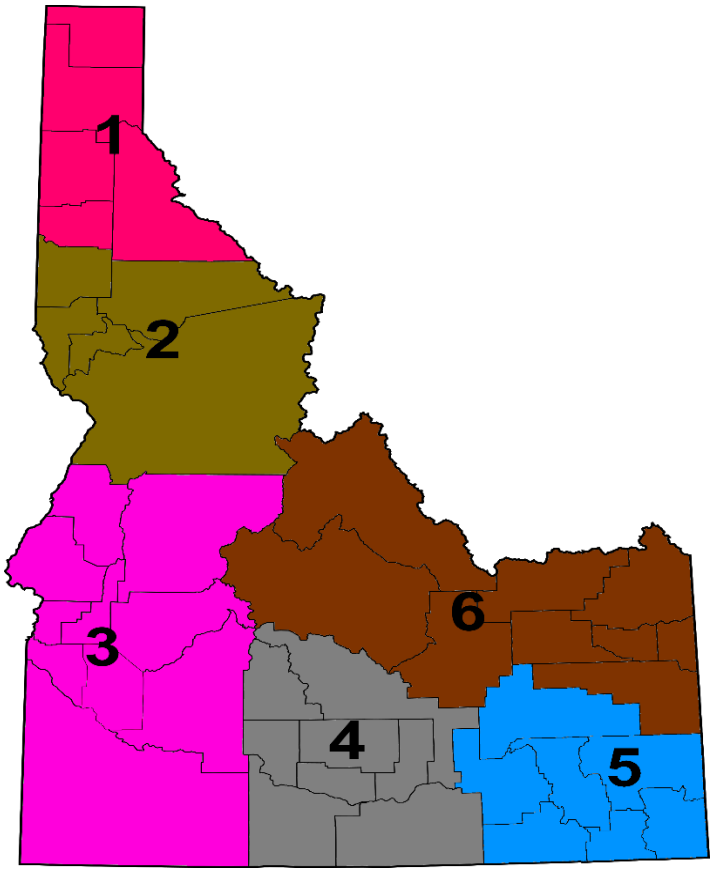

Figure 3.1 Materials collected from all six districts

3.3 Preliminary Characterization

The researcher performed preliminary characterization of the test materials that including particle-size distribution, consistency limits (i.e., Atterberg limits test), soil classification and the moisture-density relationship. This preliminary characterization is needed for classification of the materials and used for resilient modulus prediction.

3.3.1 Particle Size Distribution

The particle size distribution of test aggregates was carried out in accordance with AASHTO T 27 (AASHTO, 2011). A representative amount of each test material was obtained using a material splitter in accordance with AASHTO T 27. Two replicates (at least 5 kg [11 lb] each) were tested for sieve analysis. The test samples were dried in an oven at 110°C (230°F) for at least 24 hours. The main objective of the drying process is to get rid of any moisture in the materials before sieving. After drying the materials, they were kept to cooldown at the room temperature before sieving. A set of sieves was used to separate the

materials into different sizes. The sieve sizes include 25 mm, 19 mm, 12.5 mm, 9.5 mm, 4.75 mm, 2.36 mm, 1.18 mm, 0.6 mm, 0.3 mm, 0.15 mm, and 0.075 mm (1 in, 3/4 in, 1/2 in, 3/8 in, No.4, No.8, No.16, No. 30, No. 50, No. 100, and No. 200). Figure 3.2 shows the steps taken for sieve analysis. The weight of materials retained on each sieve after sieving was carefully measured using a scale. The percent aggregate passing (cumulative) on each sieve size was calculated. The percent material passing versus sieve size (or particle size) were plotted on semi-log graph to determine aggregate gradation parameters such as coefficient of uniformity, coefficient of curvature, etc.

3.3.2 Atterberg Limits Test

The Atterberg limits test (known also as the consistency limits test) was carried out in accordance with AASHTO T 89 (AASHTO, 2010a) and AASHTO T 90 (AASHTO, 2000). The results of this test are used to determine the liquid limit, plastic limit, and plasticity index of the test materials. Fine portion of aggregate gradation passing 0.425 mm (No. 40) sieve are used in this test. The amount of materials required is about 200 gm (0.44 lb.) and should be obtained from a thoroughly mixed and oven-dried aggregate sample. The test materials were dried in an oven at 60°C (140°F) for 24 hours.

The liquid limit test was conducted in accordance with AASHTO standard (AASHTO, 2010a) and main steps are summarized as follows:

- An amount of 60 gm (0.13 lb.) of the test material was mixed with sufficient amount of water to make a flowable paste.
- The paste was placed in a standard cup (Figure 3.3). Then a cut was made in the middle of the paste's surface using a standard grooving tool.
- The device was operated manually by turning the crank at a rate of two revolutions per second until the two sides of the groove come in contact at the bottom of the groove along a distance of 13 mm (1/2 in).
- The number of drops or blows were recorded to close the grooves at this distance at various water contents.

(a) (b)

(c) (d)

Figure 3.2 Grain size distribution of the aggregates. (a) splitting the materials, (b) drying materials in the oven, (c) using the large sieve shaker, and (d) using the small sieve shaker

- An amount of the moist test sample from the cup was taken to measure the moisture content in accordance with AASHTO T 265 (AASHTO, 2012).
- The moisture content versus number blows was plotted on a semi-log graph. The moisture content at 25 blows was designated as the liquid limit of the material as shown in Figure 3.4.

Figure 3.3 Required tools and device for Atterberg limit tests

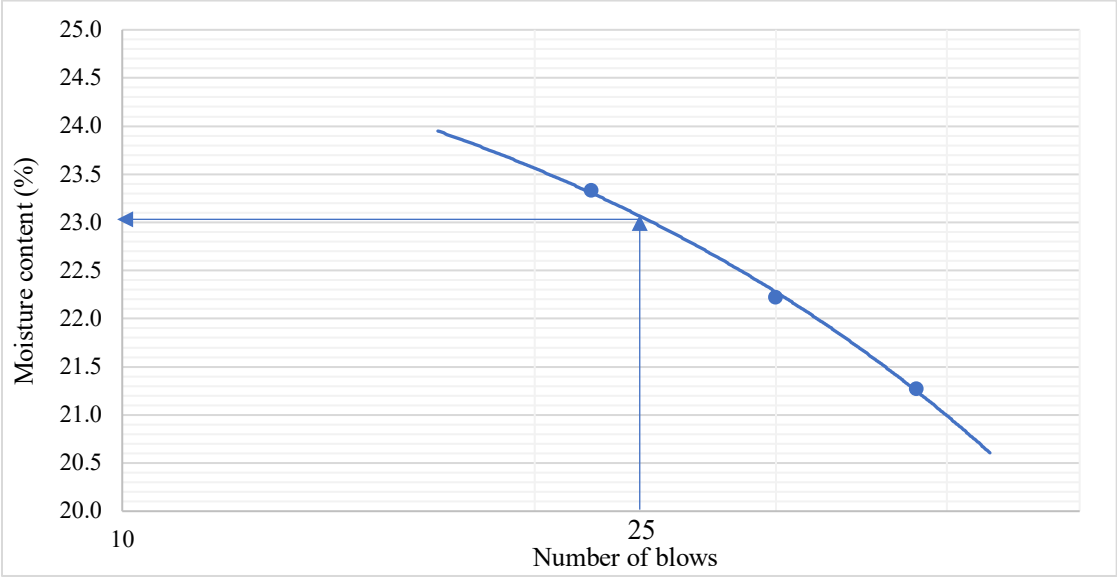

Figure 3.4 Liquid limit determination

The plastic limit test was conducted in accordance with AASHTO T 90 (AASHTO, 2000) and main steps are summarized as follows:

- An amount of 5 gm (0.011 lb.) of representative sample was taken from the sample taken for the liquid limit test and mixed with small amount of water to make a shape of a ball. The sample was squeezed and rolled to make a thread of 3.2 mm (1/8 in) in diameter.

- The kneading or rolling was repeated until the thread started to crumble. According to AASHTO T 90 (AASHTO, 2000), the minimum moisture content where the 3.2 mm (1/8 in) thread of the test material begins to break a part or crumble is defined as the plastic limit of the test material.
- The threads were placed in a container to measure the moisture content in accordance with AASHTO T 265 (AASHTO, 2012)

The plasticity index is the difference of between the liquid limit and plastic limit (Equation 3.1).

$$\text{Plasticity Index (PI)} = \text{Liquid Limit (LL)} - \text{Plastic Limit (PL)} \quad (3.1)$$

3.3.3 Soil Classification

In this study, the soil classification was carried out in accordance with AASHTO M 145 (AASHTO, 1991). The outcome of the particle size distribution and the Atterberg limits test were used as the input for the soil classification. Percent passing of the 0.075 mm (No. 200) sieve and the plasticity index of the aggregates are the most significant input for the ASSHTO soil classification. Figure 3.5 shows the soil classification system according to standard documented in AASHTO (1991).

GENERAL CLASSIFICATION	GRANULAR MATERIALS (35% OR LESS PASSING 0.075 mm SIEVE)							SILT-CLAY MATERIALS (MORE THAN 35% PASSING 0.075 mm SIEVE			
GROUP CLASSIFICATION	A - 1		A - 3	A - 2				A - 4	A - 5	A - 6	A - 7 - 5 A - 7 - 6
	A-1-a	A-1-b		A - 2 - 4	A - 2 - 5	A - 2 - 6	A - 2 - 7				
SIEVE ANALYSIS, PERCENT PASSING:											
2.00 mm (No.10)	≤ 50	-	-	-	-	-	-	-	-	-	-
0.425 mm (No. 40)	≤ 30	≤ 50	≥ 51	-	-	-	-	-	-	-	-
0.075 mm (No. 200)	≤ 15	≤ 25	≤ 10	≤ 35	≤ 35	≤ 35	≤ 35	≥ 36	≥ 36	≥ 36	≥ 36
CHARACTERSTICS OF FRACTION PASSING 0.425 SIEVE (No. 40):											
LIQUID LIMIT	-		-	≤ 40	≥ 41	≤ 40	≥ 41	≤ 40	≥ 41	≤ 40	≥ 41
PLASTICITY INDEX*	6 MAX		NP	≤ 10	≤ 10	≥ 11	≥ 11	≤ 10	≤ 10	≥ 11	≥ 11
USUAL TYPES OF CONSTITUENT MATERIALS	STONE FRAGMENTS, GRAVEL, SAND		FINE SAND	SILTY OR CLAYEY GRAVEL AND SAND				SILTY SOILS		CLAYEY SOILS	
GENERAL RATING AS SUBGRADE	EXCELLENT TO GOOD							FAIR TO POOR			

Figure 3.5 Soil classification according to AASHTO M 145 (AASHTO, 1991)

3.3.4 Moisture-Density Relationship

The Maximum dry density of granular unbound materials is typically achieved at optimum moisture content. For the same material type, maximum dry density and optimum moisture content change with the particle size distribution or gradation. The moisture-density relationship is established in accordance with AASHTO T 180 (Method D) (AASHTO, 2010c). The AASHTO T 180 is known as "Modified Compaction Method". The difference between the modified versus the standard compaction procedure is that the weight and drop height of the compaction hammer. AASHTO T 180 methods (i.e., A, B, C, and D) define the size of compaction mold and respective maximum size of materials. The moisture-density relationship was established as follows:

- A representative sample of the test material was oven-dried at 60°C (140°F) for at least 24 hours to get rid of any existing moisture. Then, the sample was cooled to the room temperature.
- The dried sample was conditioned (i.e., mixed with water) at various moisture contents ranging from 2.0% to 9.0% by the weight of dry sample on a mixing tray.
- The materials were divided into approximately five equal portions to compact in five lifts. The tray was covered with rubber cloth to prevent evaporation or moisture loss, until the last lift was compacted.
- The sample was compacted in approximately equal lifts. Each layer was compacted with 56 blows of a compaction hammer of 4.54 kg (10 lb.).
- The collar of the mold was removed after compaction and the top surface of the sample was trimmed and flattened (Figure 3.6)
- The weight of the compacted sample was measured and the bulk density was calculated since the volume of the mold is known.
- The compacted sample was extruded out of the mold and dismantled.

Figure 3.6 Compacted specimen for moisture-density relationship test

- According to AASHTO T 265 (AASHTO, 2012) required amount of material was collected from the dismantled specimen and moisture content was calculated using Equation 3.2.

$$\text{Moisture Content (\%)} = 100 \times (W_W - W_D) / W_D \quad (3.2)$$

where,

W_W = weight of wet sample (gm)
W_D = weight of dry sample (gm)

- The dry density was calculated for the test specimen according to Equation 3.3.

$$\text{Dry Density (kg/m}^3\text{)} = \gamma_{bulk} / \{1 + MC / 100\} \quad (3.3)$$

where,

γ_{bulk} = bulk density (kg/m^3)
MC = moisture content (%)

- The moisture content versus the dry density plot was used to determine the maximum dry density (MDD) and corresponding optimum moisture content (OMC) as shown in Figure 3.7. At least two replicates were tested from each aggregate source.

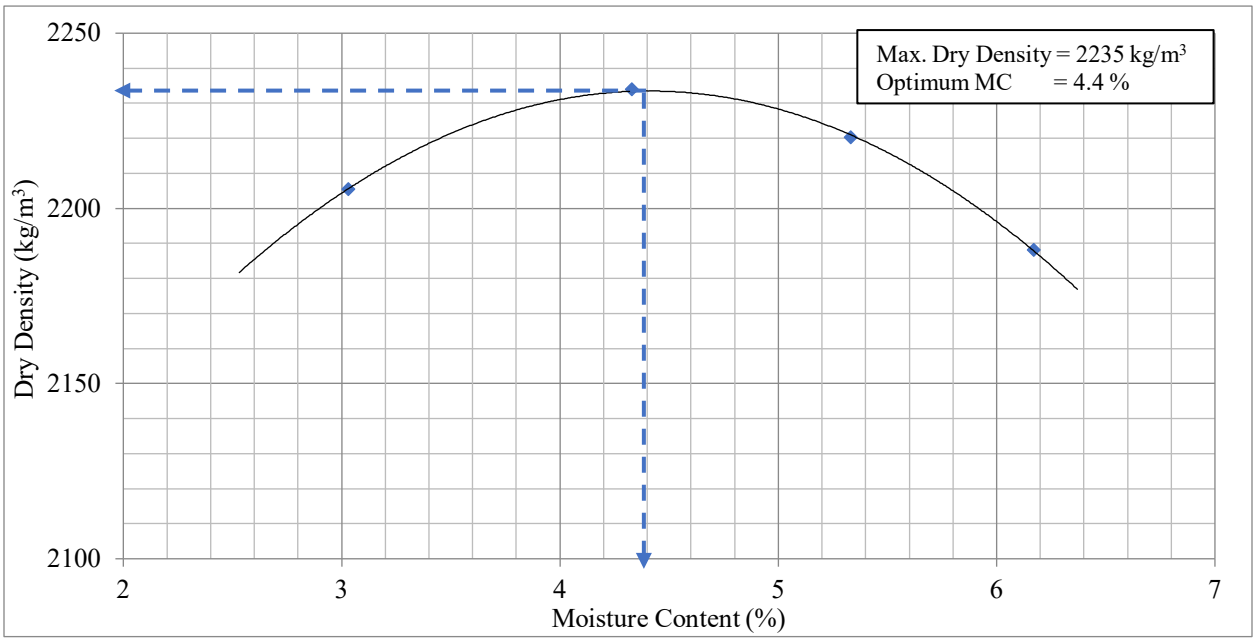

Figure 3.7 Typical graphical representation of moisture-density relationship

3.4 Resilient Modulus Test

Repeated load triaxial (RLT) testing was conducted in accordance with AASHTO T 307 (AASHTO, 1999) to determine the resilient modulus of the tested materials at different stress states. The test samples were also prepared and compacted following the procedure described in AASHTO T 307. This section discusses the triaxial test setup, sample preparation, and deformation measurements for resilient modulus test.

3.4.1 Resilient Modulus Test Setup

The repeated load triaxial test was conducted using Material Testing System (MTS) loading frame. The MTS at the University of Idaho is a closed-loop servo-hydraulic dynamic testing system. The system has a Controller (MTS Flex Test SE) with 10 channels and data acquisition to apply different loading sequences and collect the data (e.g., force, displacement, time etc.). The capacity of load frame is up to 890 kN (200 kips). Figure 3.8 shows the dynamic material testing system used in this study, while Figure 3.9 shows the

controller and data acquisition system used with the MTS system. Air was used to apply the required confining pressure. This triaxial cell can accommodate 152.4 mm by 304.8 mm (6 in by 12 in) test specimen and can withstand air pressure up to 400 kPa (58 psi). The triaxial cell is equipped with external LVDT and internal LVDTs as discussed in Section 3.4.3.

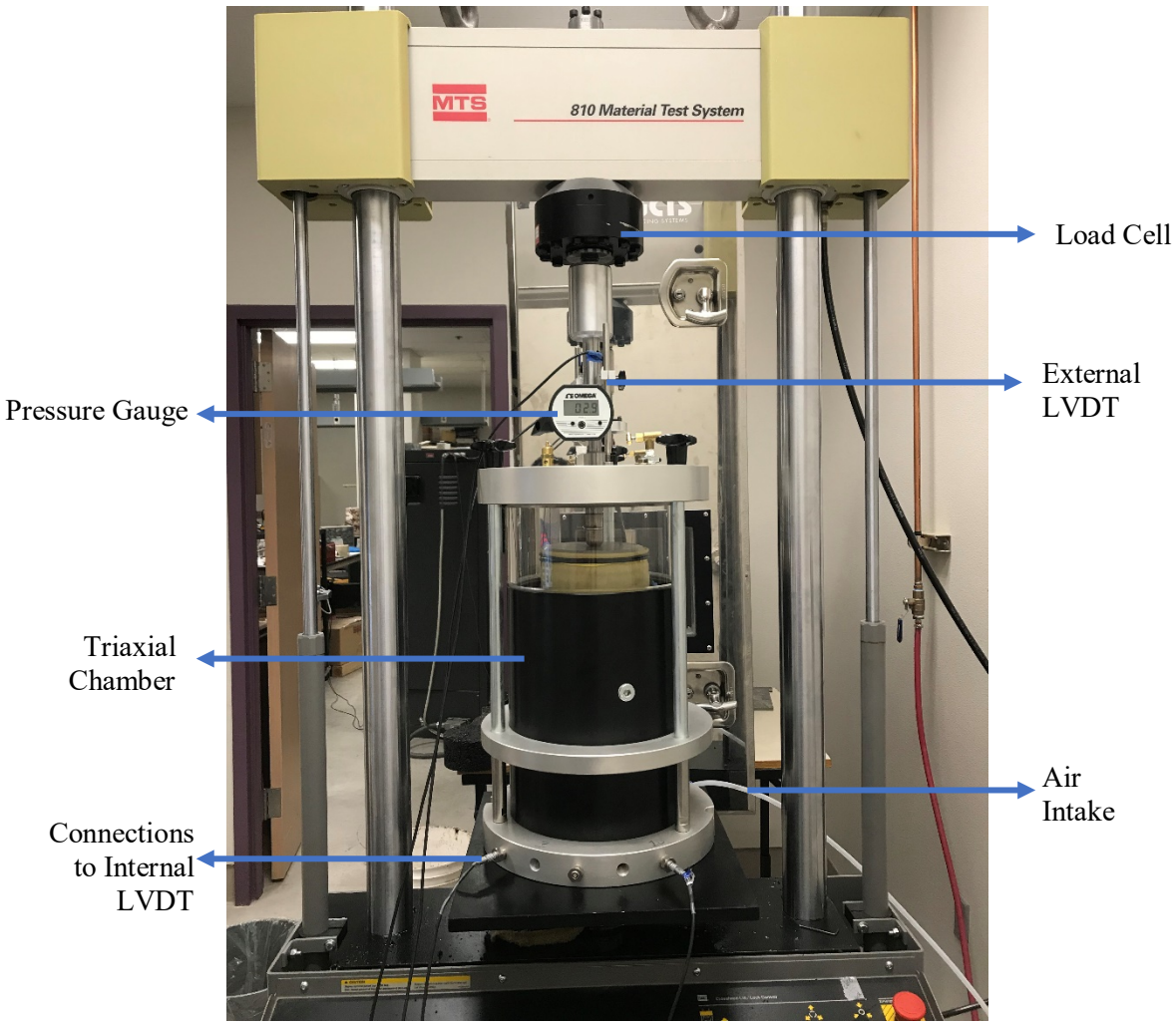

Figure 3.8 The Material Testing System at the University of Idaho

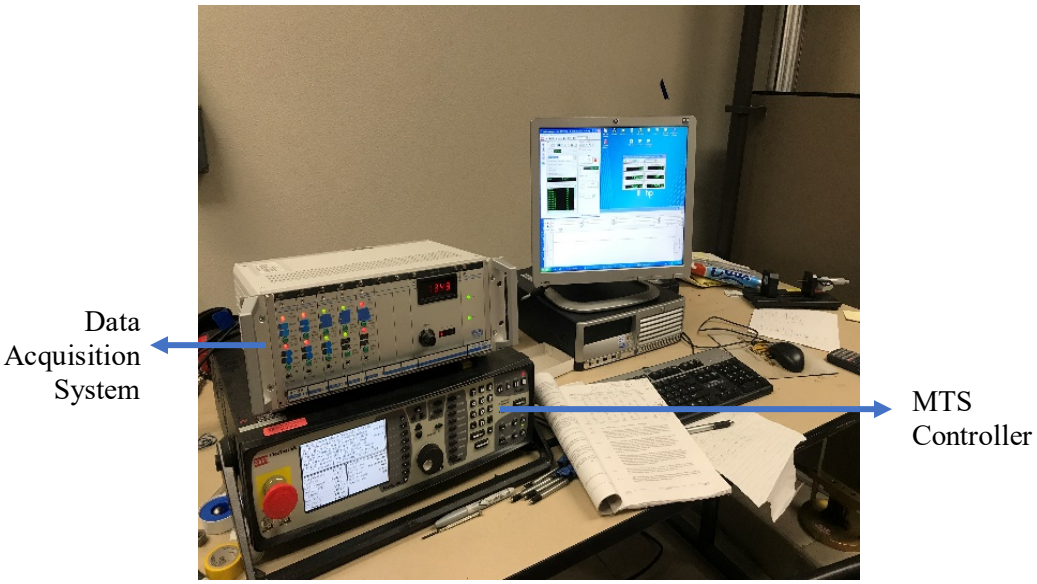

Figure 3.9 Computer operated controller and data acquisition system

Fifteen distinct haversine loading sequences in addition to a preconditioning sequence were applied to the test samples (Table 3.2) in accordance with AASHTO T 307. Each sequence except preconditioning (Sequence No. 0) consists of 100 loading cycles and each loading cycle consists of 0.1 second of loading and 0.9 second of rest period. The specimen is preconditioned with 750 cycles. The confining pressure was checked at the start of each sequence and maintained constant over the entire sequence. The applied load and the corresponding deformations were recorded with the help of the computer.

Table 3.2 Testing sequences for base/subbase materials in accordance to AASHTO T 307 (AASHTO, 1999)

Sequence No.	Confining Pressure, σ_3		Maximum Axial Stress, σ_d		Cyclic Stress σ_{cyclic}		Constant Stress, $0.1\sigma_d$		No. of Load Applications
	kPa	psi	kPa	psi	kPa	psi	kPa	psi	
0	103.4	15	103.4	15	93.1	13.5	10.3	1.5	500-1000
1	20.7	3	20.7	3	18.6	2.7	2.1	0.3	100
2	20.7	3	41.4	6	37.3	5.4	4.1	0.6	100
3	20.7	3	62.1	9	55.9	8.1	6.2	0.9	100
4	34.5	5	34.5	5	93.1	13.5	3.5	0.5	100
5	34.5	5	68.9	10	62.0	9	6.9	1	100
6	34.5	5	103.4	15	93.1	13.5	10.3	1.5	100
7	68.9	10	68.9	10	62.0	9	6.9	1	100
8	68.9	10	137.9	20	93.1	13.5	13.8	2	100
9	68.9	10	206.8	30	186.1	27	20.7	3	100
10	103.4	15	68.9	10	62.0	9	6.9	1	100
11	103.4	15	103.4	15	93.1	13.5	10.3	1.5	100
12	103.4	15	206.8	30	93.1	13.5	20.7	3	100
13	137.9	20	103.4	15	93.1	13.5	10.3	1.5	100
14	137.9	20	137.9	20	124.1	18	13.8	2	100
15	137.9	20	275.8	40	248.2	36	27.6	4	100

3.4.2 Specimen Preparation

The aggregates were oven dried at 60°C (140°F) for at least 24 hours. After drying, the aggregates were placed at the room temperature to cool down then were conditioned at optimum moisture content. The test samples were compacted in approximately six equal lifts or layers. Each layer was compacted with 60 blows of a compaction hammer of 4.54 kg (10 lb.). The number of blows were selected to produce a density of 95% of the maximum dry density at optimum moisture content. The compaction method provided uniformly compacted lifts while using the same weight of aggregate for each lift. The samples were compacted outside the triaxial chamber (Figure 3.10).

Figure 3.10 Compaction of specimen for resilient modulus

A split mold was used with membrane stretcher to facilitate specimen preparation procedure. Figure 3.11 shows the split mold, membrane stretcher, unmolded specimen after compaction, and test specimen with the membrane. During the placing of the rubber membrane on the test sample with the help of membrane stretcher, vacuum was applied. A metal base plate with a porous stone on top was placed on the pedestal of the triaxial chamber. Then the test specimen was placed on the metallic plate and porous stone assembly. A porous stone and metal plate were also placed on the top of the test sample. The specimen's top and bottom were properly sealed with O-rings. Before starting the test, vacuum was applied once again thorough the vacuum inlet to make sure the full contact between the membrane and the aggregate. It is also check for leakage in the membrane.

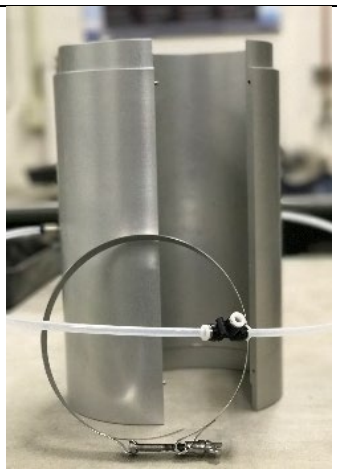

(a)

(b)

(c)

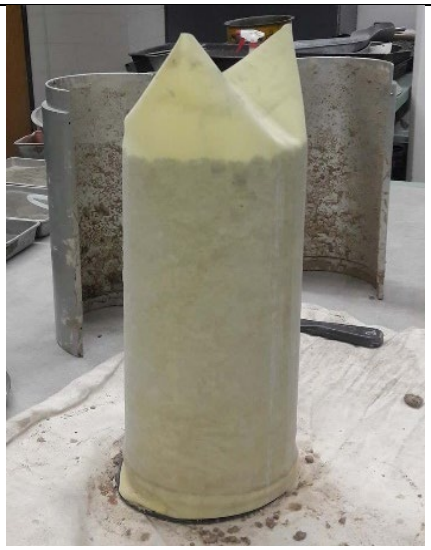

(d)

Figure 3.11 Preparation of specimen for resilient modulus test (a) split mold, (b) membrane stretcher, (c) unmolded specimen after compaction, (d) specimen with rubber membrane

3.4.3 Deformation Measurements and Testing of Specimen

Resilient modulus is a stress-controlled test. Both stress and resilient/recoverable strain are used to calculate the resilient modulus value. Thus, accurate measurements of load and deformations are needed to calculate resilient modulus. The influence of load cells and the deformation measurement techniques were discussed in previous studies (Camargo et al., 2012; Ping and Ge, 1996; Ping et al., 2003 and Kancherla, 2004). According to AASHTO T 307 (AASHTO, 1999), the load cell is placed outside the triaxial cell. For deformation

measurements, The AASHTO T 307 utilizes external measurements in the calculations of resilient modulus. However, the NCHRP 1-28A research project recommended the use of internal measurements. In this study, both external and internal deformation measurements were considered and the difference in resilient modulus values was studied. For the internal deformation measurement, the clamps with the internal LVDTs were placed at quarter points of the specimen to measure the deformations over the middle half of the length of the specimen, whereas external LVDTs were placed on top of the chamber to measure deformations of entire specimen length (Figure 3.12). The external LVDTs were fixed with fixtures outside the triaxial chamber where a circular disc was used as datum for them. Figure 3.13 depicts the triaxial chamber setup with a prepared specimen within the chamber.

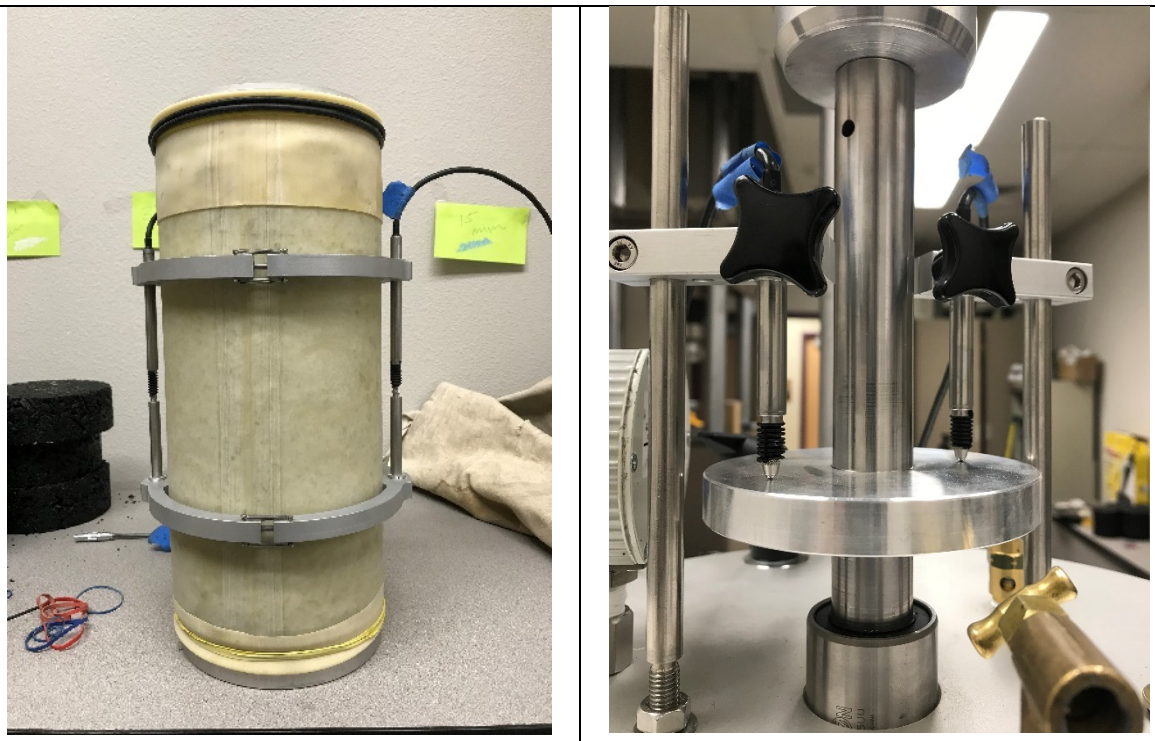

(a) (b)

Figure 3.12 Deformation measurements (a) internal LVDT (b) external LVDT

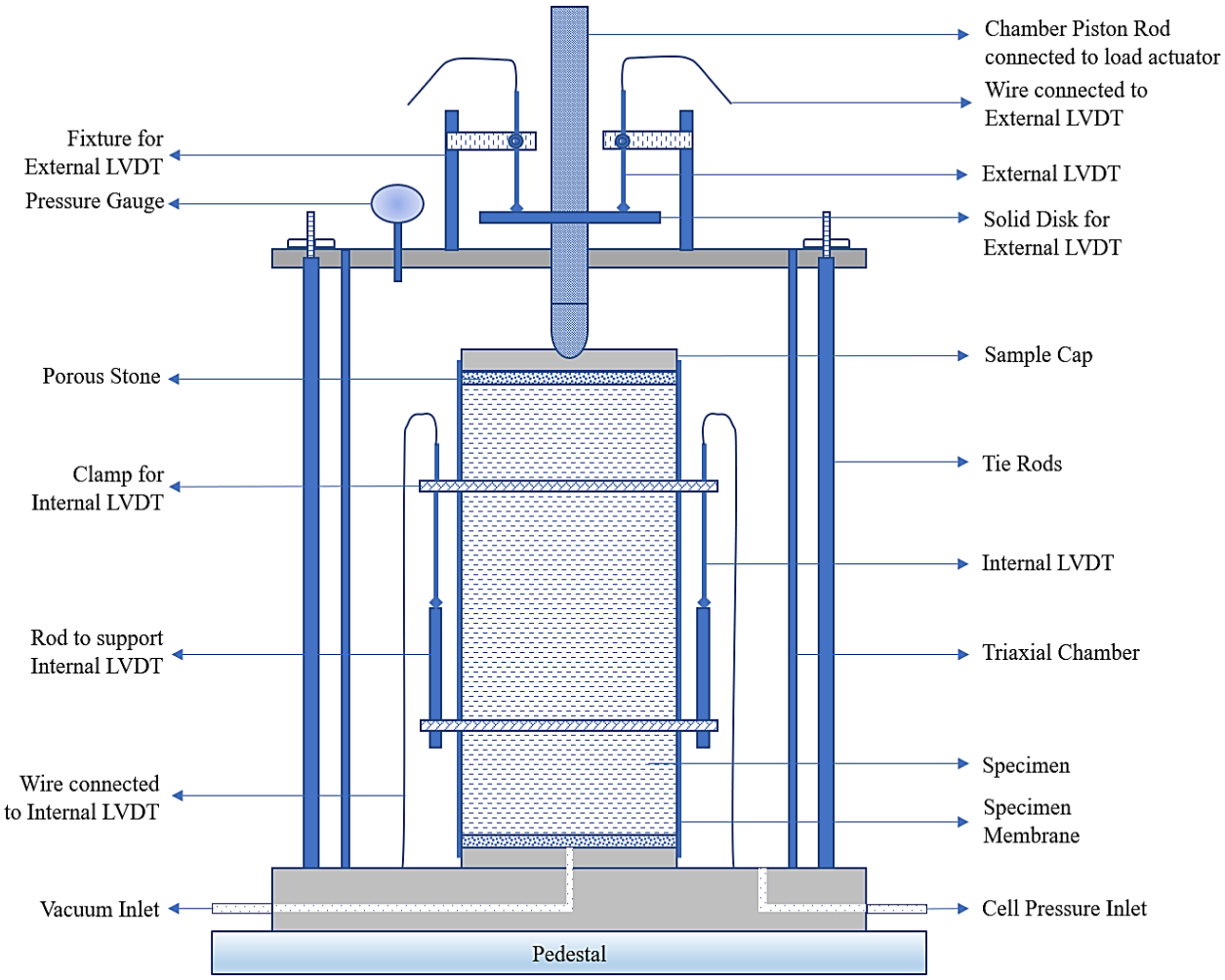

Figure 3.13 Schematic diagram of the triaxial chamber with prepared specimen for repeated load triaxial testing

3.5 Alternative Stiffness Tests for Granular Unbound Materials

The main objectives of this study were to populate a database of the resilient modulus values for commonly used base/subbase materials in Idaho and develop prediction models for the resilient modulus as function of material properties and gradation. These information assists Idaho Transportation Department (ITD) to implement MEPDG in pavement design as discussed in Chapter 1. Additionally, the researcher explored other alternative simpler tests for assessing the stiffness of granular unbound materials including California Bearing Ratio and Light Weight Deflectometer (LWD). This section provides a discussion of these two alternative tests.

3.5.1 California Bearing Ratio

The California Bearing Ratio test is conducted in accordance with AASHTO T 193 (AASHTO, 2010d). This test is a monotonic, strain-controlled test. Thus, it is considered much simpler; however, unlike the resilient modulus test, it doesn't characterize the materials at different stress states. In this test, the materials are placed and compacted in a metal mold in approximately five equal lifts. The metal mold is 152.4 mm (6 in) in diameter and 177.8 mm (7 in) in height with a spacer disk of 61.4 mm (2.42 in) high inside the mold. Thus, the mold allows the compaction of test samples that are 152.4 mm (6 in) in diameter and 116.3 mm (4.58 in) in height. In this study, two replicates were prepared and tested in unsoaked conditions at the maximum dry density and optimum moisture content. The maximum dry density and optimum moisture content were determined from the density-moisture relationship discussed in Section 3.3.4. The main steps followed in this study for preparing the CBR test specimens and conducting the test are summarized as follows:

- The test materials were dried in an oven at 60°C (140°F) for at least 24 hours. The materials were conditioned at the optimum moisture content after they cooled down at the room temperature.
- The test specimens were compacted in approximately five equal layers. Each layer was compacted with 56 blows of a modified proctor hammer of 4.54 kg (10 lb.).
- The collar of the mold was removed after compaction and the top surface of the test specimen was leveled using a straightedge.
- The compacted specimen was flipped upside down and the spacer disk was removed from the mold.
- For the unsoaked CBR test, a surcharge load of 2.27 kg (5 lb.) was placed on top of the compacted specimen.
- The compression machine was used to apply a constant penetration rate of 1.3 mm/min (0.05 in/min) that pushed the loading piston into the top surface of the test specimen (Figure 3.14). The CBR compression machine at the University of Idaho has a loading cell of 50 kN (10,000 lbf).

- The penetration of the loading piston into the test specimen was measured using an external linear variable differential transducer (LVDT) with a range of 25.4 mm (1 in). Figure 3.14 shows the compression machine setup, load cell, loading piston, clamped LVDT, and test specimen during loading.

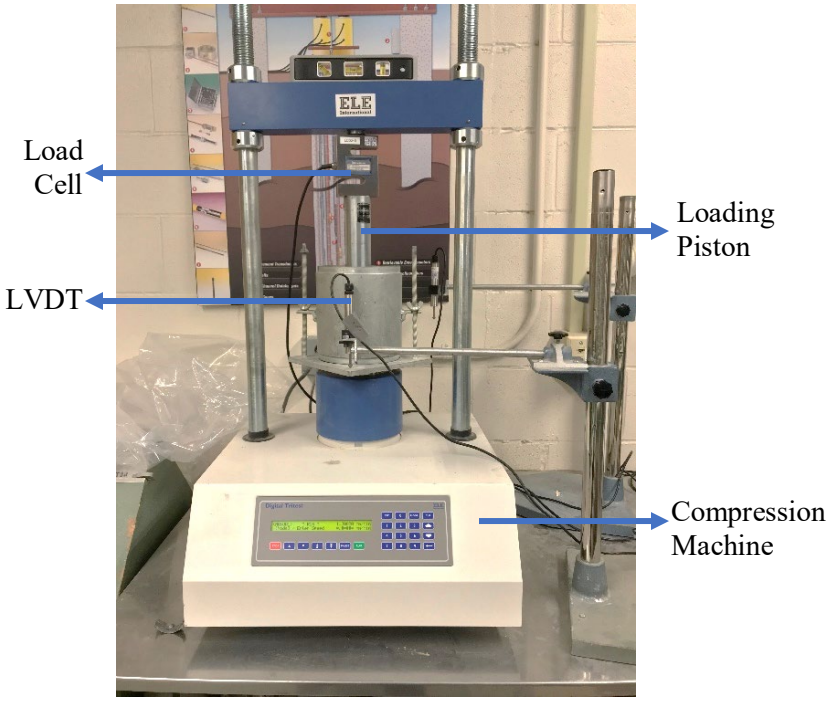

Figure 3.14 Machine set up for CBR test with mounted specimen

A data acquisition system that consists of a mini data logger and a laptop was used to record the penetration and applied load during the test (Figure 3.15). AASHTO T 193 requires penetration and corresponding loads at 0.64 mm, 1.27 mm, 1.91 mm, 2.54 mm, 3.81 mm, 5.08 mm and 7.62 mm (0.025 in, 0.050 in, 0.075 in, 0. 100 in, 0.150 in, 0.200 in, and 0.300 in). The stress versus penetration was plotted and the CBR was calculated at 2.54 mm (0.1 in) and 5.08 mm (0.2 in) according to Equations 3.4 and 3.5 respectively. The corrected load was calculated for 2.54 mm (0.1 in) and 5.08 mm (0.2 in) penetration according to AASHTO T 193 (AASHTO, 2010d) (Equations 3.4 and 3.5).

$$\text{CBR (\%)} = 100 \times \text{Corrected load for 2.54 mm penetration (MPa)} / \text{Standard load (6.9 MPa)} \quad (3.4)$$

CBR (%) = 100 x Corrected load for 5.08 mm penetration (MPa) / Standard load (10.3 MPa) (3.5)

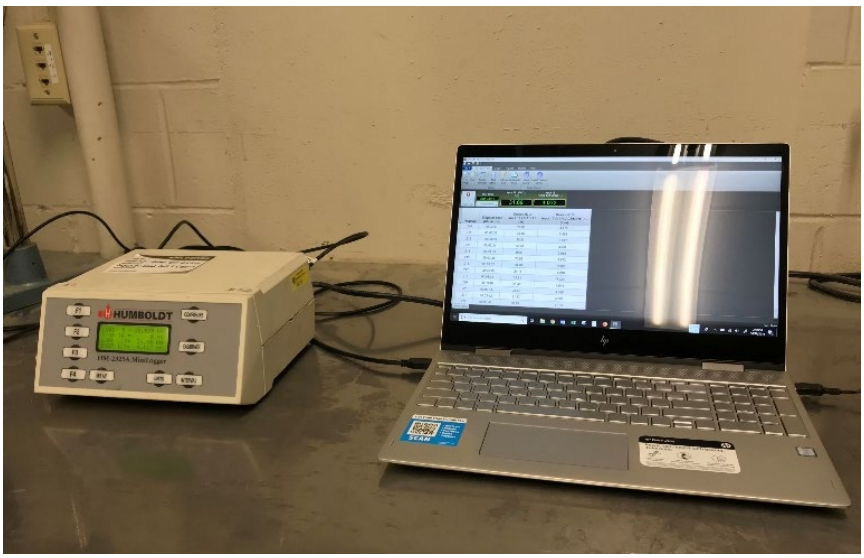

Figure 3.15 Data acquisition system for the CBR testing

Figure 3.16 shows an example of the stress versus penetration and CBR at 2.54 mm (0.1 in) and 5.08 mm (0.2 in) with recommended correction.

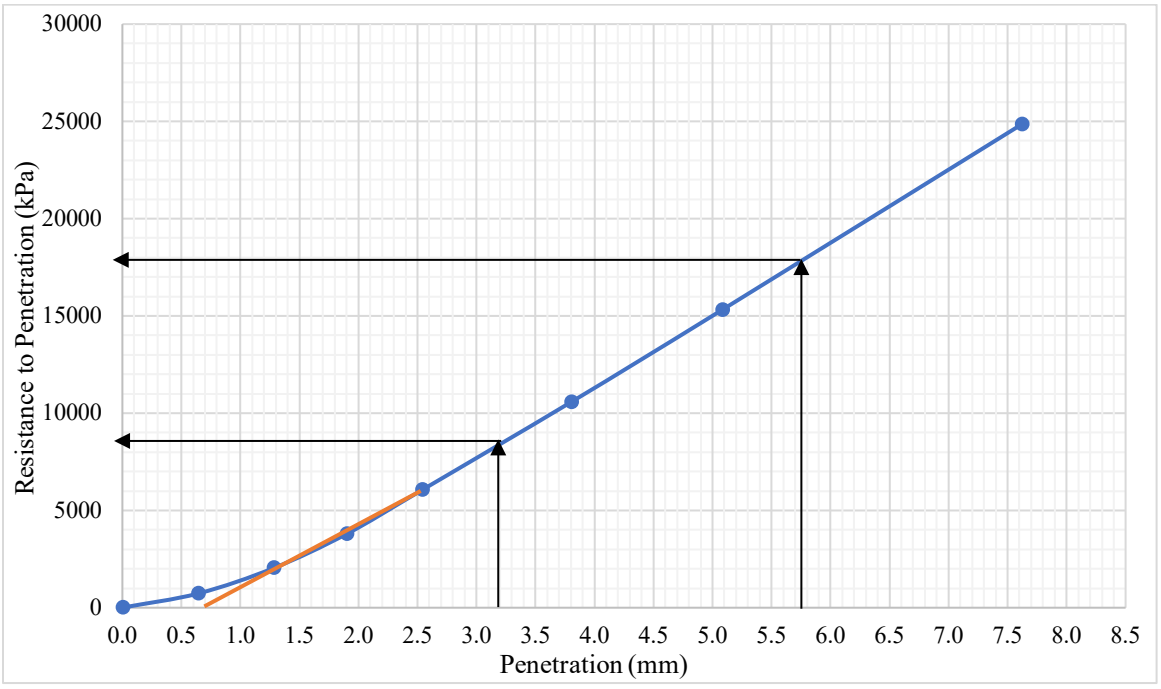

Figure 3.16 Typical load penetration plot for CBR test with correction

3.5.2 Light Weight Deflectometer (LWD)

Light Weight Deflectometer (LWD) is recently used by several researchers (Schwartz et al., 2017; Mohammad et al. 2008 and Mousavi et al. 2017) to assess the stiffness of the subgrade and base/subbase layers. It is a relatively new test. The guidelines for LWD test was proposed as an ASTM standard E 2583 (ASTM, 2007). In this study, the LWD manufactured by Olson was used and guidelines documented by Schwartz et al. (2017) was followed to conduct the test on a mold. The LWD has a loading cell of 10 kg (22.05 lb.) and a base plate of 152.4 mm (6 in) was mounted on the device. This equipment setup is for base and subbase material with mold for modified compaction. The deformation is measured using geophones or velocity transducers. The following steps summarize the LWD testing:

- Similar to the CBR test specimens, the test materials were dried in an oven at 60°C (140°F) for at least 24 hours and then conditioned at the optimum moisture content after they cooled down at the room temperature.
- The test specimen was prepared and compacted at the maximum dry density corresponding optimum moisture content.
- The test specimens were compacted in a mold (152.4mm by 116.4 mm [6 in by 4.58 in]) in approximately five equal lifts, which is used for modified compaction.
- All five layers were compacted with 56 blows per layer.
- The collar was removed, top surface was trimmed and straightened after finishing the compaction of all five layers.
- The LWD was placed on the top of the surface after attaching the collar back to the mold (Figure 3.17). Care was taken to make sure the base plate was placed properly on top of the aggregate surface.
- A few numbers of seating drops and testing drops were performed on each specimen and corresponding deflections were recorded. Schwartz et al. (2017) proposed three seating followed by three test drops to conduct the test. But the author made a modification to the drop combinations to explore the effect of drops on the $E_{LWD.}$
- A data cable was connected to the laptop computer from the LWD by which the load deflection data was collected.

- The computer was equipped with the required software to produce the modulus value of the material automatically. The modulus value was obtained instantly.

Figure 3.17 LWD testing conducted at Boise State University

- The E_{LWD} is calculated using Equation 3.6

$$E_{LWD} = \{1 - 2\upsilon^2 / (1 - \upsilon)\} \times 4 H k / \pi D^2 \quad (3.6)$$

$$k = | F_{peak} | / | w_{peak} | \quad (3.7)$$

where,

k = stiffness

υ = Poisson's ratio

H = mold height

F_{peak} = average maximum applied load

w_{peak} = average maximum deflection

D = plate diameter

Figure 3.18 shows the typical interface of the software for the LWD (manufactured by OLSON) used in this study to measure the E_{LWD}.

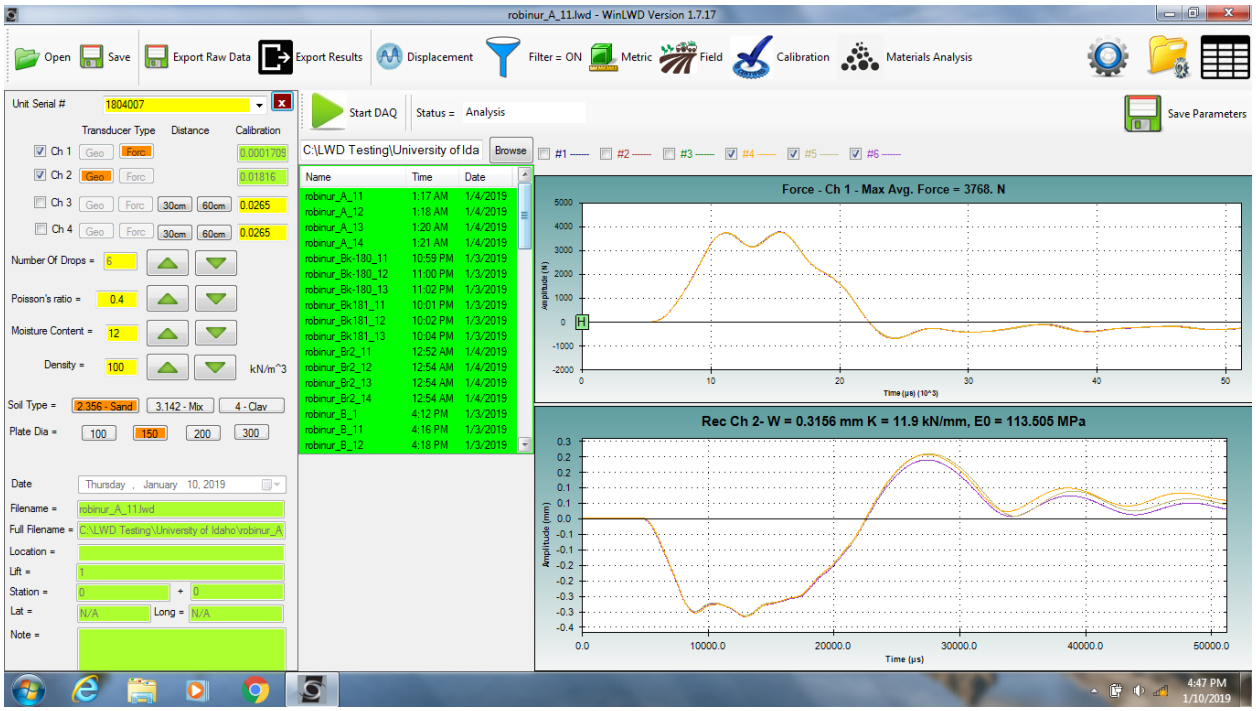

Figure 3.18 Typical interface of the LWD software (manufactured by OLSON)

CHAPTER 4 RESULTS AND ANALYSIS

4.1 Overview

This chapter discusses the results and analysis of various tests conducted in this study. The laboratory tests include particle-size distribution, Atterberg limits, material classification, moisture-density relationship, resilient modulus, CBR, and LWD. In addition, the proposed models for resilient modulus and associated statistical analyses were also discussed in this chapter.

4.2 Particle Size Distribution

Table 4.1 and Figure 4.1 present and show the particle size distribution of the test materials. Several parameters can be determined from the gradation curve. These parameters include:

- **Maximum and Nominal Maximum Aggregate Size**
  The smallest sieve opening that passes 100% of aggregates is defined as the maximum aggregate size. One sieve size smaller than the maximum aggregate size is known as nominal maximum aggregate size.
- **Effective grain size (D_{10})**
  The diameter of the particle/grain corresponding to 10% finer is defined as the effective grain size (D_{10}).
- **D_{30} and D_{60}**
  The diameter of the particle/grain corresponding to 30% finer and 60% finer is defined as the D_{30} and D_{60}, respectively.
- **Coefficient of Uniformity (C_u)**
  The coefficient of uniformity is defined as the ratio of D_{60} to D_{10} (Equation 4.1)
- **Coefficient of Curvature (C_c)**
  Coefficient of curvature is also known as coefficient of gradation. The coefficient of curvature is calculated according to Equation 4.2

$$C_u = D_{60} / D_{10} \quad (4.1)$$

$$C_c = (D_{30})^2 / (D_{10} \times D_{60}) \quad (4.2)$$

Table 4.1 Particle size distribution of the test materials

Sieve Size (mm)	25	19	12.5	9.5	4.75	2.36	1.18	0.6	0.3	0.15	0.075
A	100	100	88	74	48	34	26	19	12	4	1.4
B	100	100	81	60	36	31	26	20	13	4	1.3
BK - 100	100	98	87	79	57	35	20	12	8	5	3.4
BK - 181	100	96	77	65	41	25	17	12	8	4	2.4
BR - 2	100	99	83	67	37	21	12	7	4	3	1.8
CS - 184	100	97	79	64	45	32	22	14	8	4	2.6
EL - 132	93	89	78	70	53	42	33	25	14	6	2.3
IMC - 140	100	97	76	65	51	43	35	19	8	4	1.7
KT - 215	100	97	87	78	54	32	21	14	9	6	3.4
LE - 160	100	96	76	62	41	29	22	16	7	3	2.0
LN - 80	100	98	87	77	53	38	29	19	8	3	1.2
NP - 82	100	100	95	82	51	29	18	13	9	6	4.2
PW - 84	100	97	87	81	65	48	32	19	11	6	4.3
VY - 63	100	96	63	45	24	12	6	3	2	2	1.2
WCW	100	100	93	81	57	36	23	16	12	9	4.6
CN - 148 SB	98	90	79	71	61	55	49	34	15	8	5.1
CS - 184 SB	100	93	86	78	58	42	31	21	12	6	2.1
PY - 720 SB	100	84	73	69	62	57	49	36	21	7	2.6

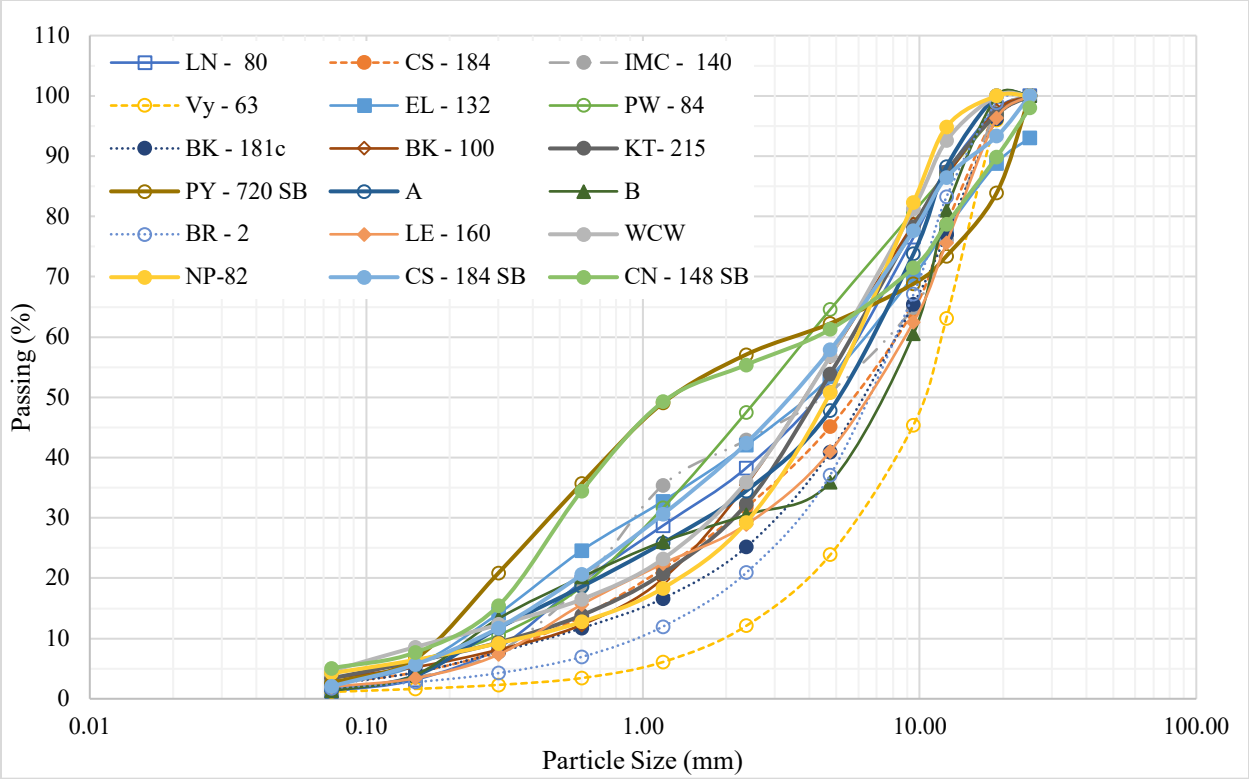

Figure 4.1 Sieve analysis of all the materials collected from all six districts

According to AASHTO T 307, the minimum diameter of the test specimen should be at least five times larger than the maximum aggregate size. The results in Table 4.1, shows that approximately all the materials have the maximum aggregate size of 25.4 mm (1.0 in). The basic difference between the base and subbase materials is the gradation. The subbase materials are much sandy, have less crushed aggregates and contain much finer particles compare to the base material. In general, the base materials are coarser compared to subbase materials as shown in Figure 4.1. Subbase materials (e.g., CN-148 SB, PY-720 SB, and CS–184 SB) have more fine particles compared to base materials (e.g., NP-82, WCW, LE-160 etc.) which are coarser in size. Among all base materials, "BR-2" and "VY-63" materials have relatively larger particles compare to other base materials. Table 4.2 summarizes various parameters calculated from the particle size analysis (e.g., D_{10}, D_{30}, D_{60}, C_c, C_u).

Table 4.2 Aggregate gradation parameter

Material ID	D_{10} (mm)	D_{30} (mm)	D_{60} (mm)	C_c	C_u
A	0.27	1.78	6.84	1.74	25.81
B	0.25	2.36	9.5	2.38	38.76
BK - 100	0.45	1.93	5.3	1.55	11.78
BK - 181	0.47	3.05	8.35	2.37	17.77
BR - 2	1.05	3.75	8.25	1.62	7.86
CS - 184	0.42	2.14	8.34	1.32	20.10
EL - 132	0.23	0.91	6.35	0.56	27.61
IMC - 140	0.36	0.94	7.65	0.32	21.25
KT - 215	0.32	2.20	5.75	2.63	17.97
LE - 160	0.40	2.48	8.8	1.77	22.28
LN - 80	0.35	1.23	6.04	0.72	17.26
NP - 82	0.39	2.43	5.93	2.58	15.39
PW - 84	0.29	1.13	3.85	1.15	13.51
VY - 63	1.95	6.05	12.35	1.52	6.35
WCW	0.20	1.80	5.10	3.18	25.5
CN - 148 SB	0.19	0.51	4.00	0.34	21.05
CS - 184 SB	0.13	1.20	5.19	2.14	39.88
PY - 720 SB	0.19	0.46	2.60	0.44	14.05

4.3 Material Properties and Classification

Table 4.3 summarizes the results of the material characterization tests conducted to evaluate the material properties. Several properties and parameters were measured including fines content (percentage passing of 0.075 mm Sieve or No. 200 sieve), consistency limits (liquid limit, plastic limit, and plasticity index) for the AASHTO soil classification. In this study, the evaluated base and subbase materials cover only the coarse-grained soils. For every test parameter, the reported value is the average of two replicates. Test material “VY-63” has the highest Liquid Limit (LL) of 23%, while, larger size materials (e.g., BR-2 and VY-63) had the highest Plasticity Index (PI) of 6%. Tet material “LE-160” has the highest plastic limit (PL) value of 19. All the test materials were classified as “A-1-a” according to ASSHTO classification (AASHTO, 1991).

Table 4.3 Properties of the tested materials

Material ID	Percent Passing #200 (%)	Liquid Limit (LL, %)	Plastic Limit (PL, %)	Plasticity Index (PI, %)	AASHTO Soil Classification
A	1.4	No Value	No Value	Non-Plastic	A-1-a
B	1.3	No Value	No Value	Non-Plastic	A-1-a
BK – 100	3.4	18	14	4	A-1-a
BK – 181	2.4	19	14	5	A-1-a
BR - 2	1.8	21	15	6	A-1-a
CS – 184	2.6	No Value	No Value	Non-Plastic	A-1-a
EL – 132	2.3	No Value	No Value	Non-Plastic	A-1-a
IMC – 140	1.7	No Value	No Value	Non-Plastic	A-1-a
KT – 215	3.4	18	18	Non-Plastic	A-1-a
LE – 160	2.0	19	19	Non-Plastic	A-1-a
LN – 80	1.2	No Value	No Value	Non-Plastic	A-1-a
NP - 82	4.2	17	15	2	A-1-a
PW - 84	4.3	18	16	2	A-1-a
VY – 63	1.2	23	17	6	A-1-a
WCW	4.6	No Value	No Value	Non-Plastic	A-1-a
CN - 148 SB	5.1	No Value	No Value	Non-Plastic	A-1-a
CS - 184 SB	2.1	20	18	2	A-1-a
PY - 720 SB	2.6	No Value	No Value	Non-Plastic	A-1-a

4.4 Moisture Density Relationship

Table 4.4 summarizes the results of the moisture-density relationships. At least two replicates were tested at each moisture content. The maximum dry density of subbase materials was comparatively lower than the base materials. Test material "BK – 181" had the highest MDD of 2445 kg/m^3 while "CS – 184 SB" (subbase material) has the lowest MDD of 2148 kg/m^3. The MDD for the base materials was between 2445 kg/m^3 and 2210 kg/m^3, while the subbase materials had MDD of about 2160 kg/m^3. The dense gradation provides higher mass per unit volume.

The range for OMC was between 3.5% to 6.5% for base materials and 5.5% to 8.1% for subbase materials. As explained earlier, the subbase materials are finer thus they have higher specific surface area compared to base materials. An aggregate with higher specific surface area may absorb more moisture. The lowest OMC was 3.5% for "NP-82" material while the highest OMC was 8.1% for "CS-184 SB" material.

The values of MDD and OMC of the test materials were comparable to values obtained by other researchers. Hajj et al (2018) reported an average MDD of 2298.7 kg/m^3 and OMC of 5.3% for nine granular base aggregates tested in Nevada. Jackson (2015) tested eight base materials in Utah, and reported an average MDD of 2248.9 kg/m^3 with an average OMC of 6.1%.

Table 4.4 Moisture density relationship test results

Material ID	MDD (kg/m^3)	OMC (%)
A	2245	4.4
B	2253	4.4
BK – 100	2290	4.7
BK – 181	2445	5.7
BR – 2	2280	5.6
CS – 184	2210	6.5
EL – 132	2275	6.0
IMC – 140	2290	6.2
KT – 215	2265	4.8
LE – 160	2235	4.4
LN – 80	2250	5.8
NP – 82	2261	3.5
PW – 84	2365	5.6
VY – 63	2265	4.3
WCW	2300	4.9
CN - 148 SB	2168	5.5
CS - 184 SB	2148	8.1
PY - 720 SB	2165	6.6

4.5 Resilient Modulus Test Results

According to AASHTO T 307, the recoverable strain should be calculated from the last five cycles of each loading sequence. For each sequence, the last five cycles provide five resilient modulus values which were averaged and reported as resilient modulus for a given sequence per AASHTO T 307. Thus, each test material has 15 stress-dependent resilient modulus values. In addition, this study utilized external as well as internal LVDTs to measure the resilient modulus, therefore the resilient modulus based on both external and internal deformations were calculated and summarized in Tables 4.4 and 4.5, respectively. At least two replicates were tested from each test material.

In both cases, material “CS – 184 SB” has the lowest resilient modulus compare to rest of materials, while material “BR – 2” has the highest resilient modulus at the corresponding loading sequences. This particular material (BR – 2) has relatively larger particles compared to the other materials. Although, material “PW – 84” is considered a base material, it exhibited lower resilient modulus which is similar to subbase material “CS – 184 SB”. Test materials “PW – 84” and “CS – 184 SB” experienced higher deformations, which yielded comparatively larger value of recoverable strains, led to lower resilient modulus values. On the other hand, “BR – 2” did not undergo comparatively higher deformation.

The results showed that maximum resilient modulus occur at test sequence number 15, while the lowest resilient modulus occur at test sequence number 1 which is in good agreement with previous studies (Hajj et al., 2018; Ceylan and Kim, 2009). The range of resilient modulus values obtained in this study were comparable to those obtained by other researchers in the nearby states of Nevada (Hajj et al. 2018) and Utah (Jackson 2015). In this study, the base materials had a range of 42 MPa to 441 MPa, while the subbase materials had a range of 33.2 MPa 352.8 MPa. Hajj et al. (2018) obtained a minimum resilient modulus of 63.8 MPa and a maximum resilient modulus of 408.8 MPa for the base materials tested in Nevada. While, Jackson (2015) obtained a minimum resilient modulus of 37.6 MPa and a maximum resilient modulus of 383.7 MPa for base materials tested in Utah. Meanwhile, it should be noted that the base materials evaluated in these three studies had different gradations and percent fines.

Table 4.5 Calculated resilient modulus using external deformations

Material ID	Sequence Number (Resilient Modulus in MPa)														
	1	**2**	**3**	**4**	**5**	**6**	**7**	**8**	**9**	**10**	**11**	**12**	**13**	**14**	**15**
A	79.9	95.3	107.2	118	137.5	151.9	200.7	227.1	237.3	229.5	248.3	289.4	289.2	314.1	350.7
B	84.1	98.6	113.1	123.9	146.4	157.5	210.7	238.8	245.4	236.9	256	294.3	293.9	318.8	355.4
BK - 100	60.5	87.2	100.9	103.6	128.5	141	183.1	207.8	216.5	213.2	227	263.7	263.9	281.6	319.9
BK - 181	42.0	58.7	80.2	68.1	97	110.1	127.9	159.7	182.1	144.5	159	211.1	187.5	204.9	277.8
BR - 2	119.5	135.2	151.8	168.5	190.5	207.6	269.2	300.3	311	316.9	329.6	371.1	382.6	401.3	441
CS - 184	61.8	77.7	89.5	93.6	109.4	121.8	149.2	172.5	184.2	174.3	184.7	216.6	217.1	230.1	264.7
EL - 132	57.6	82.7	95.7	102.1	128.6	138.9	184.8	209.3	218.2	212.6	228.5	265.5	271.3	288.5	328.4
IMC - 140	62.8	80.0	95.6	105.2	126.3	136.7	176.8	197.4	213.4	197.3	216	253	251.9	269.4	307.1
KT - 215	43.6	74.7	95.3	76.4	122.3	139.5	152.4	200.9	214	159.8	206.7	253.6	233.7	268.2	309.9
LE - 160	82.4	101.2	114.4	123.5	146.5	159.3	196.2	230	246.8	227.2	248.5	293.4	287.1	311	357.1
LN - 80	58.6	93.1	109.2	108.8	140.9	154.7	190	222.4	225.5	214.5	232.5	275.7	272.4	291.6	338.2
NP - 82	86.1	96.6	110.0	117.5	137.1	150.9	197.3	222.2	237.4	231.9	244.1	284.9	291.3	310.3	348.7
PW - 84	32.9	53.7	71.4	50.5	82.8	103.9	97.1	137.8	161.5	96.9	122.7	179.8	135	165.1	227.4
VY - 63	63.4	84.0	106.7	94.2	134.3	155.1	181.4	228.1	245.7	197.7	236.4	290.2	268.6	299.3	350.2
WCW	76.6	89.8	101.5	107.1	124.9	140.7	174.2	201	219.7	209.4	217.2	256.1	258.3	271.6	313.9
CN - 148 SB	88.1	105.5	120.7	137.9	152	161.4	212.3	234.8	243.4	249.4	255.1	286	303.3	316.4	352.8
CS - 184 SB	33.1	48.9	61.5	43.4	63.7	79.6	63.4	92.3	115.3	69.3	77.6	119.1	82	96.9	144.7
PY - 720 SB	84.5	100.5	114.3	123.4	144.3	153.4	197	217.7	227.4	226.7	243.6	273.4	280.1	295	321.9

Table 4.6 Calculated resilient modulus using internal deformations

Material ID	Sequence Number (Resilient Modulus in MPa)														
	1	**2**	**3**	**4**	**5**	**6**	**7**	**8**	**9**	**10**	**11**	**12**	**13**	**14**	**15**
A	105.2	117.9	130.8	144.4	163.6	174.2	236.6	258.7	260.7	270.5	284.2	321.8	338.9	354.1	392.5
B	121.2	132.8	145.3	163.9	183.3	193.2	268.2	293.2	295.7	319.1	329	364.9	388.2	410.1	446.5
BK - 100	96.6	109.9	122.5	138.3	152.4	164.6	224.7	240.9	246.7	262.9	270.8	302.7	315.5	330.5	367.3
BK - 181	66.8	95.6	122.7	99.2	137.6	151.8	168.1	204.5	230	200.2	210.9	262.7	252.7	269	322.7
BR - 2	166.5	181	205.3	227.4	249.3	263	349.1	377.3	393.2	432.8	439.1	472.7	527.9	532.1	573.1
CS - 184	81.0	89.2	98.3	107.5	118.5	136.7	169.5	198.9	209.3	208.7	214.2	243.9	257.8	265.3	313.6
EL - 132	110.6	121.4	145	158.7	189.5	195.7	257.3	304.9	297.9	308.2	311.4	363.3	379.4	395	470.2
IMC - 140	114	124.3	165.4	158.1	204.3	221.4	256.3	324.4	331.9	302.3	313.8	385.3	374.2	386.9	487.4
KT - 215	103.4	113.8	124.3	141.2	155.9	168.2	217	245.7	256.3	257.1	272.4	307.6	323.5	336.2	376.3
LE - 160	121.0	127.8	139.5	160.1	177.9	187	241.4	271.8	286.8	296.6	304.9	342.5	360.6	379	423.9
LN - 80	103.6	120.6	132.5	144	165.5	175.7	231.6	257.1	250.3	262.8	271.3	309.9	328	339.2	386.2
NP - 82	105.4	110.4	119.4	128.6	146.9	160.1	217.2	236.6	252.7	267.7	270.5	305.2	323.8	337.6	376.4
PW - 84	47.9	69.3	89.5	69.0	100.2	125.9	116.1	157.2	182.7	125.9	140.9	199.1	165.8	187.1	251.6
VY - 63	128.6	138.7	155.7	166.9	199	215.8	276.7	318.8	331.1	332.2	331.8	403	397.9	418.7	497
WCW	87.4	97.5	106.9	113.5	129.5	143.1	181.1	207.4	225.5	224	227.6	266.8	278.8	290	335.1
CN - 148 SB	102.3	138.5	132	154.4	164.9	173.5	235.6	255.6	257.8	277.9	281.2	308.6	342.6	369.8	384.8
CS - 184 SB	35.7	54.7	71.5	44.9	70.0	89.3	64.8	98	126.3	68.6	77.7	125.8	79.6	97.8	153.8
PY - 720 SB	132.1	134.5	143.3	172.7	182.1	185.4	253.6	265.6	272.6	303.8	309.1	334.1	363.5	376.5	397.6

4.6 Comparison between Internal and External Resilient Modulus

As mentioned earlier AASHTO T 307 utilizes external deformation measurements in the calculations of resilient modulus; however, NCHRP 1-28A research project recommended the use of internal measurements. In this study, the researcher calculated the resilient modulus using both external as well as internal deformations and the difference in resilient modulus values was studied. Figures 4.2 and 4.3 show the resilient modulus values for the test materials at different bulk stress levels using external and internal deformation measurements, respectively. As the sequence of the test progresses, and applied bulk stresses increases as well. It is clear that the resilient modulus increases with bulk stress for all test materials due to stress hardening as a result of increased aggregate interlock. The aggregate skeleton within the specimen develops more particle-to-particle interlock as the confining and the deviatoric stress increase. These results are in good agreement with the ones reported in the literature by other researchers (Ceylan and Kim, 2009; Camargo et al., 2012, Hajj et al., 2018). Test material "BR – 2" had the highest resilient modulus values using both external deformations (441 MPa) and internal deformations (573 MPa). While, test material "CS – 184 SB" had the lowest resilient modulus values using both external deformations (144.7 MPa) and internal deformations (153.8 MPa). Higher modulus values are associated with lower recoverable (resilient) deformation and vice versa. Test material "CS – 184 SB" had the highest recoverable deformations measured using both external and internal LVDTs, thus it had lowest resilient modulus compared to other materials.

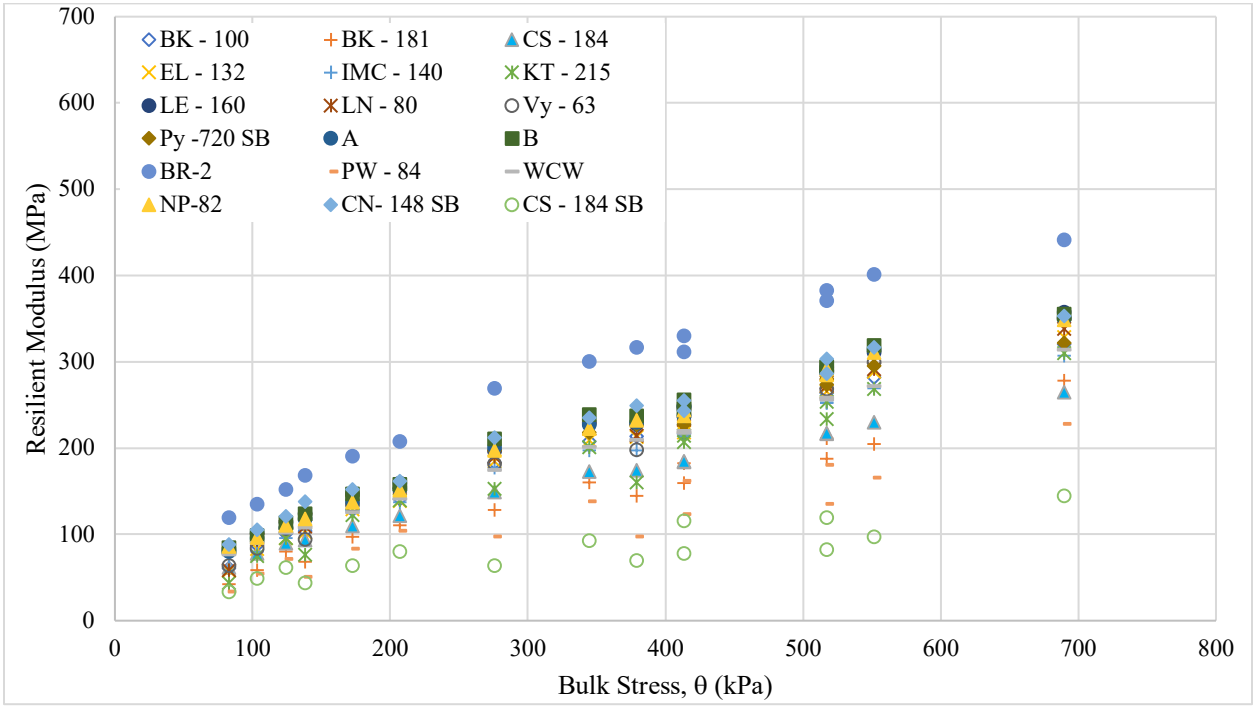

Figure 4.2 Resilient modulus calculated using external deformation versus bulk stress

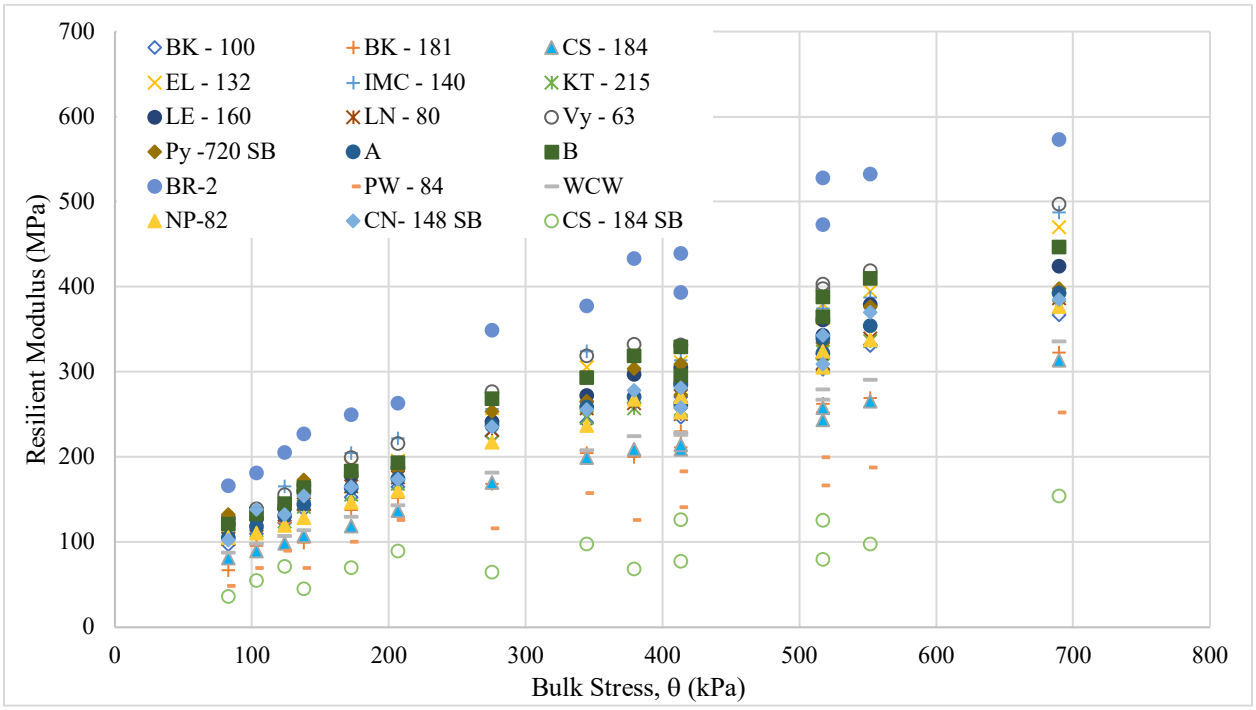

Figure 4.3 Resilient modulus calculated using internal deformation versus bulk stress

The resilient modulus calculated based on internal deformation measurements were consistently higher than those measured using the external deformation measurements as shown in Figures 4.2 and 4.3. The ratio of internal to external resilient modulus was found 0.97, for test material "CS – 184 SB", to 2.37, for test material "VY – 63". Figures 4.4 shows the ratio of internal resilient modulus values to external ones with respect to the external resilient modulus. It can be seen that the ratio was higher at low resilient modulus before it stabilized at higher resilient modulus. Figures 4.5 demonstrates that the ratio of internal resilient modulus to external resilient modulus decreases with the number of the test sequence. Figure 4.6 provides a direct correlation between both resilient moduli. The findings of this section are in good agreement with previous studies (Camargo et al., 2012; Ping et al., 2003).

Camargo et al. (2012) reported similar numbers for their study where they found the internal resilient moduli is 1.5 times higher than the external ones based on the tests conducted on base materials acquired from Minnesota and Wisconsin. Ping and Ge (1996) in Florida conducted similar studies on cemented limerock base and found a ratio from 0.85 to 1.48 between the internal to external resilient modulus.

Ping et al. (2003) conducted extensive study where they examined the impact of the internal LVDT positions (e.g., top half, bottom half and the middle half). They found that the ratio of internal to external was from 1.19 to 1.35 for A-3 soils and 1.14 to 1.30 for A-2-4 soils. Several factors may affect the external LVDT measurements including sample end effects, bedding error, machine compliance (Jardine et al. 1984; Goto et al., 1991; Tatsuoka et al., 1994; Bejarano et al., 2003; Boudreau and Wang, 2003; Ping et al., 2003). The term, "system compliance" or "machine compliance" is referred to the deflection of the resilient modulus testing equipment parts, such as the load cell, top cap, and piston (Camargo et al., 2012). For the internal deformation measurements, the LVDTs were mounted on the test specimen along the middle half. In this region (middle half), there was no friction, end bearing effect, or bedding error, therefore the deformation at the middle half was typically lower than the full length of the specimen.

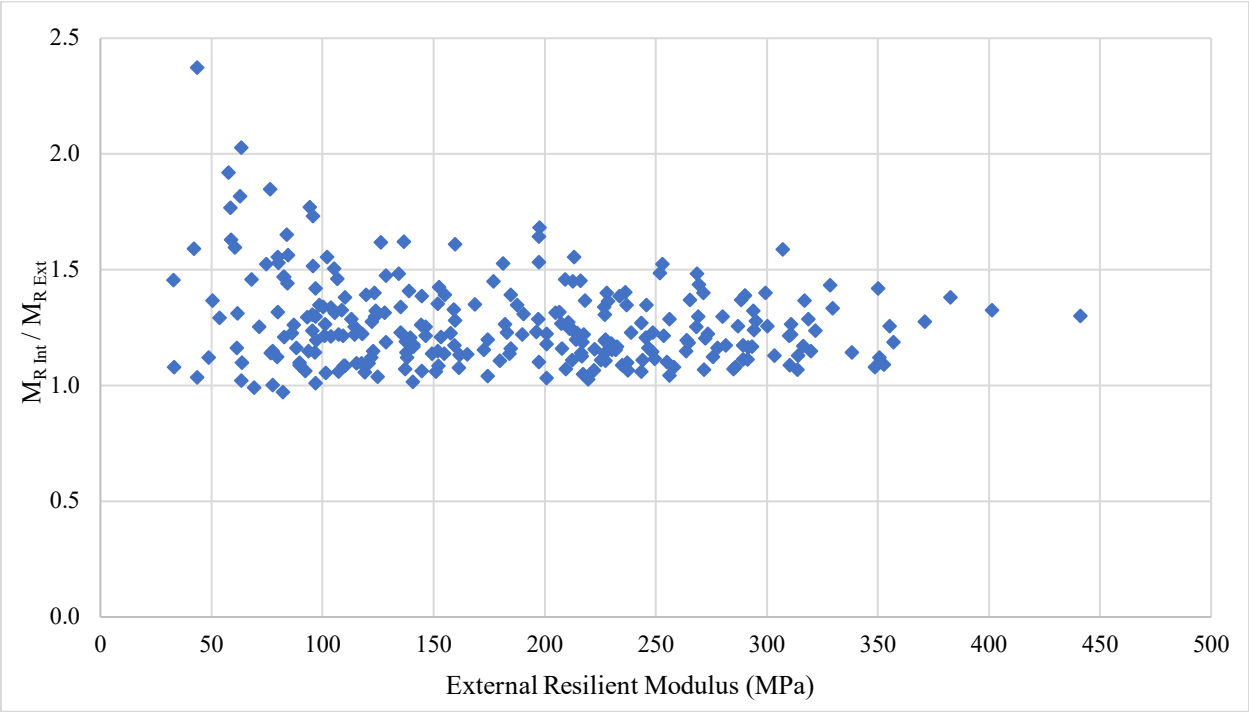

Figure 4.4 Ratio of internal M_R to external M_R with respect to external M_R

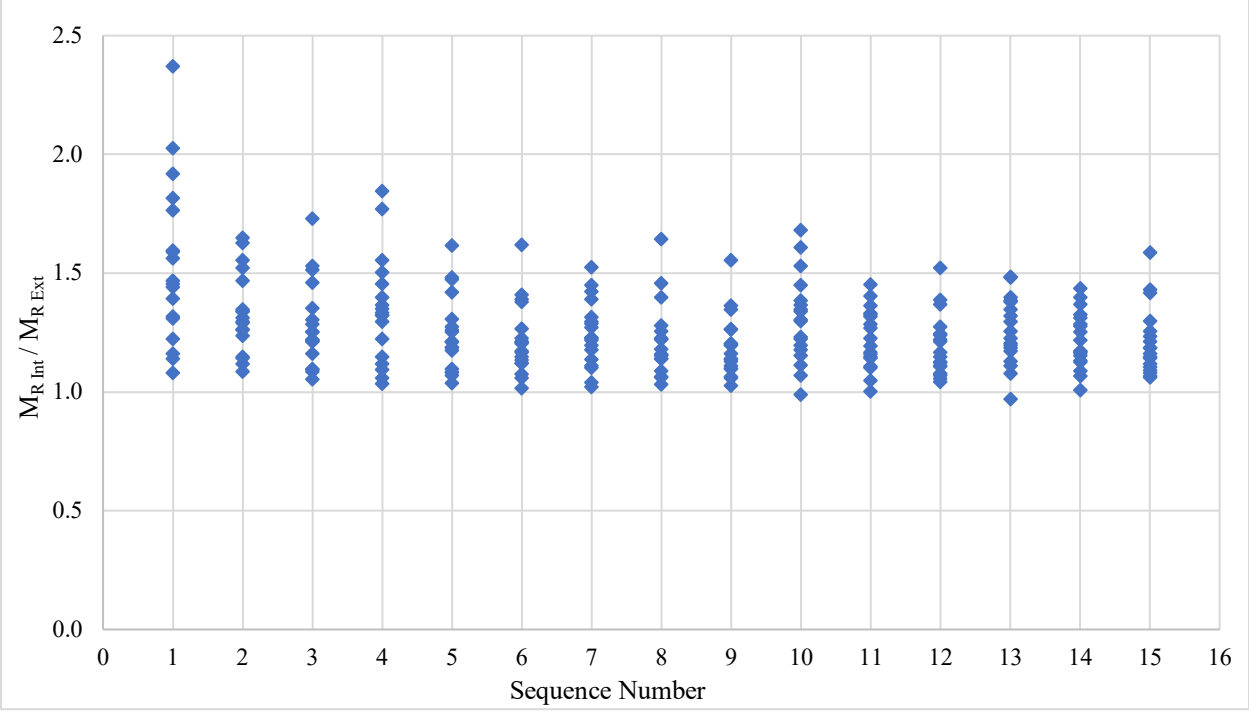

Figure 4.5 Ratio of internal M_R to external M_R with respect to sequence number

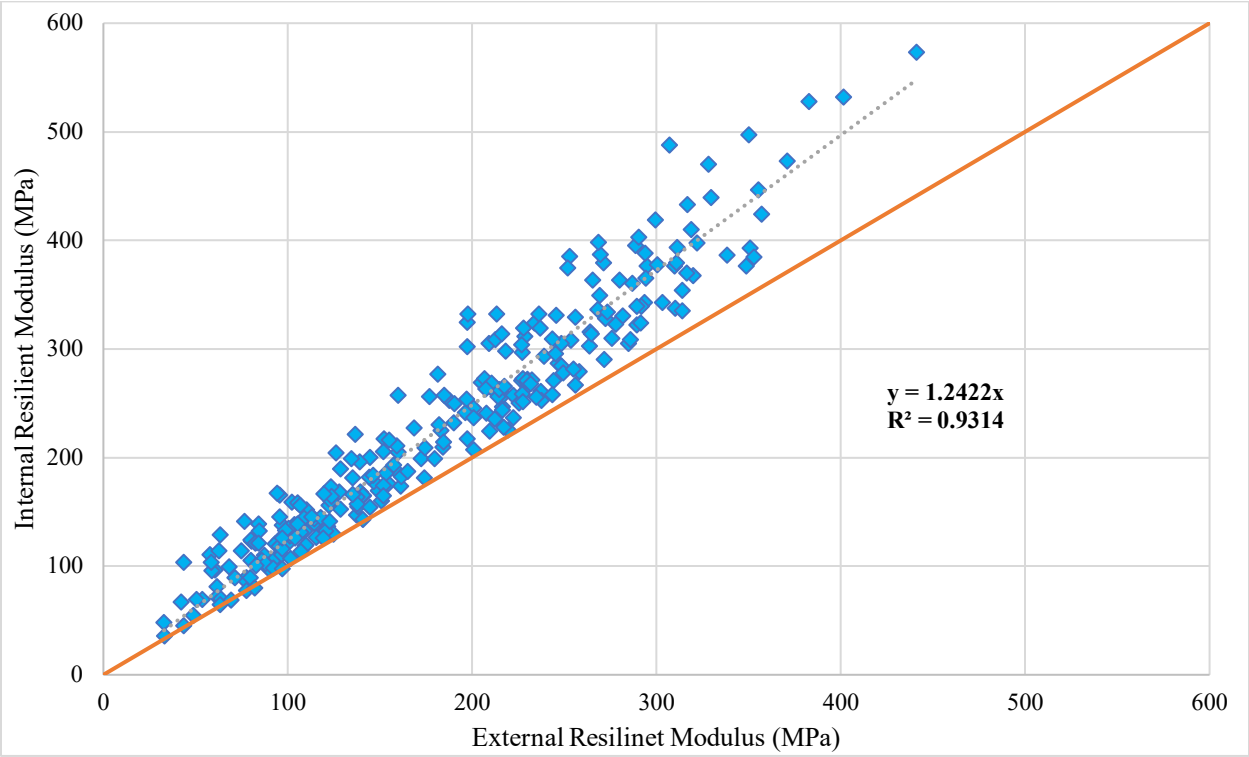

Figure 4.6 Relationship between internal M_R and external M_R

The results demonstrate that there is a linear correlation between the external and internal resilient modulus as shown in Figure 4.6. On average, the internal resilient modulus was about 24 percent higher than the external resilient modulus in this study. A linear regression analysis was carried out to check if there any statistically significant relationship existed between the internal and external resilient moduli for all test materials. In this analysis, the obtained *p-value* (0.0001) was lower than 0.05. Therefore, the null hypothesis (slope is zero, e.g., no relationship) was rejected and concluded that there was a statistically significant relationship exist between internal and external resilient moduli. Equation 4.3 presents the relationship between the internal and external resilient moduli.

$$M_{R\ Int} = 1.2422 \times M_{R\ Ext} \quad (4.3)$$

The resilient modulus of aggregate base and subbase is generally reported at a bulk stress of 206.8 kPa (30 psi) (i.e., resilient modulus obtained from the sixth loading sequence of AASHTO T 307), which is known as the summary resilient modulus (SRM) (Witczak, 2003). Since the current version of AASHTOWare allows only one value for resilient modulus of unbound layers, the summary resilient modulus or SRM is used as an input in the software (Figure 4.7). Table 4.7 summarizes the SRM of all test materials in this study using the external as well as the internal deformations. In addition, Table 4.7 presents the ratio of internal to external resilient modulus. The ratio is greater than 1.00 with an average of 1.22 (based on Sequence No. 6) which is close to 1.24 (based on the average of all 15 sequences). Figure 4.8 shows a visual comparison of the internal and external summary resilient modulus. It is more conservative to use the resilient modulus measured using the external deformation compared to the internal modulus. In addition, it is simpler to measure the external deformation compared to internal deformation measurements. Thus, the current practice and standards (e.g., AASHTO T 307) is to use the external deformation measurements. Furthermore, the summary resilient modulus can be used as a single, standard value to compare two or more materials (Camargo et al., 2012).

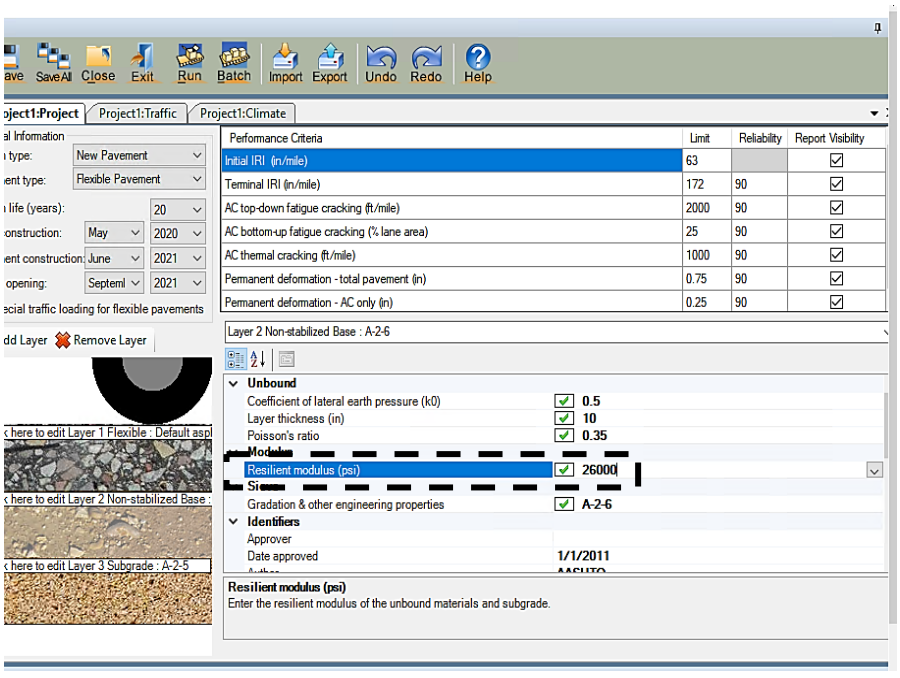

Figure 4.7 Resilient modulus input for base layer in AASHTOWare

Table 4.7 Summary resilient modulus of the selected base and subbase materials

Material ID	External M_R (MPa)	Standard Deviation of external M_R	Internal M_R (MPa)	Standard Deviation of internal M_R	Ratio (Int/Ext)
A	151.9	4.04	174.2	3.04	1.15
B	157.5	5.51	193.2	13.28	1.23
BK - 100	141.0	4.84	164.6	2.22	1.17
BK - 181	110.1	2.62	151.8	12.45	1.38
BR - 2	207.6	6.50	263.0	0.04	1.27
CS - 184	121.8	1.15	136.7	3.40	1.12
EL - 132	138.9	3.31	195.7	3.91	1.41
IMC - 140	136.7	3.15	221.4	31.87	1.62
KT - 215	139.5	2.79	168.2	5.91	1.21
LE - 160	159.3	4.80	187.0	0.16	1.17
LN - 80	154.7	0.10	175.7	0.77	1.14
NP - 82	150.9	8.83	160.1	7.07	1.06
PW - 84	103.9	2.75	125.9	6.67	1.21
VY - 63	155.1	1.83	215.8	21.91	1.39
WCW	140.7	5.70	143.1	3.87	1.02
CN - 148 SB	161.4	4.08	173.5	4.95	1.07
CS - 184 SB	79.6	1.17	89.3	2.48	1.12
PY - 720 SB	153.4	3.48	185.4	3.05	1.21

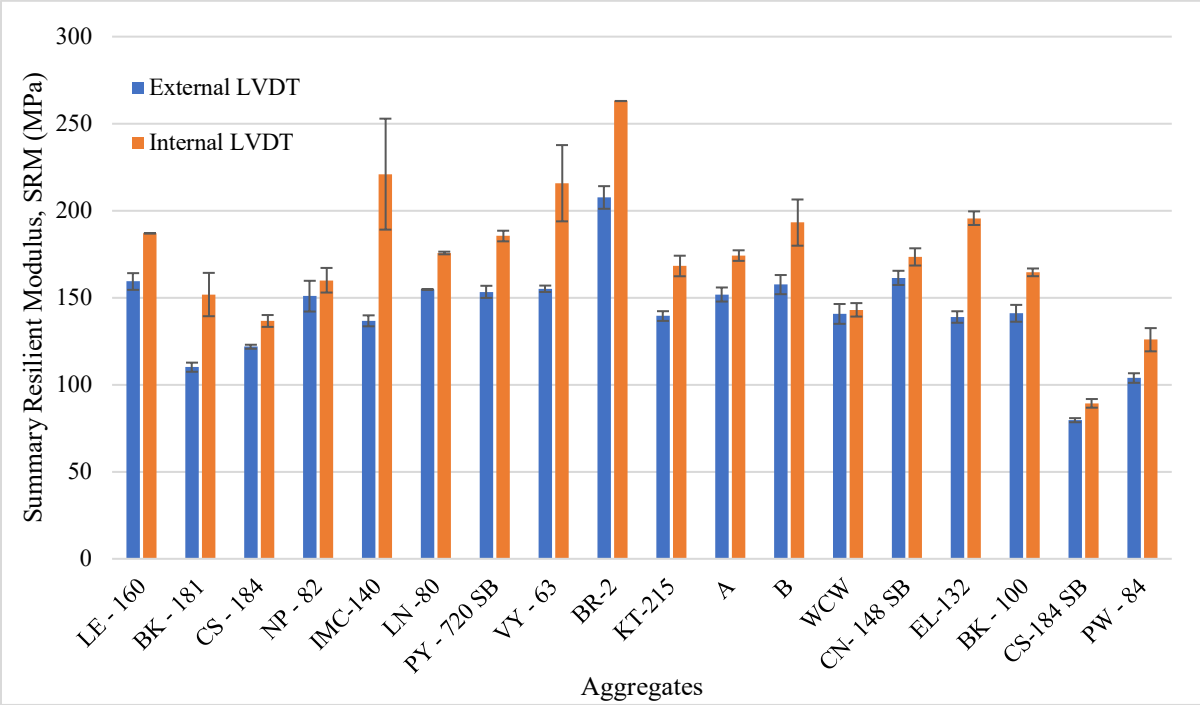

Figure 4.8 Comparison between internally and externally measured SRM

4.7 Summary Resilient Modulus Prediction Model

Since the resilient modulus test is time consuming that requires expensive equipment and well-trained personnel, the resilient modulus can be estimated based on base and subbase material properties that are simple to measure. AASHTOWare Pavement ME Design (PMED) software (V 2.5.3) requires the summary resilient modulus (SRM) as input for the unbound layers, therefore the researcher used multivariate regression analysis to develop a prediction model for the summary resilient modulus as a function of inherent properties of aggregates that were measured in this study. The statistical prediction model was developed using "Minitab" statistical software (Minitab, 2017). The SRM obtained from 13 randomly chosen materials were used as "trained data" or "development data" while SRM for remaining 5 materials were used as "tested data" or "validation data". In Minitab software, the "stepwise" regression analysis technique was used to develop the prediction model. The average summary resilient modulus (externally measured) of each material was considered as the response variable where the material properties like MDD, OMC, percent passing of #4 sieve, particle size of 10% and 30% finer were considered as explanatory variables. Equation 4.4 presents the relationship between resilient modulus and various material parameters.

$$M_R = 198.2 + 1.405 \frac{MDD^{0.73}}{OMC^{1.3863}} - 16.82 (D_{10} + D_{30})^{1.18} - 1.081 P_4 + 123 L - 53.24 H \qquad (4.4)$$

where,

M_R = summary resilient modulus (MPa)
MDD = maximum dry density (kg/m^3),
OMC = optimum moisture content (%),
D_{10} = particle diameter corresponding to 10 percent finer (mm),
D_{30} = particle diameter corresponding to 30 percent finer (mm),
P_4 = percent passing of 4.75 mm (No. 4) sieve,
L and H are categorical variables:
L = 1, if $D_{10} \geq 1.00$ mm; otherwise L = 0
H = 1, if OMC > 8.0%, otherwise H = 0.

The measured and predicted resilient modulus values of test materials are depicted in Figure 4.9*a*. The validation data points are well covered by the envelop of 95% confidence interval except for one material. The goodness of fit or coefficient of determination (R^2) of the proposed model is high (0.9572) with adjusted R^2 of 0.9266. The plot of normal probability (Q-Q plot) satisfies the requirement, (i.e., most of the data points are on or very close to the line) (Figure 4.9b).

The *p-value* of each independent variables was less than 0.05 which means all the estimates for independent variables are significant. Also, the researcher checked the multicollinearity. Multicollinearity defines how the independent variables are correlated to each other. This could result an incorrect estimate of the coefficients. Variance Inflation Factor (VIF) is the measure of the multicollinearity. The lower the VIF value, the less the independent variables are correlated to each other. A VIF of 10.0 is considered a proper cutoff to ensure that the independent variables are not correlated or not highly correlated to each other (Kutner et al., 2004). The researcher can choose the cut off values based on their proposed model and statistics. Different authors/statistician (Hines and Montgomery, 1980; Sheather, 2009) proposed different VIF cutoffs. All the statistical analysis of the model parameters is provided in Table E.1 of Appendix E.

The following observations can be made from Equation 4.4.

- The resilient modulus increases with the increase of maximum dry density and decreases with the increase in optimum moisture content
- The resilient modulus decreases with effective grain size (D_{10} and D_{30}) up to certain limit, and with percent passing of 4.75 mm (No. 4) sieve but at lower rate compared to effective grain size (D_{10} and D_{30}).

Hajj et al. (2018) reported that the resilient modulus base aggregate decreases with the increase in optimum moisture content. Rahim (2005) also reported that the resilient modulus increases with maximum dry density and decreases with moisture content (Equation 2.3).

Jackson (2015) found that an increase in MDD of one unit increases the resilient modulus by 1.94 units, while one unit increase of OMC decreases the resilient modulus value by 3.09 units (Equation 2.4). The findings from this study are in well agreement with findings of previous two studies (Rahim, 5005; Jackson, 2015; Hajj et al. 2018).

The material of "PW – 84" was not covered by the 95% confidence interval of the prediction model. According to the prediction model (Equation 4.4), if the MDD increases, the resilient modulus should also increase. The resilient modulus for "PW – 84" yielded lower resilient modulus (less than 110 MPa) while it had a maximum dry density of 2365 kg/m^3 with OMC of 5.5%. With almost same moisture-density relationship of test material "WCW" (MDD = 2300 kg/m^3 and OMC = 4.85) which had an average resilient modulus of 140.7 MPa. To investigate this low result, third replicate was prepared and tested. The results of summary resilient modulus of all three replicates for "PW – 84" were 101.1 MPa, 106.1 MPa and 89.88 MPa. From the visual inspection by the author, it was found that, "PW – 84" had finer particle with very smooth surface. When compacting this test material "PW – 84" for moisture-density relationship and resilient modulus test, the authors noticed an unstable condition (i.e., unexpected movement of aggregates). This movement of particles could be affected by the smooth surface of this aggregate which could lead to lower resilient modulus.

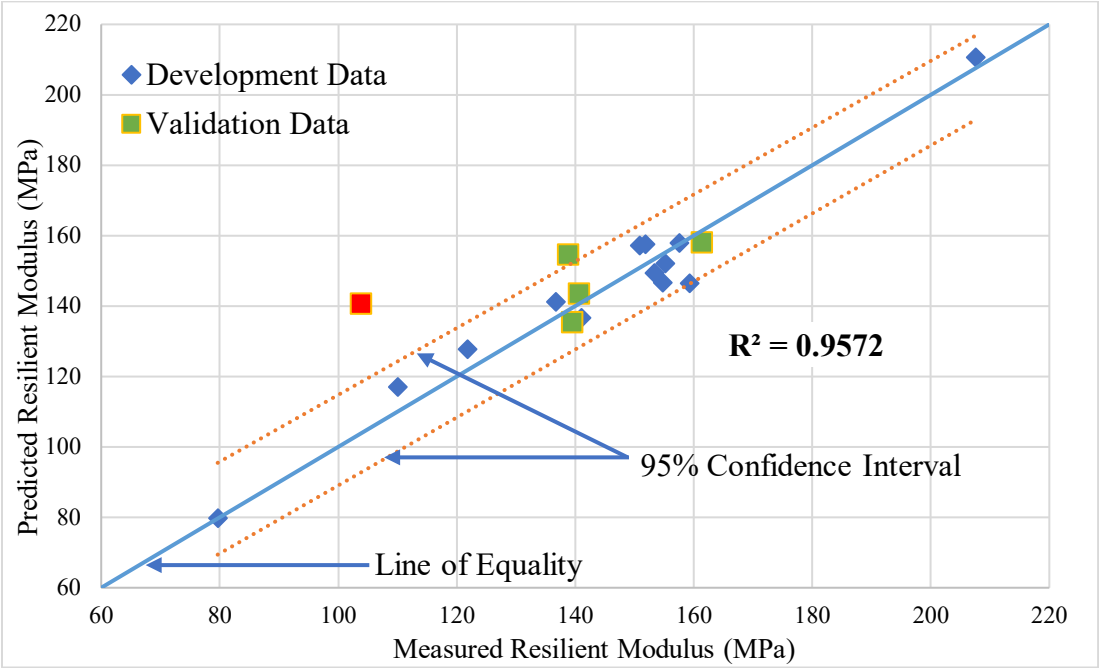

(a)

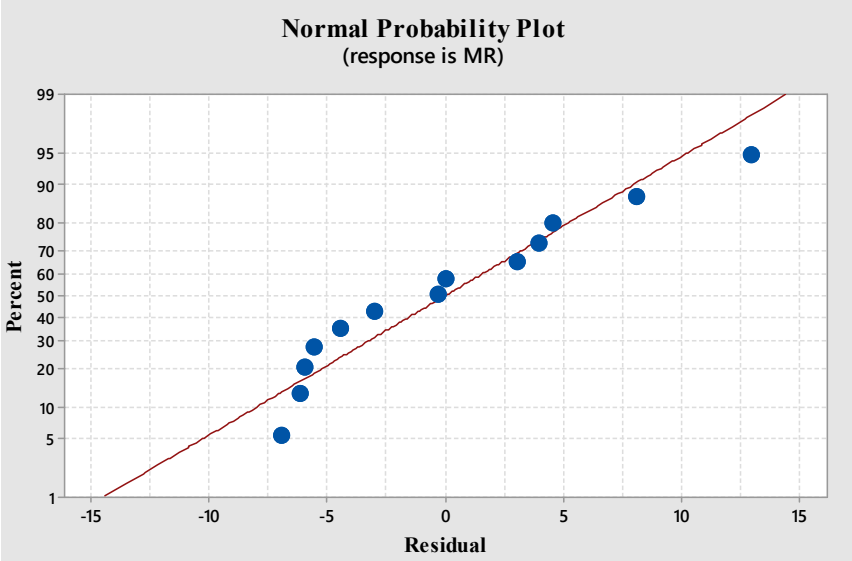

(b)

Figure 4.9 Statistical analysis of the prediction model (a) measured vs predicted value of resilient modulus, (b) normal Q-Q plot

4.8 Analysis of Resilient Modulus Models as Function of Stress State

As discussed in Section 2.10, there are over 20 constitutive models used to describe the resilient modulus of the base/subbase materials. These models are summarized in Table 2.1. Four out of these models are commonly used to describe the change of resilient modulus for granular materials at various stress conditions. These four models are (1) K-θ model (Hicks and Monismith, 1971), (2) Uzan Model (Uzan, 1985), (3) Modified Uzan Model (Witczak and Uzan, 1988), and (4) MEPDG Model (ARA Inc., 2004). These various models are fitted against the resilient modulus data obtained from all the stress state denoted in standard test of AASHTO T 307 to obtain the parameters for each model. These models were discussed in Section 2.10.

For all the selected constitutive models, the resilient modulus is in MPa, while the bulk stress, shear stress and atmospheric pressure are in kPa. The regressions parameters (i.e., k_1, k_2, k_3) are dimensionless except for "K-θ" model. For "K-θ" model, "K" is in MPa and "n" is dimensionless. Figure 4.10 shows an example of the correlation between measured versus predicted resilient modulus using MEPDG Model (external deformations). Table 4.8 summarize the regression coefficients for the MEPDG Model (Equation 2.18), for external resilient modulus while the regression coefficients for internal resilient modulus are included in Appendix D. Appendix A, B, and C include the results of all the other models for the test materials including both external and internal resilient modulus.

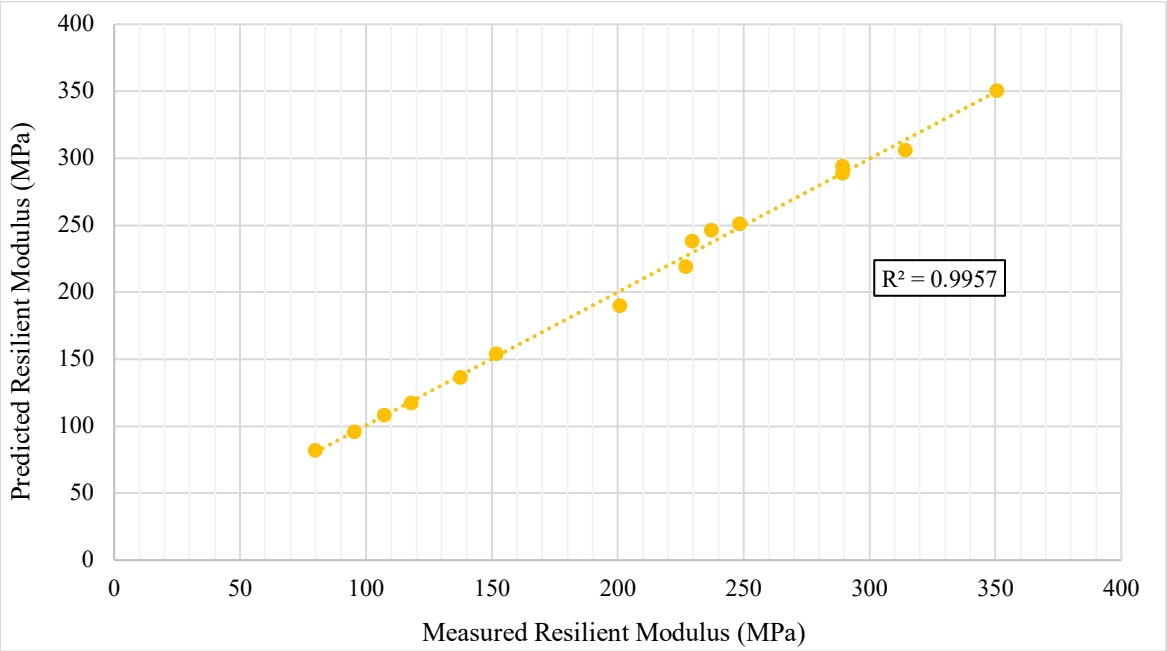

Figure 4.10 An example of the correlation between measured vs. predicted resilient modulus using MEPDG Model

Table 4.8 Summary of regression coefficients for *"MEPDG Model"* for external resilient modulus

Material ID	k_1	k_2	k_3	R^2
A	940.475	0.708	-0.069	0.996
B	1002.486	0.681	-0.066	0.994
BK - 100	852.193	0.713	-0.071	0.994
BK - 181	562.601	0.613	0.486	0.993
BR - 2	1373.348	0.664	-0.152	0.998
CS - 184	751.953	0.639	0.017	0.997
EL - 132	823.403	0.752	-0.091	0.994
IMC - 140	825.294	0.685	-0.013	0.995
KT - 215	705.926	0.659	0.284	0.974
LE - 160	978.308	0.645	0.053	0.997
LN - 80	898.157	0.672	0.026	0.988
NP - 82	949.280	0.701	-0.077	0.997
PW - 84	467.246	0.420	0.960	0.978
VY - 63	836.145	0.660	0.220	0.988
WCW	868.372	0.660	0.001	0.999
CN - 148 SB	1072.674	0.670	-0.154	0.995
CS - 184 SB	391.217	0.142	1.276	0.978
PY - 720 SB	1011.395	0.655	-0.136	0.997

From Equation 2.18, it is evident that, k_1 is directly proportional to resilient modulus. If k_1 increases, the resilient modulus also increases (k_1 is positive). From Figure 4.2 and Figure 4.3, as the bulk stress increases, the resilient modulus also increases (k_2 is positive). In case of k_3, it should be negative since the increase in shear stress will likely weaken the specimen, exhibiting stress softening behavior (Tutumluer, 2013). Meanwhile, from Table 4.13, the values of k_3 are mixed with positive and negative. The reason for these positive k_3 values is the stress hardening behavior. Since octahedral stress is a function of deviator

stress, as the deviator stress increases (or, octahedral stress increases), for the unbound aggregates the aggregate interlock also increases, resulting increase in resilient modulus. This phenomenon yielded positive k_3 values for the increasing resilient modulus values. Similar observations were also reported by Ceylan and Kim (2009).

From Table 4.10, the k_1 ranges from 391 to 1373, k_2 ranges from 0.1416 to 0.713 and for the k_3 has wide range of -0.154 to 1.2763. Since test material "CS – 184 SB" yielded the lowest resilient modulus value, it has the lowest k_1, k_2 and highest k_3 values. This highest k_3 value was registered to "CS – 184 SB" because, the resilient modulus of this material was increasing with the deviatoric stress at higher rate compare to other materials. Since the material "PW – 84" and the "CS – 184 SB" yielded the lower resilient modulus, the regression coefficients for these materials were significantly different than others. It is interesting to note that if the range and average of estimates of k_2 are made without considering these two materials, the range is between 0.673 to 0.752 with an average of 0.673.

The goodness of fit (R^2) for all selected constitutive models are satisfactory. The range of R^2 for "K – θ model" model is in between 0.787 to 0.999. The range of R^2 for "Uzan model" and "Modified Uzan model" is same, in between 0.981 to 0.999. The MEPDG model have a range of R^2 in between 0.974 to 0.999. All the constitutive models were fitted well by the selected aggregates and incorporation of deviator stress (or octahedral stress) increased the R^2 significantly. The R^2 value based on the internal measurement for all four selected models are reported in Appendix A, B, C and D.

4.9 Prediction Model for Regression Parameters of MEPDG Model

The current version of AASHTOWare Pavement ME Design (PMED) software (V 2.5.3) requires a single value of resilient modulus as input for unbound materials (Figure 4.7). This input value can be referred to the summary resilient modulus (SRM) and it represents the resilient modulus obtained from one stress state. Since the resilient modulus is stress sensitive, one single value resilient modulus does not represent the true stress dependent behavior. To capture the stress dependent behavior of aggregate, resilient modulus obtained from all sequence, the regression coefficients (or model constants) of the MEPDG

model (Equation 2.18), k_1, k_2, k_3 are good alternative and can be used as Level 1 input for AASHTOWAre Pavement M-E Design (PMED) software (Tutumluer 2013, Ceylan and Kim 2009). The next version of AASHTOWare Pavement ME Design (PMED) software will incorporate these regression parameters (e.g., k_1, k_2, k_3) as input for the MEPDG model (Equation 2.18) instead of SRM, meaning instead of one value of resilient modulus, one value of k_1, k_2, k_3 (total three values) will be needed as input. In this study, the researcher developed predictive models for these regression parameters.

The Minitab (Minitab, 2017) software was used to perform the statistical analysis and develop equations for three MEPDG model parameters (i.e., k_1, k_2, k_3). The "stepwise" regression technique was used to these parameters as a function of inherent material properties such as MDD, OMC, and aggregate gradation. Since the summary resilient modulus of "PW – 84" could not be explained by the prediction Equation 4.4, it was not considered to develop the prediction model of MEPDG model parameters. Equations 4.5 through 4.7 presents the prediction equations for k_1, k_2, k_3, respectively.

$$k_1 = 1130.1 - 749\ D_{10} + 188\ (MDD^{0.719064} / OMC^{3.90237}) - 79\ Cc + 1109\ L - 486.2\ H \quad (4.5)$$

$$k_2 = 0.5901 + 0.001198\ P_{3/8} - 0.5419\ H \quad (4.6)$$

$$k_3 = -4.22 + 0.001873\ MDD + 1.475\ H \quad (4.7)$$

where,

k_1, k_2, k_3 are the regression parameters of the MEPDG model
MDD = maximum dry density (kg/m^3),
OMC = optimum moisture content,
Cc = coefficient of curvature (Equation 4.2),
$P_{3/8}$ = percent passing of 9.5 mm (3/8 in) sieve,
L and H are categorical variables;
L = 1, if $D_{10} \geq 1.00$ mm; otherwise L = 0
H = 1, if OMC > 8.0%, otherwise H = 0

After developing the prediction equations for k_1, k_2, k_3, the basic assumptions of the multilinear regression were checked. The check for multicollinearity was also conducted. All the statistical analysis of these three prediction models is given in Appendix E. It should be noted that, Equations 4.5, 4.6 and 4.7 do not yield resilient modulus value individually. These three equations are part of a single equation (Equation 2.18). Substituting these three equations (4.5, 4.6 and 4.7) in Equation 2.18, yields the resilient modulus at a particular stress state denoted in AASHTO T 307 (AASHTO, 1999). So, if the MDD of the aggregate increases by a unit, the model parameter "k_1"and "k_3" will increases which means that resilient modulus value increases as well. The increase of MDD increases the value of k_3 which leads to an increase in resilient modulus provided that the resilient modulus of aggregates increases with the deviator stress (or octahedral stress). An increase of percent passing of 9.5 mm (3/8 in) sieve increases the value of k_2. Since k_2 is related to bulk stress, the resilient modulus will increase with the increase of k_2.

Substituting these three equations (4.5, 4.6 and 4.7) in Equation 2.18 provides the resilient modulus as presented in Equation 4.8. The resilient modulus (M_R) in Equation 4.8 is in MPa, while the bulk stress, octahedral stress and atmospheric pressure are in kPa. Since the resilient modulus is obtained from a direct measurement of a physical test, the prediction Equation of 4.5, 4.6 and 4.7 can be validated in terms of Equation 4.8 with these measured resilient modulus data.

$$M_R = \left\{(1130.1 - 749\, D_{10} + 188\, (MDD^{0.719064} / OMC^{3.90237}) - 79\, Cc + 1109\, L - 486.2\, H)\, P_a \times \left(\frac{\theta}{P_a}\right)^{0.5901 + 0.001198\, P_{3/8} - 0.5419\, H\_1} \times \left(\frac{\tau_{oct}}{P_a} + 1\right)^{-4.22 + 0.001873\, MDD + 1.475\, H}\right\} / 1000 \quad (4.8)$$

Figure 4.11 shows the measured resilient modulus versus the predicted values using Equation 4.8. It can be observed that Equation 4.8 provides accurate predictions of the resilient modulus values for all 18 test materials. The coefficient of determination (R^2) is

0.9457 which is very good. Tutumluer (2013) documented that the goodness of fit should be higher than 0.9 to obtain proper correlation coefficients which is achieved using model developed in this study. Figure 4.12 shows the statistical analysis (normal probability plot) of the prediction models (Equation 4.5, 4.6, and 4.7). The normal probability plot of residuals of the predicted resilient modulus values shows that all the data points are on the line, which is in good agreement with the basic assumptions for regression analysis for these prediction equations (Equation 4.5, 4.6, and 4.7).

Yau and Von Quintus (2004) conducted an extensive research on long-term pavement performance (LTPP) database to predict the regression coefficient (k_1, k_2, and k_3) as a function of inherent material properties (e.g., percent passing of 9.5 mm (3/8 in) sieve and 0.425 mm (No. 40), liquid limit, OMC, etc.). They obtained good correlations between the observed and predicted resilient modulus of the unbound base and subbase aggregates. For crushed stone, the increase in percent passing of 3/8" sieve increases the value of k_1 reported by Yau and Von Quintus (2004) and this trend is also observed for this study (Equation 4.5). Hani and Titi (2006) predicted the MEPDG model coefficients for 17 subgrade materials as function of percent passing of 0.425 mm (No. 40) sieve, 0.075 mm (No. 200) sieve, MDD etc. The predicted modulus values had good correlations with measured resilient modulus obtained. Similar approach was used in the study herein and a good correlation between measured and predicted resilient modulus was also found (Figure 4.11).

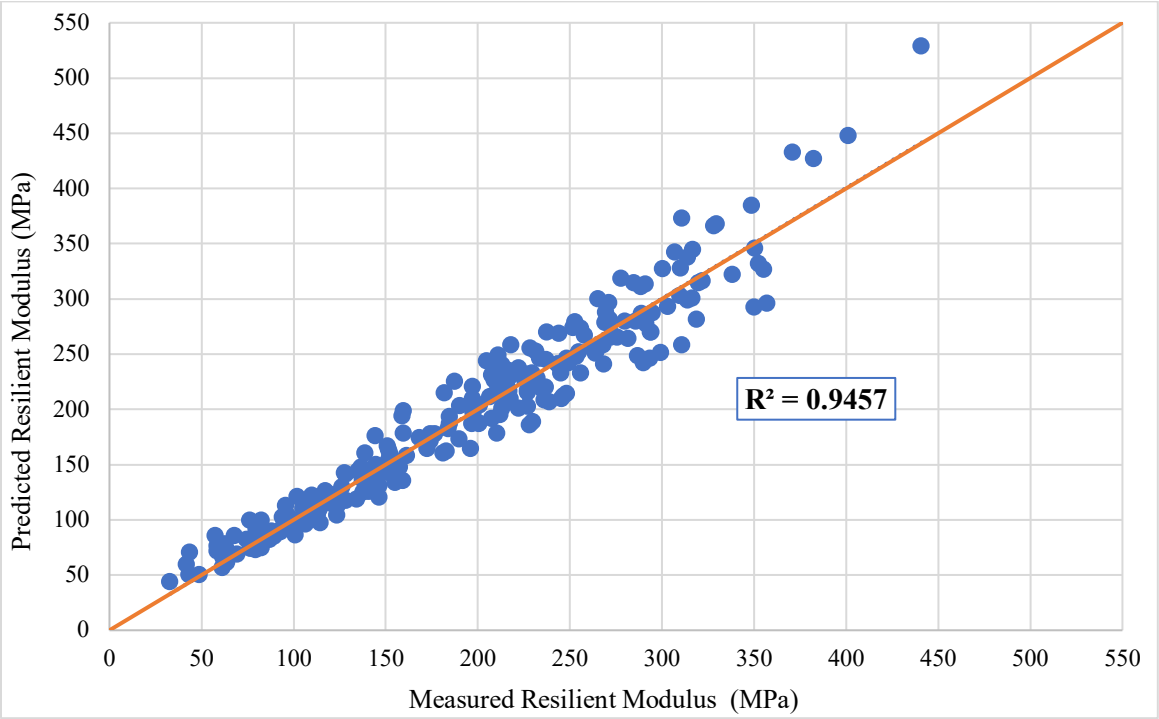

Figure 4.11 Measured vs. predicted resilient modulus using Equation 4.8

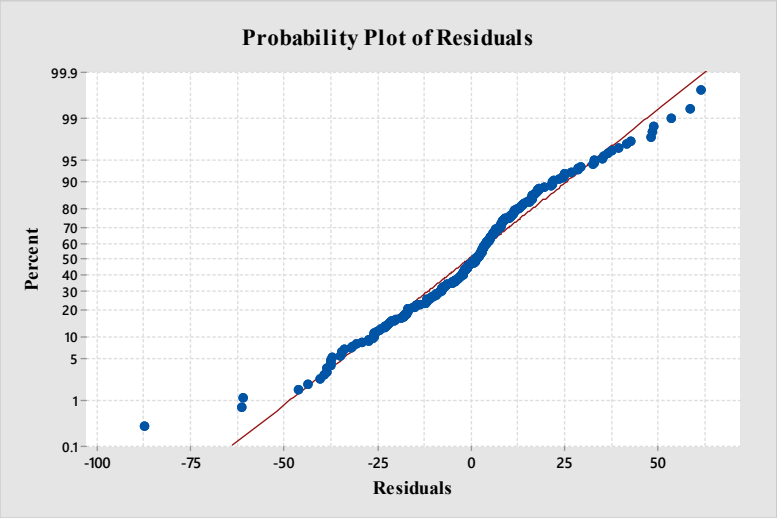

Figure 4.12 Normal probability plot of residuals using Equation 4.8

4.10 Correlation between Resilient Modulus and Alternative Stiffness Tests

The researcher utilized the remaining materials from the resilient modulus testing and conducted further simpler tests including CBR and LWD to explore any correlation between these tests and the resilient modulus. Since the resilient modulus test requires an advanced system that is not available in most of pavement laboratories of department of transportation or transportation agencies, such correlations could be used if the resilient modulus test is not available. This section discusses the results of the CBR and LWD testing.

4.10.1 California Bearing Ratio (CBR) Test Results

Table 4.9 presents the CBR results of the test materials. Due to the limited materials remaining from the resilient modulus and material characterization tests, the CBR was conducted on two replicates at only one condition (i.e., 100% of MDD at OMC and unsoaked). In this study, the CBR values were calculated at two different penetrations (i.e., 2.54 mm [0.1 in] and 5.08 mm [0.2 in]) to assess the correlation between CBR and resilient modulus at these two different penetrations.

Table 4.9 CBR values for the base and subbase materials at various penetrations

Material ID	CBR (%) at 2.54 mm	CBR (%) at 5.08 mm
A	146.4	204.4
B	195.2	242.7
BK - 100	162.3	211.0
BK - 181	105.1	142.7
EL - 132	87.7	129.9
IMC - 140	174.3	239.8
KT - 215	113.1	160.0
LE - 160	118.8	168.0
LN - 80	160.9	216.5
NP - 82	98.6	139.3
PW - 84	93.5	133.1
VY - 63	137.0	169.9
WCW	135.5	194.2
CN – 148 SB	146.8	168.7
CS - 184 SB	57.3	78.7

In most cases, the increase in penetration decreases CBR values (Huang, 2004). The denser the aggregate, the higher CBR values. The CBR values of angular crushed stones

tested in the laboratory are greater than 100 (Tutumluer, 2013). The base and subbase materials obtained from crush rock sources often have higher CBR at 5.08 mm (0.2 in) penetration which was observed in this study. In addition, the CBR at unsoaked conditions is always higher compared to soaked CBR values (Osouli et al., 2017). In addition, Erlingsson (2007) reported that the CBR increases with the increased MDD. This study used modified compaction method which results in higher MDD compared to standard compaction method leading to increased CBR. It is noted that, unsoaked CBR is carried out to simulate the natural filed condition whereas the soaked CBR is carried out simulate the extreme condition which can be resulted from the moisture variation.

The results in Table 4.9 demonstrate that test material "B" has the highest CBR values at both penetrations (e.g., 195.2% at 2.54 mm [0.1 in] and 242.7% at 5.08 mm [0.2 in] penetration). While, test material "CS – 184 SB" has the lowest CBR values at both penetrations (e.g., 57.3% at 2.54 mm [0.1 in] and 78.7% at 5.08 mm [0.2 in] penetration). Test material "B" consisted of purely crushed rock particles whereas "CS – 184 SB" has more fine-grained particles, which absorbs and hold huge amount of water (e.g. OMC of 8.1%).

The CBR values summarized in Table 4.9 were correlated with the SRM measured using the external deformations and reported in Table 4.7. Figures 4.13 and 4.14 show the correlation between CBR and SRM at 5.08 mm and 2.54 mm penetration, respectively. The relationship between the two measures is nonlinear. For CBR at 5.08 mm (0.2 in) penetration, the goodness of fit (R^2) is 0.5626, while the correlation yielded R^2 of 0.5668 at 2.54 mm (0.1 in) penetration. This correlation is considered fair given the fact that the SRM is calculated from a dynamic test while the CBR is calculated from a monotonic test at different stress state. Even though there is difference between resilient modulus and CBR test, the parameter estimates were found statistically significant (i.e., *p-value* = 0.001 < 0.05), means correlation of SRM and CBR is statistically significant. Very limited research has been conducted to correlate the CBR to resilient modulus for base materials, although there are plenty of studies evaluated such correlation for subgrade materials. Jackson (2015)

evaluated the correlation between the average M_R and CBR for the base materials in Utah but found an insignificant correlation (*p-value* of 0.402 and an R^2 value of 0.119).

Based on the results of the correlation between CBR and resilient modulus in this study, the author recommends that the use of material properties to estimate the resilient modulus using the proposed model (Equation 4.2) instead of estimating the resilient modulus as a function of CBR values. Equation 4.2 provides better prediction for the resilient modulus compared to the direct correlation with CBR.

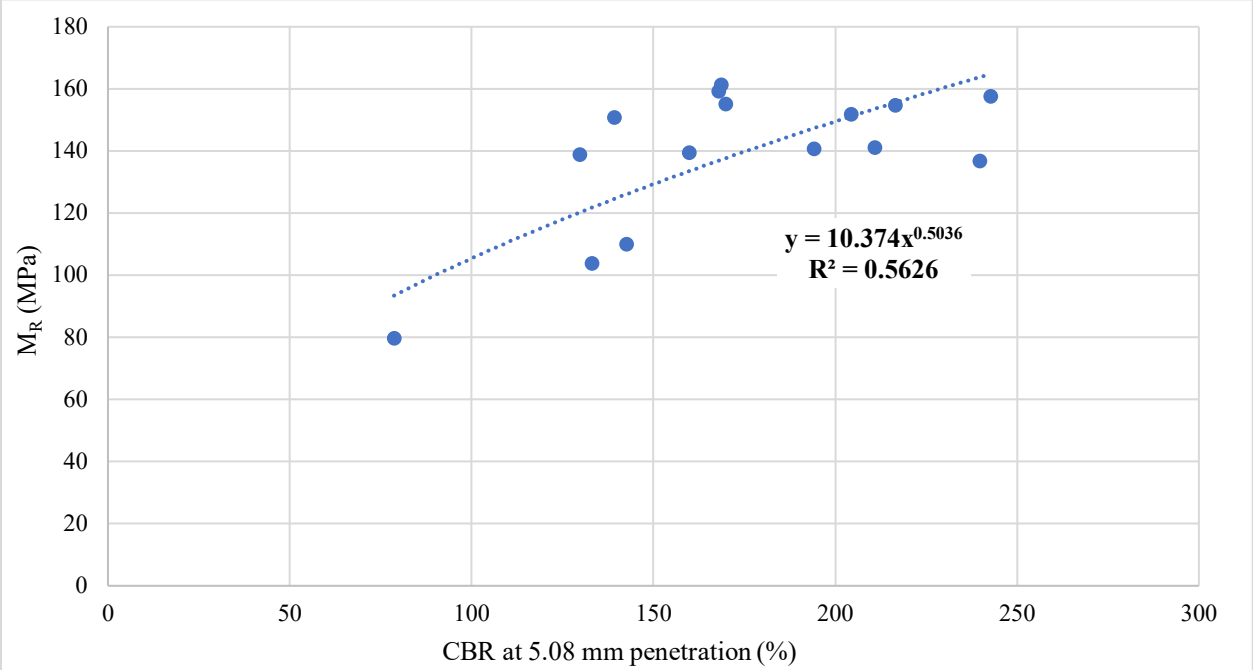

Figure 4.13 Correlation between SRM and CBR for 5.08 mm (0.2 in) penetration

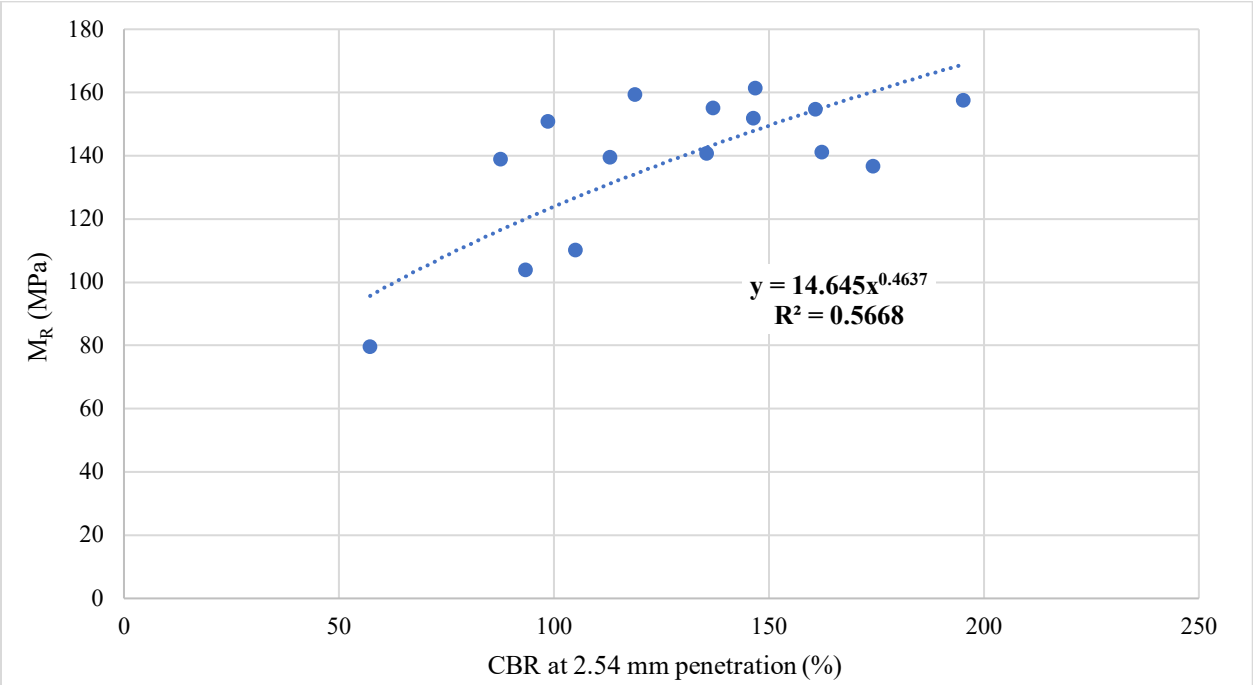

Figure 4.14 Correlation between SRM and CBR for 2.54 mm (0.1 in) penetration

4.10.2 Light Weight Deflectometer Results

The researcher conducted the LWD testing at Boise State University where LWD was available. Loose mixtures were transported to Boise and tests samples were prepared and tested there. In this study, three seating drops followed by three test drops were followed. This combination of loading is referred to as "3+3" which means three seating drops followed by three test drops. The first three drops were made for assuring full contact of the base plate and the aggregate surface and the following three for deflection calculation. In addition, two more drop combinations; "6+3" and "9+3" were applied on the same specimen. The loading designation "6+3" indicates six seating drops followed by three testing drops. While loading designation "9+3" indicates nine seating drops followed by three testing drops. The applied load and the obtained deflection data were used to obtain the modulus (E_{LWD}) value as outlined in the report of Schwartz et al. (2017). All the calculations associated with modulus calculations are performed with the associated software provided with the LWD device. A Poisson's ratio of 0.4 was assumed in this study which is a typical value for unbound granular materials. Table 4.10 summarizes the modulus values obtained by the LWD (E_{LWD}).

Table 4.10 LWD modulus (E_{LWD} [MPa]) of the test materials

Material ID	3+3 Drops	6+3 Drops	9+3 Drops
A	113.5	122.5	132.8
B	148.7	157.8	177.5
BK - 100	133.6	151.9	139.7
BR - 2	174.4	188.7	185.7
CS -184	140.8	141.7	142.1
EL - 132	140.8	147.3	151.0
IMC - 140	110.4	122.8	124.0
KT - 215	146.5	157.5	161.0
LE - 160	150.6	173.8	174.8
LN - 80	135.5	144.1	139.7
NP - 82	159.9	161.6	161.1
PW - 84	80.2	89.0	91.4
VY - 63	145.8	147.8	162.6
WCW	136.1	156.8	162.1
CN -148 SB	145.0	154.7	161.1
CS -184 SB	33.9	32.7	34.1

The results from Table 4.10 showed that the E_{LWD} increased when the drop combination was shifted changed from "3+3 drops" to "6+3 drops". Same trend also observed when there was shift from "6+3 drops" to "9+3 drops". The modulus increased with the increase of test drops as a result of reduction in deformation for most of test specimens. However, four test materials (e.g., BK – 100, BR – 2, LN – 80, and NP – 82) didn't experience increase in modulus when the number of test drops increased from six to nine. This could be due to over compaction. Similar to resilient modulus test "BR – 2" had the highest ELWD values while test material "CS – 184 SB" had the lowest E_{LWD}.

The statistical analysis of "*t-test"* demonstrated that the there is significant difference between the results of "3+3" combination compared to "6+3" combinations (*p-value* = 0.0001), and "3+3" combination compared to "9+3" combinations (*p-value* = 0.0001), while there was no significant different between "6+3" and "9+3" test results (*p-value* = 0.115).

Figure 4.15 through 4.17 show the correlation between SRM and E_{LWD} at "3+3", "6+3", and "9+3" loading combinations, respectively. The coefficient of determination (R^2) for such correlation was higher (0.827) for the "9+3" combination compared to the other two

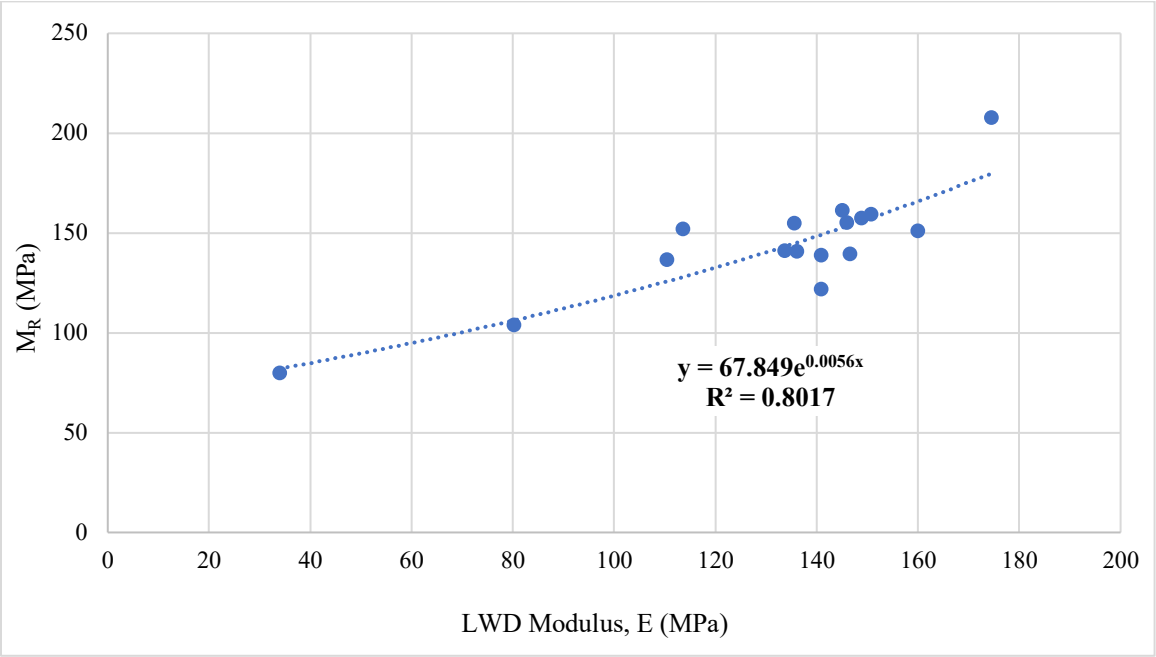

Figure 4.15 Correlation between SRM and LWD modulus (3+3 drops)

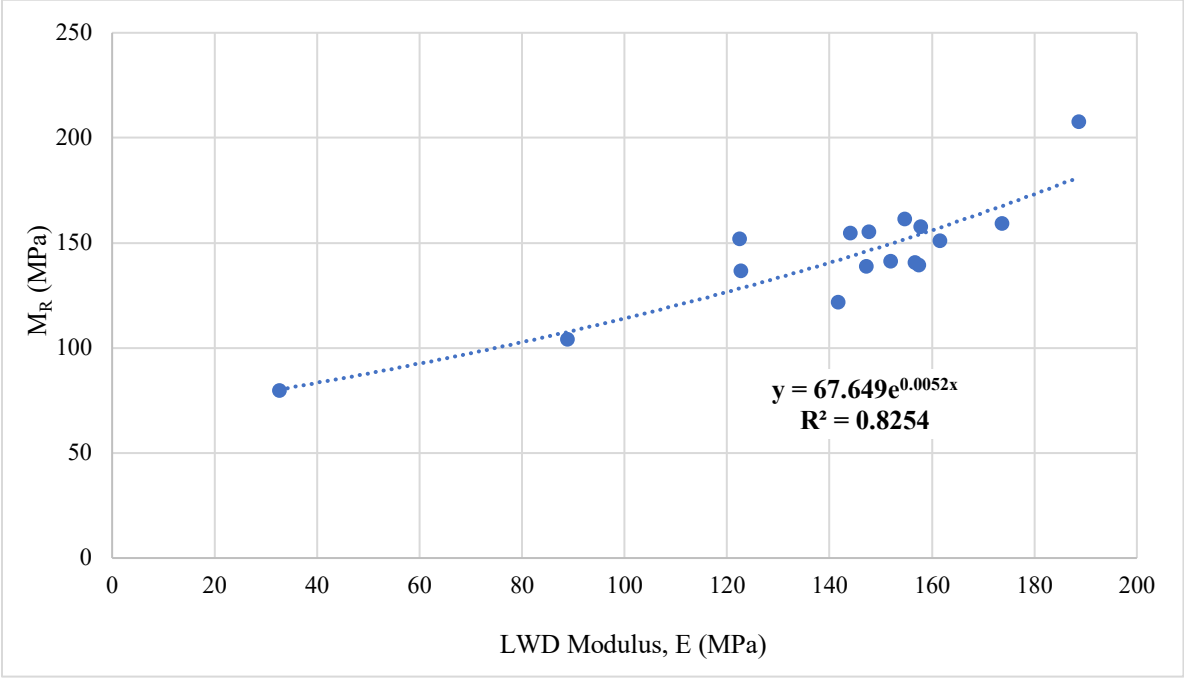

Figure 4.16 Correlation between SRM and LWD modulus (6+3 drops)

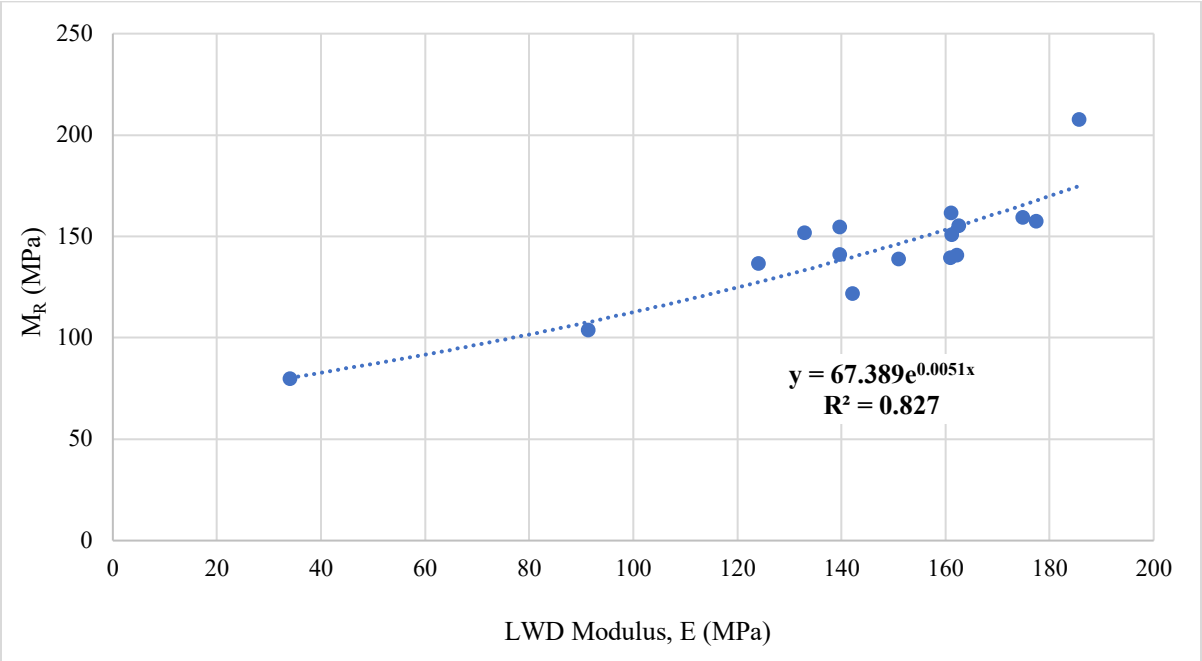

Figure 4.17 Correlation with SRM and LWD modulus (9+3 drops)

combinations. The statistical analysis for these three correlations is provided in Table 4.11 below. For all different combination, the *p-value* was less than 0.05 which means that SRM and E_{LWD} are significantly correlated. Meanwhile, the relationship of SRM and modulus obtained from "9+3" combination had the least summation of squared errors.

Table 4.11 Statistical analysis correlation between SRM and E_{LWD}

Variables		R^2	SSE	*p-value*
SRM	E_{LWD} (3+3 drops)	0.8017	0.131786	3.87E-16
SRM	E_{LWD} (6+3 drops)	0.8254	0.115982	1.4E-16
SRM	E_{LWD} (9+3 drops)	0.827	0.114921	1.4E-16

It is evident from the Figure 4.15, 4.16 and 4.17, that the relationship between the SRM and the E_{LWD} obtained from the "9+3 drops" yielded higher coefficient of determination (R^2) value of 0.827 compare to other two R^2 values (0.8017 and 0.8254) with an exponential relationship. For all cases, the *p-value* is less than 0.05, means M_R and E_{LWD} values are significantly correlated. The proposed correlation is presented in Equation 4.9.

$$SRM = 67.389\ e^{0.0051\ E_{LWD}} \quad (4.9)$$

where,

SRM = summary resilient modulus in MPa

E_{LWD} = the modulus in MPa calculated using LWD of "9+3" loading combination.

From Figure 4.17, the SRM and E_{LWD} has nonlinear (exponential) relationship. As the E_{LWD} increases, the SRM also increases proportionally. The goodness of fit (R^2 = 0.827) of Equation 4.9 proposed in this study is higher compared to the one obtained by Schwartz et al. (2017). Schwartz reported R^2 of 0.73 for the correlations between resilient modulus and E_{LWD}. Meanwhile, the researcher recommends validating Equation 4.9 with additional materials from different sources and types.

CHAPTER 5 CONCLUSIONS

5.1 Summary

The resilient modulus is a primary parameter needed for base and subbase materials in MEPDG. This study aimed to populate a database of resilient modulus values for the most common base and subbase materials used in the state of Idaho. This study evaluated 18 base and subbase materials from the six ITD highway districts. The resilient modulus test was conducted in accordance with AASHTO T 307 test standard. The deformation of the test specimens was measured using both internal and external LVDTs. At least two replicates of 152.4 mm (6 in) in diameter and 304.8 mm (12 in) in height were tested from each material type. In addition, basic materials properties (e.g., grain size distribution, Atterberg limits, optimum moisture content [OMC], maximum dry density [MDD]) were also determined for the test materials.

A model was developed for predicting the summary resilient modulus using material parameters that can be easily measured. In addition, a predictive model for the resilient modulus as a function of stress state was also proposed. The latter model overcomes the limitations of the former model in terms of predicting resilient modulus at all stress states, as documented in AASHTO T 307 while the former model can only predict the resilient modulus at only one state. These predictive models will help to generate Level 1 input for the MEPDG.

The strength index properties of the aggregates such as CBR and LWD modulus were also determined. Correlations between resilient modulus and strength index properties were also explored. Such correlations can provide Level 2 input for the MEPDG.

5.2 Findings

Based on the results of this study, the research findings are summarized below:

Laboratory Test Results

- Direct measurement of resilient properties of aggregates is quite expensive, time-consuming and very complex to conduct. The developed prediction models of resilient modulus shall assist transportation agencies to accurately estimate the resilient modulus

values for coarse unbound materials from basic properties that are typically determined from compaction and gradation tests.

- The internally-measured resilient modulus was about 24% (on average) higher than the externally-measured resilient modulus. The ratio of internal to externally measured resilient modulus had a range of 0.97 to 2.37. All the internally-measured summary resilient modulus values were higher than the externally-measured ones.

- The recoverable deformations measured using the external LVDTs were higher compare to the ones measured by the internal LVDTs (middle half length). The higher recoverable deformations resulted in lower externally-measured resilient modulus and vice versa.

- The stress dependency of resilient modulus of the unbound aggregates was examined and evaluated using four constitutive models: (1) K-θ model, (2) Uzan model, (3) Modified Uzan model, and (4) MEPDG model. The goodness of fit (R^2) was higher than 0.9 for all the models except for the K-θ model. The incorporation of the deviatoric stress yielded higher R^2 values for the other three models (i.e., Uzan model, Modified Uzan model, and MEPDG model).

Development of Prediction Model

- A summary resilient modulus prediction model was developed as a function of material properties including maximum dry density, optimum moisture content, particle diameter corresponding to 10% and 30% finer and percent passing through 4.75 mm (#4) sieve. The model provided good correlation with the laboratory-measured resilient modulus for typical unbound materials used in road construction in Idaho.

- Predictive models were also developed to predict the regressions parameters of the MEPDG model for resilient modulus at various stress states. These models showed good correlations with the laboratory-measured resilient modulus.

- The summary resilient modulus prediction model provides an estimate for the resilient modulus at a single stress state. Whereas, the predictive models for the MEPDG regression model for resilient modulus provides estimates for the resilient modulus at

any stress states thus it is more recommended over the summary resilient modulus prediction model.

- The developed prediction models can be used to estimate the unbound materials resilient modulus values for Level 1 input in the AASHTOWare Pavement ME Design (PMED) software.

Correlation with Index Properties

- Modulus values obtained from LWD were correlated with measured resilient modulus. Such correlation was found to predict the resilient modulus with a reasonable accuracy (R^2 = 0.82). This correlation can be used as Level 2 input in MEPDG. However, it is strongly recommended to validate this correlation with more materials from different sources and types.

- The CBR data were used to develop a correlation between resilient modulus and CBR. This correlation equation can predict resilient modulus with fair accuracy (R^2 = 0.56).

5.3 Recommendations for Future Work

- The sensitivity of resilient modulus to moisture content of base and subbase materials should be investigated.
- The effect of adding plastic fines up to certain limit in base and subbase should be investigated.
- The correlation between resilient modulus and LWD modulus could be further validated at different levels of compaction and moisture content as well as including more materials of different sources and types.
- Aggregate shape properties such as angularity, roughness, toughness can be incorporated in prediction models for resilient modulus.
- More resilient modulus tests should be conducted on Idaho aggregates with a view to improving the predictions models proposed in this study.

REFERENCES

Adu-Osei, A. (2000). *Characterization of Unbound Granular Materials*. Doctoral dissertation. Department of Civil Engineering, Texas A&M University, College Station, Texas.

Allen, J. (1973). *The Effect of Non-Constant Lateral Pressures of the Resilient Response of Granular Materials.* Doctoral dissertation, University of Illinois at Urbana-Champaign, Urbana, Illinois.

Allen, J.J. and Thompson, M.R. (1974). Resilient Response of Granular Materials Subjected to Time Dependent Lateral Stresses*, Transportation Research Record,* 510, 1-13. Transportation Research Board, Washington, D.C.

Amber, Y., and H. L. Von Quintus. (2002). *Study of LTPP Laboratory Resilient Modulus Test Data and Response Characteristics*, Report FHWA-RD-02-051, Federal Highway Administration, Washington, D.C.

American Association of State Highway and Transportation Officials (AASHTO) (2010a). *Determining the Liquid Limits of Soils.* T 89. Standard Specifications for Transportation Materials and Methods of Sampling and Testing: Part 2A Tests. American Association of State Highway and Transportation Officials, Washington D.C.

American Association of State Highway and Transportation Officials (AASHTO) (2010b). *Moisture-Density Relations of Soils Using a 2.5-kg (5.5 lb) Rammer and a 305-mm (12-in.) Drop.* T 99. Standard Specifications for Transportation Materials and Methods of Sampling and Testing: Part 2A Tests. American Association of State Highway and Transportation Officials, Washington D.C.

American Association of State Highway and Transportation Officials (AASHTO) (2010c). *Moisture-Density Relations of Soils Using a 4.54-kg (10 lb) Rammer and a 457-mm (18-in.) Drop.* T 180. Standard Specifications for Transportation Materials and Methods of Sampling and Testing: Part 2A Tests. American Association of State Highway and Transportation Officials, Washington D.C.

American Association of State Highway and Transportation Officials (AASHTO) (2010d). *The California Bearing Ratio.* T 193. Standard Specifications for Transportation Materials and Methods of Sampling and Testing: Part 2A Tests. American Association of State Highway and Transportation Officials, Washington D.C.

American Association of State Highway and Transportation Officials (AASHTO) (2012). *Laboratory Determination of Moisture Content of Soils.* T 265. Standard Specifications for Transportation Materials and Methods of Sampling and Testing: Part 2B Tests. American Association of State Highway and Transportation Officials, Washington D.C.

American Association of State Highway and Transportation Officials (AASHTO) (2011). *Sieve Analysis of Fine and Coarse Aggregates.* T 27. Standard Specifications for Transportation Materials and Methods of Sampling and Testing: Part 2A Tests. American Association of State Highway and Transportation Officials, Washington D.C.

American Association of State Highway and Transportation Officials (AASHTO) (1999). *Determining the Resilient Modulus of Soils and Aggregate Materials.* T 307. Standard Specifications for Transportation Materials and Methods of Sampling and Testing: Part 2B Tests. American Association of State Highway and Transportation Officials, Washington D.C.

American Association of State Highway and Transportation Officials (AASHTO) (2000). *Determining the Plastic Limit and Plasticity Index of Soils.* T 90. Standard Specifications for Transportation Materials and Methods of Sampling and Testing: Part 2A Tests. American Association of State Highway and Transportation Officials, Washington D.C.

American Association of State Highway and Transportation Officials (AASHTO) (1993). *AASHTO Guide for Design of Pavement Structures*. American State Highway and Transportation Officials, Washington D.C.

American Association of State Highway and Transportation Officials (AASHTO) (1991). *The Classification of Soils and Soil-Aggregate Mixtures for Highway Construction Purposes.* M 145. Standard Specifications for Transportation Materials and Methods of Sampling and Testing: Part 1A Specifications and Practices. American Association of State Highway and Transportation Officials, Washington D.C.

American Association of State Highway and Transportation Officials (AASHTO) (2015). *Mechanistic-Empirical Pavement Design Guide: A Manual of Practice.* MEPDG-2. American Association of State Highway and Transportation Officials, Washington D.C.

American Society of Testing and Materials (ASTM) (2007). Standard Test Method for Measuring Deflections with a Light Weight Deflectometer (LWD). E2583. Annual Book of ASTM Standards, American Society of Testing and Materials, West Conshohocken, Pennsylvania

ARA Inc. (2004). *NCHRP 1-37A: Guide for Mechanistic-Empirical Pavement Design of New and Rehabilitated Pavement Structures*, Final Report 1-37A, National Cooperative Highway Research Program, Federal Highway Administration, Washington, DC.

Barksdale, R. D. (1971). Compressive Pulse Times in Flexible Pavements for Use in Dynamic Testing. *Highway Research Record No. 345*, Highway Research Board, National Research Council, Washington, D.C.

Barksdale, R.D. and Itani, S.Y. (1989). Influence of Aggregate Shape on Base Behavior, *Transportation Research Record,* 1227, 173-182. Transportation Research Board, Washington, D.C.

Bejarano, M., Heath, A., and Harvey, J., (2003). A Low-cost High-performance Alternative for Controlling a Servohydraulic System for Triaxial Resilient Modulus Apparatus, ASTM Special Technical Publication,1437: 129–140.

Biarez, J. (1961). *Contribution on 1 etude des properietes mechaniques des sols et des materiaux pulverulents,* Doctoral dissertation, University of Grenoble, France.

Bishop, A. W. and Green, G. E. (1965). "The Influence of End Restraint on the Compression Strength of a Cohesionless Soil." *Geotechnique*, 15(3), 243- 265.

Boudreau, R., and Wang, J., (2003). Resilient Modulus Test– Triaxial Cell Interaction. *ASTM Special Technical Publication,* 1437: 176–188. https://doi.org/10.1520/STP12531S

Boyce, J. R. (1976). *The Behavior of a Granular Material Under Repeated Load.* Doctoral dissertation, University of Nottingham, Department of Civil Engineering, U.K.

Boyce, J. R., Brown, S. F. and Pell, P. S. (1976). The resilient Behavior of a Granular Material Under Repeated Loading. *Proceedings, Australia Road Research Board*, 28, pp. 8-19.

Boyce, J.R. (1980). *A Nonlinear Model for the Elastic Behavior of Granular Materials Under Repeated Loading.* International Symposium on Soils Under Cyclic and Transient Loading, Swansea.

Brown, S. F. (1996). Soil Mechanics in Pavement Engineering. *Geotechnique*. 46 (3), 383-426.

Brown, S. F., O'Reilly, M. P., and Pappin, J. W. (1989). *A Repeated Load Triaxial Apparatus for granular Materials.* Unbound Aggregates in Roads, London, Butterworth, pp. 143-158.

Camargo, F., Benson, C. and Edil, T. (2012). An Assessment of Resilient Modulus Testing: Internal and External Deflection Measurements. *Geotechnical Testing Journal*, 35(6): 837-844. https://doi.org/10.1520/GTJ20120077

Carmichael, III, R. F., and Stuart, E. (1978). Predicting Resilient Modulus: A Study to Determine the Mechanical Properties of Subgrade Soils, *Transportation Research Record*, 1043, 20-28. Transportation Research Board, Washington, D.C.

Ceylan, H., & Kim, K. G. S. (2009). *Characterization of Unbound Materials (Soils / Aggregates) for Mechanistic-Empirical Pavement Design Guide*. Center for Transportation Research and Education, Iowa State University: Iowa Department of Transportation.

Ceylan, H., & Kim, K. G. S. (2009). *Characterization of Unbound Materials (Soils / Aggregates) for Mechanistic-Empirical Pavement Design Guide*. Center for Transportation Research and Education, Iowa State University: Iowa Department of Transportation.

Crockford, W.W., L.J. Bendana, W.S. Yang, S.K. Rhee, and S.P. Senadheera, (1990). *Modeling Stress and Strain States in Pavement Structures Incorporating Thick Granular Layers,* Final Report F08635-87-C-0039, The Texas Transportation Institute, The Texas A&M University, College Station, Texas.

Cunningham, C. N., Evans, T. M., and Tayebali, A. A. (2013). Gradation Effects on the Mechanical Response of Crushed Stone Aggregate*, International Journal of Pavement Engineering*, 14(3), 231-241.

Dawson, A.R., Thom, N.H., and Paute, J.L. (1996). Mechanical Characteristics of Unbound Granular Materials as a Function of Condition*,* Flexible Pavements, *Proceedings of European Symposium Euroflex 1993*, A.G. Correia, ed., Balkema, Rotterdam, The Netherlands, pp. 35-44.

Dehlen, G. L. (1969). *The effect of non-linear material response on the behavior of pavements subjected to traffic loads,* Doctoral dissertation, University of California, Berkeley, Berkeley, California.

Dione, A., Fall, F., Berthaud, Y., Benboudjema, F., and Michou, A. (2015). Implementation of Resilient Modulus - CBR relationship in Mechanistic-Empirical (M. -E) Pavement Design. Revue Cames – Sci. Appl. & de l'Ing., Vol. 1(2), 65-71. ISSN 2312-8712.

Drumm, E., Boateng-Poku, Y., and Johnson Pierce, T. (1990). Estimation of Subgrade Resilient Modulus from Standard Tests*, Journal of Geotechnical Engineering*, 116(5), 774-789.

Duncan, J. M. and Dunlop, P. (1968). "The Significance of Cap and Base Restraint." *Journal of the Soil Mechanics and Foundations Division*, ASCE, 94(1), 271-290.

Dunlap, W.S. (1963). *A Report on a Mathematical Model Describing the Deformation Characteristics of Granular Materials.* Technical Report 1, Project 2-8-62-27, Texas Transportation Institute, Texas A&M University, College Station, Texas.

Elias, Mohammed & Titi, Hani. (2006). Evaluation of Resilient Modulus Model Parameters for Mechanistic–Empirical Pavement Design. *Transportation Research Record*, 1967, 89-100. Transportation Research Board. Washington D.C. doi: 10.1177/0361198106196700110

Elliot, R.P. and Thornton, S.I. (1988). Resilient Modulus and AASHTO Pavement Design, *Transportation Research Record*, 1196, 116-124. Transportation Research Board, Washington D.C.

Erlingsson, Sigurdur. (2007). On Forecasting the Resilient Modulus from the CBR Value of Granular Bases. *Road Materials and Pavement Design*. 8, 783-797. doi: 10.1080/14680629.2007.9690099

Farrar, M. J., and Turner, J. P. (1991). *Resilient Modulus of Wyoming Subgrade Soils*. Report No. 91-1, Mountain Plains Consortium, University of Wyoming, Laramie, Wyoming.

Figueroa, J. L., and Thompson, M. R. (1980). Simplified Structural Analysis of Flexible Pavements for Secondary Roads Based on ILLI-PAVE, *Transportation Research Record*, 776,17-23. Transportation Research Board, Washington D.C.

George, K. P. (2004). *Resilient Modulus Prediction Employing Soil Index Properties.* Report No. FHWA/MS-DOT-RD-04-172, Mississippi Department of Transportation, Jackson, Mississippi.

Goto, S., Tatsuoka, F., Shibuya, S., Kim, Y., and Sato, T., (1991). A Simple Gauge for Local Small Strain Measurements in the Laboratory. *J-STAGE Journal of Soils and Foundations*, 31(1): 169–180.

Gray, J.E., (1962). Characteristics of Graded Base Course Aggregates Determined by Triaxial Tests*, Engineering Research Bulletin No. 12*, National Crushed Stone Association.

Hajj, Elie Y., Thavathurairaja, Jeyakaran, Stolte, Sarah, E. Sebaaly, Peter, Piratheepan, Murugaiyah, and Motamed, Ramin. (2018). *Resilient Modulus Prediction Models of Unbound Materials for Nevada.* Final Report: P224-14-803. University of Nevada, Nevada Department of Transportation.

Heukelom W. and Foster (1960). Dynamic Testing of Pavement. *Journal of the Structural Division, ASCE*, SM 1, 86.

Heukelom, W., and Klomp, A J. G. (1962). Dynamic Testing as a Means of Controlling Pavements during and after Construction*, Proceedings of the First International Conference on Structural Design of Asphalt Pavements*, University of Michigan, Ann Arbor, Michigan.

Hicks, R. G. (1970). *Factors Influencing the Resilient Properties of Granular Materials*. Doctoral dissertation. University of California, Berkeley, California.

Hicks, R.G. and Monismith, C.L. (1971). *Factors Influencing the Resilient Properties of Granular Materials, Transportation Research Record*, 345, 15-31. Transportation Research Board, Washington D.C.

Hines, W. W., and Montgomery, D. C. (1980). *Probability and Statistics in Engineering and Management Science,* 2nd ed. John Wiley & Sons Inc., New York.

Holubec, I. (1969). Cyclic Creep of Granular Materials. *Report No. RR147*, Department of Highways, Ontario, Canada.

Hossain, Z., M. Zaman, and C. Doiron (2013). Mechanistic Empirical Pavement Design Guide Input Parameters for Unbound Aggregates in Oklahoma. *In Proceedings of the Second International Conference on Geotechnical and Earthquake Engineering*, China, International Association of Chinese Geotechnical Engineers (IACGE), pp. 578–585. https://doi.org/10.1520/STP12527S

Huang, Y. H. (2004). *Pavement Analysis and Design*, 2nd Ed., Upper Saddle River, New Jersey.

Itani, S.Y. (1990). *Behavior of Base Materials Containing Large-Sized Particles.* Doctoral dissertation, School of Civil and Environmental Engineering, Georgia Institute of Technology, Georgia.

Jackson, K. D. (2015). *Laboratory Resilient Modulus Measurements of Aggregate Base Materials in Utah,* MS Thesis, Brigham Young University, Provo, Utah.

Jardine, R., Symes, M., and Burland, J., (1984). The Measurement of Soil Stiffness in the Triaxial Apparatus," *Geotechnique*, 34(3), 323–340.

Kamal, M.A., Dawson, A.R., Faroi, O.T., Hughes, D.A.B., and Sha'at, A.A. (1993). Field and Laboratory Evaluation of the Mechanical Behavior of Unbound Granular Materials in Pavements. *Transportation Research Record*, 1406, 88-97. Transportation Research Board, Washington D.C.

Kirkpatrick, W. M. (1965). Effects of Grain Size and Grading on the Shearing Behavior of Granular Materials. *Proceedings of the 6th International Conference on Soil Mechanics and Foundation Engineering*, University of Toronto, Montreal, Quebec, 1, pp. 273-277.

Knight, J.A. (1935). Gradation of aggregate as applied to stabilization of gravel roads. *Canadian Engineer*, 69(23) 9–10, 13.

Knutson, R.M. and Thompson, M.R. (1977). Resilient Response of Railway Ballast. *Transportation Research Record*, 651, 31-39. Transportation Research Board, Washington, D.C.

Kolisoja, P. (1997). *Resilient Deformation Characteristics of Granular Materials*. Doctoral dissertation. Tampere University of Technology, Publication No 223, Tampere, Finland.

Kutner, M. H.; Nachtsheim, C. J.; Neter, J. (2004). *Applied Linear Regression Models* (4th ed.). McGraw-Hill Irwin.

Kyalham, V., and Willis, M. (2001). Predictive Equations for Determination of Resilient Modulus, Suitability of Using California Bearing Ratio Test to Predict Resilient Modulus, *Proceedings of the Federal Aviation Administration Airport Technology Transfer Conference*, Galloway, New Jersey.

Lade, P.V. and R.B. Nelson, (1987). Modeling the Elastic Behavior of Granular Materials. *International Journal for Numerical and Analytical Methods in Geomechanics*, 11, 521-542.

Lee, K. L. and Frank J. Vernese. (1978). End Restraint Effects on Cyclic Triaxial Strength of Sand. *Journal of the Geotechnical Division, ASCE*, GT6, 705-719.

Lekarp, F., U. Isacsson, & A. Dawson. (2000). State of the art. I: Resilient response of unbound aggregates. *Journal of Transportation Engineering*, *ASCE,* 126(1), 66-75.

Leslie, D. (1963). Large Scale Triaxial Tests on Gravelly Soils, *Proceedings of the 2nd Pan-american Conference on Soil Mechanics and Foundation Engineering*, Rio de Janeiro, Brazil, 1, pp. 181-202.

Lister, N. W. and Powell, D. (1987). Design Practices for Pavement in the United Kingdom. *Proceedings to 6th Internal Conference of the Structural Design of Asphalt Pavements*, University of Michigan, Ann Arbor, Michigan.

Lytton, R.L., (1987). Foundations and Pavements on Unsaturated Soils. *1st International Conference on Unsaturated Soils*, Paris, France.

Minitab Inc. (2017). *Minitab 18 Statistical Software.* [Computer Software]. State College, PA (www.minitab.com)

Mitry, F. G. (1964). *Determination of the modulus of resilient deformation of untreated base course materials.* Doctoral dissertation, University of California, Berkeley, Berkeley, California.

Mohammad, L.N., Herath, A., Gudishala, R., Nazzal, M.D., Abu-Farsakh, M.Y., Alshibli, K. (2008). *Development of models to estimate the subgrade and subbase layers' resilient modulus from in situ devices test results for construction control*. Publication FHW-LA-406. FHWA, U.S. Department of Transportation.

Monismith, C. L., D. A. Kasianchuk, and J. A. Epps. (1967). *Asphalt mixture behavior in repeated flexural: A study on in-service pavement near Morro Bay, California.* IER Report TE67-4. University of California, Berkeley, CA.

Moossazadeh, J., & M. W. Witczak, (1981). Prediction of subgrade moduli for soil that exhibits nonlinear behavior. *Transportation Research Record* 810, 9-17. Transportation Research Board, Washington, D.C.

Morgan, J.R. (1966). The response of granular materials to repeated loading. *Proceedings of the 3rd Conference of ARRB*, pp. 1178-1192.

Mousavi, S. Hamed, Gabr, Mohammed A., Borden, Roy H. (2017). Subgrade resilient modulus prediction using light-weight deflectometer data. *Canadian Geotechnical Journal*, 54:304-312, https://doi.org/10.1139/cgj-2016-0062

Ni, B., T.C. Hopkins, L. Sun, and T.L. Beckham (2002). Modeling the Resilient Modulus of Soils. *Proceedings of the 6th International Conference on the Bearing Capacity of Roads,* Railways, and Airfields, Vol. 2, A.A. Balkema Publishers, Rotterdam, the Netherlands, pp. 1131–1142.

Ooi, P.S.K., A.R. Archilla, and K.G. Sandefur (2004). Resilient Modulus for Compacted Cohesive Soils. *Transportation Research Record*, 1874, 115-124, Transportation Research Board, Washington, D.C.

Osouli, A., Salam, S., Othmanawny, G., Tutumluer, E., Beshears, S., Shoup, H., and Eck, M. (2017). Soaked and Unsoaked CBR Test Results on Unbound Aggregates with Varying Amounts of Fines and Dust Ratios. *Transportation Research Record*, 2655. 13-19, Transportation Research Board, Washington, D.C.

Pappin, J. W. (1979). *Characteristics of a Granular Material for Pavement Analysis.* Doctoral dissertation, University of Nottingham, Department of Civil Engineering, U.K.

Paterson, W.D.L., and Maree, J.H. (1978). *An Interim Mechanistic Procedure for the Structural Design Pavements*. National Institute for Transport and Road Research, Pretoria, South Africa.

Pezo, R.F. (1993). *A General Method of Reporting Resilient Modulus Tests of Soils—A Pavement Engineer's Point of View*. Paper No: 93082, presented at 72nd Annual Meeting of the Transportation Research Board, Washington, D.C.

Ping, W. and Ge, L., (1996). Evaluation of Resilient Modulus of Cemented Limerock Base Materials in Florida. *Transportation Research Record, 1546, 1-12,* Transportation Research Board, Washington, D.C. https://doi.org/10.3141/1546-01

Ping, W. V., Xiong, W. and Yang, Z. (2003). *Implementing Resilient Modulus Test for Design of Pavement Structure in Florida.* Final Report: FL/DOT/RMC/BC-352-6(F), Research Center, MS30, Florida Department of Transportation, Tallahassee, Florida.

Puppala, A.J., (2008). *Estimating Stiffness of Subgrade and Unbound Materials for Pavement Design,* National Cooperative Highway Research Program (NCHRP) Synthesis No. 382, Transportation Research Board of the National Academies, Washington, D.C.

Rada, G., and Witczak, M. W. (1982). Material Layer Coefficients of Unbound Granular Materials from Resilient Modulus. *Transportation Research Record*, 852, 15-21. Transportation Research Board, Washington, D.C.

Radjai, F., Wolf, D. E., Jean, M., and Moreau, J. J. (1998). Bimodal Character of Stress Transmission in Granular Packings. *Physical Review Letters*, 80(1), pp. 61-64.

Rahim, A. M. (2005). Subgrade Soil Index Properties to Estimate Resilient Modulus for Pavement Design. *International Journal of Pavement Engineering*, 6(3), 163-169.

Rao, C., Tutumluer, E. and Kim, I. T. (2002). Quantification of Coarse Aggregate Angularity Based on Image Analysis. *Transportation Research Record* 1787:117-124. Transportation Research Board, Washington D.C.

Rowe, P. W. and Barden, L. (1964). "Importance of Free Ends in Triaxial Testing." *Journal of the Soil Mechanics and Foundations Division*, ASCE, SM1, 1-27.

Rowshanzamir, M.A. (1995). *Resilient Cross-Anisotropic Behavior of Granular Base Materials Under Repetitive Loading.* Doctoral dissertation, University of New South Wales, School of Civil Engineering, Australia.

Schwartz, Charles W, Afsharikia, Zahra, and Khosravifar, Sadaf (2017). *Standardizing Light Weight Deflectometer Modulus Measurements for Compaction Quality Assurance.* Final Report, Contract No: TPF-5(285)/SP409B4P, University of Maryland, College Park, Maryland.

Seed, H. B., Mitry, F. G., Monismith, C. L., and Chan, C. K. (1967). *Prediction of flexible pavement deflections from laboratory repeated load tests*. NCHRP Report No. 35, National Cooperative Highway Research Program.

Seed, H. B., Mitry, F. G., Monismith, C. L., and Chan, C. K. (1965). *Predictions of pavement deflection from laboratory repeated load tests.* Report No. TE-65-6, Soil Mech. and Bituminous Mat. Res. Lab., University of California, Berkeley, Berkeley, California.

Seyhan, U. (2001). *Characterization of Anisotropic Granular Layer Behavior in Flexible Pavements.* Doctoral dissertation, University of Illinois at Urbana-Champaign, Urbana, Illinois.

Shackel, B. (1973), Repeated Loading of Soils–A Review. *Australian Road Research*, 5 (3), 22-49.

Sheather, S. (2009). *A modern approach to regression with R*. New York, NY: Springer. ISBN 978-0-387-09607-0.

Smith, W. S., and Nair, K. (1973). *Development of procedures for characterization of untreated granular base coarse and asphalt-treated base course materials.* Rep. No. FHWA-RD-74-61, Federal Highway Administration, Washington, D.C.

Sweere, G. T. H. (1990). *Unbound granular basis for roads.* Doctoral dissertation, University of Delft, Delft, The Netherlands.

Tatsuoka, F., Teachavorasinskun, S., Dong, J., Kohata, Y., and Sato, T. (1994) Importance of Measuring Local Strains in Cyclic Triaxial Tests on Granular Materials, *ASTM Special Technical Publication*, 1213: 288–302.

Taylor, A. (2008). *Mechanistic characterization of resilient moduli for unbound pavement layer materials.* Doctoral dissertation*,* Auburn University, Alabama.

Taylor, A. J., & Timm, D. H. (2009). *Mechanistic Characterization of Resilient Moduli for Unbound Pavement Layer Materials*. NCAT Report 09-06. National Center for Asphalt Technology, Auburn University, Alabama.

Taylor, D. W. (1941). *7th Progress Report on Shear Strength to U.S. Engineers.* Massachusetts Institute of Technology, Massachusetts.

Thom, N.H. (1988). *Design of Road Foundations.* Doctoral dissertation, University of Nottingham, Department of Civil Engineering, May, U.K.

Thom, N.H., and Brown, S.F. (1988). The Effect of Grading and Density on the Mechanical Properties of a Crushed Dolomitic Limestone. *Proceedings of the 14th ARRB Conference,* Part 7, pp. 94-100.

Tian, P., Zaman, M., and Laguros, J. (1998). Gradation and Moisture Effects on Resilient Moduli of Aggregate Bases. *Transportation Research Record*, 1619, 75-84, Transportation Research Board, Washington, D.C.

Tutumluer, E. (2013). *Practices for Unbound Aggregate Pavement Layers*. National Cooperative Highway Research Program (NCHRP) Synthesis No. 445, Transportation Research Board of the National Academies, Washington, D.C.

Tutumluer, E. and Seyhan, U. (1998). Neural Network Modeling of Anisotropic Aggregate Behavior from Repeated Load Triaxial Tests. *Transportation Research Record*, 1615, 86-93, Transportation Research Board, Washington, D.C.

Uzan, J. (1985). Characterization of Granular Material. *Transportation Research Record,* 1022, 52-59, Transportation Research Board, Washington, D.C.

Wambura, G. (2003). *Characterization of Unbound Pavement Materials for Mechanistic-Empirical Performance Prediction.* MS Thesis, University of Maryland, College Park.

Webb, W. M., and Campbell, B. E. (1986). *Preliminary Investigation into Resilient Modulus Testing for New AASHTO Pavement Design Guide.* Office of Materials and Research, Georgia Department of Transportation, Atlanta, Georgia.

White, D., Thompson, M., and Vennapusa, P. (2007). *Field validation of intelligent compaction monitoring technology for unbound materials*. Report No. MN/RC-2007-10. Department of Civil, Construction and Environmental Engineering, Iowa State University. Minnesota Department of Transportation.

Witczak, M. W. (2003). *NCHRP 1-28A: Harmonized Test Methods for Laboratory Determination of Resilient Modulus for Flexible Pavement Design*. Final Report 1-28A, National Cooperative Highway Research Program, Federal Highway Administration.

Witczak, M. W., Qi, X. and Mirza, M. W. (1995). Use of Nonlinear Subgrade Modulus in AASHTO Design Procedure. *Journal of Transportation Engineering*, ASCE. 121(3), 273.

Witczak, M.W. and J. Uzan, (1988). *The Universal Airport Pavement Design System, Report I of V: Granular Material Characterization.* University of Maryland, College Park, Maryland.

Yau, A. and Von Quintus, H. L. (2004). Predicting Elastic Response Characteristics of Unbound Materials and Soils, *Transportation Research Record*, 1874(1), 47–56. doi: 10.3141/1874-06.

Zaman, M., Chen, D., and Laquros, J. (1994). Resilient Moduli of Granular Materials. *Journal of Transportation Engineering*, 120(6), 967–988.

Zeghal, M. (2000). Variability of Resilient Moduli of Aggregate Materials Due to Different Gradations. *Proceedings of the Canadian Society for Civil Engineering Annual Conference*, National Research Council Canada Institute for Research in Construction, London, Ontario, pp. 363-367.

Appendix A: K - θ Model fitting

Table A.1: Regression coefficients for *"K - θ Model"*

Material ID	External Measurement			Internal Measurement		
	K (MPa)	n	R^2	K (MPa)	n	R^2
A	3.802	0.694	0.997	6.134	0.632	0.992
B	4.306	0.677	0.995	6.816	0.642	0.989
BK - 100	2.886	0.826	0.987	5.777	0.637	0.992
BK - 181	1.590	0.778	0.969	4.408	0.653	0.967
BR - 2	7.485	0.628	0.996	10.940	0.609	0.988
CS - 184	3.740	0.651	0.996	4.447	0.646	0.996
EL - 132	2.340	0.762	0.987	5.712	0.670	0.992
IMC - 140	3.047	0.710	0.991	6.615	0.651	0.985
KT - 215	1.662	0.803	0.945	6.314	0.625	0.995
LE - 160	4.702	0.661	0.997	7.506	0.615	0.992
LN - 80	3.067	0.723	0.971	7.134	0.608	0.991
NP - 82	4.323	0.672	0.998	5.499	0.646	0.988
PW -84	1.577	0.743	0.892	3.266	0.648	0.915
VY - 63	2.468	0.760	0.980	7.038	0.647	0.995
WCW	4.195	0.659	0.999	4.819	0.645	0.996
CN - 148 SB	5.644	0.635	0.992	7.539	0.603	0.977
CS - 184 SB	4.020	0.520	0.787	5.463	0.475	0.672
PY -720 SB	5.564	0.625	0.995	10.055	0.565	0.976

Graphical representation of *"k - θ Model"* fitting

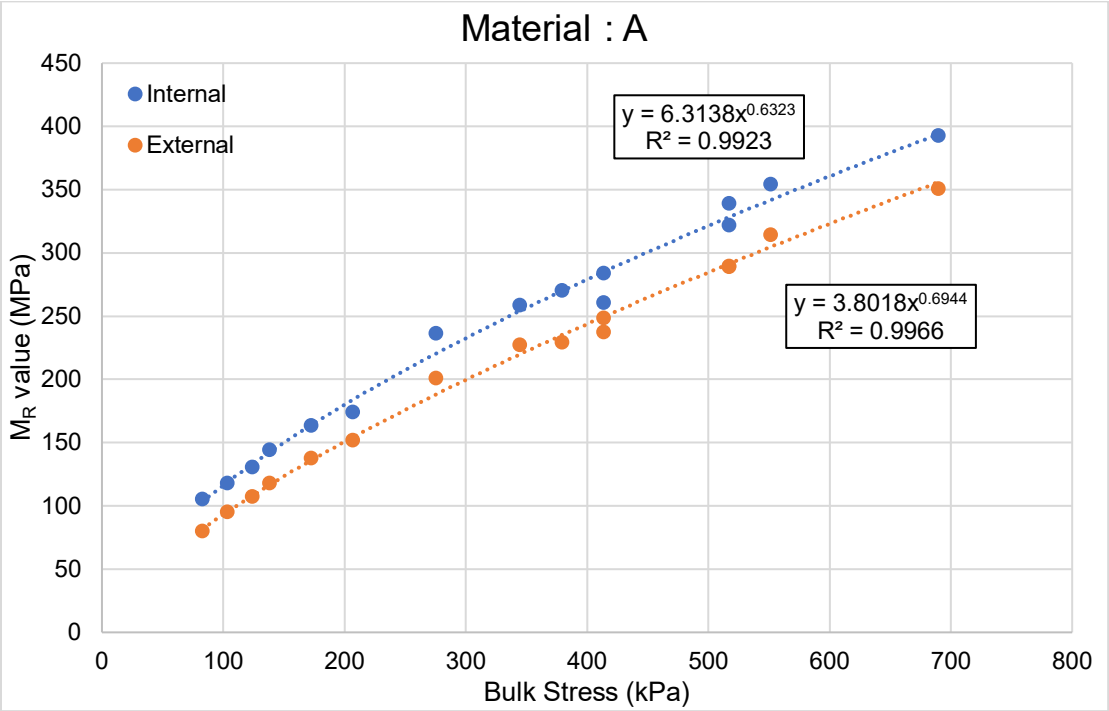
Material : A
Internal
External
y = 6.3138x^0.6323
R² = 0.9923
y = 3.8018x^0.6944
R² = 0.9966
M_R value (MPa)
Bulk Stress (kPa)
0
50
100
150
200
250
300
350
400
450
0
100
200
300
400
500
600
700
800

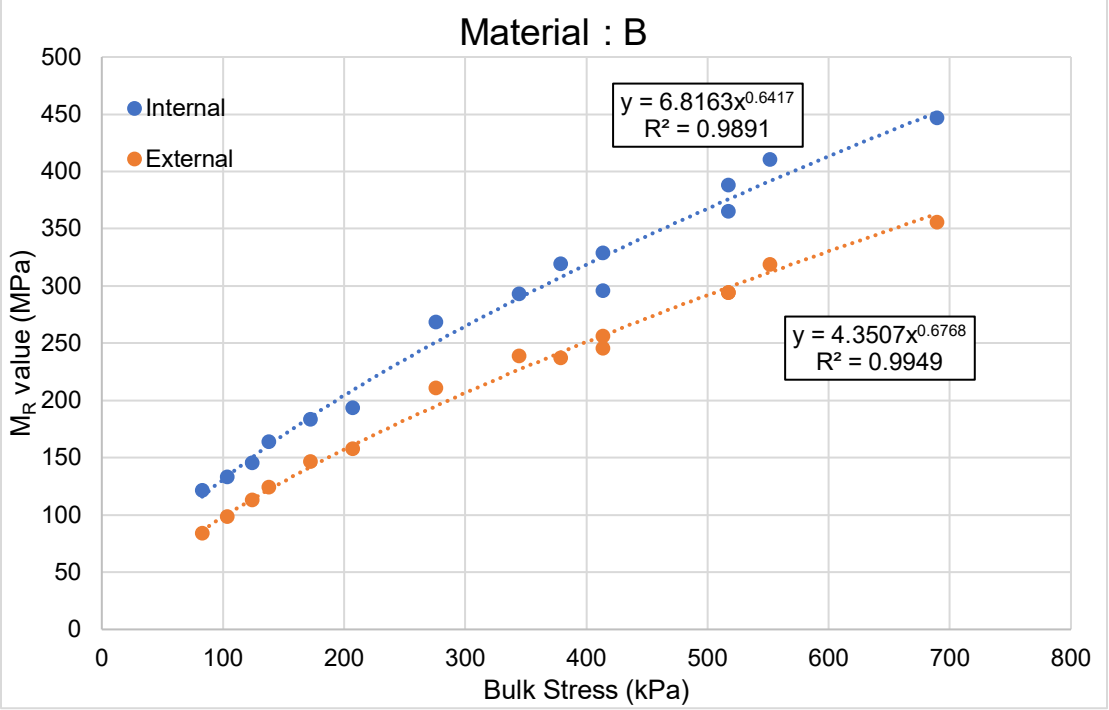
Material : B
Internal
External
y = 6.8163x^0.6417
R² = 0.9891
y = 4.3507x^0.6768
R² = 0.9949
M_R value (MPa)
Bulk Stress (kPa)
0
50
100
150
200
250
300
350
400
450
500
0
100
200
300
400
500
600
700
800

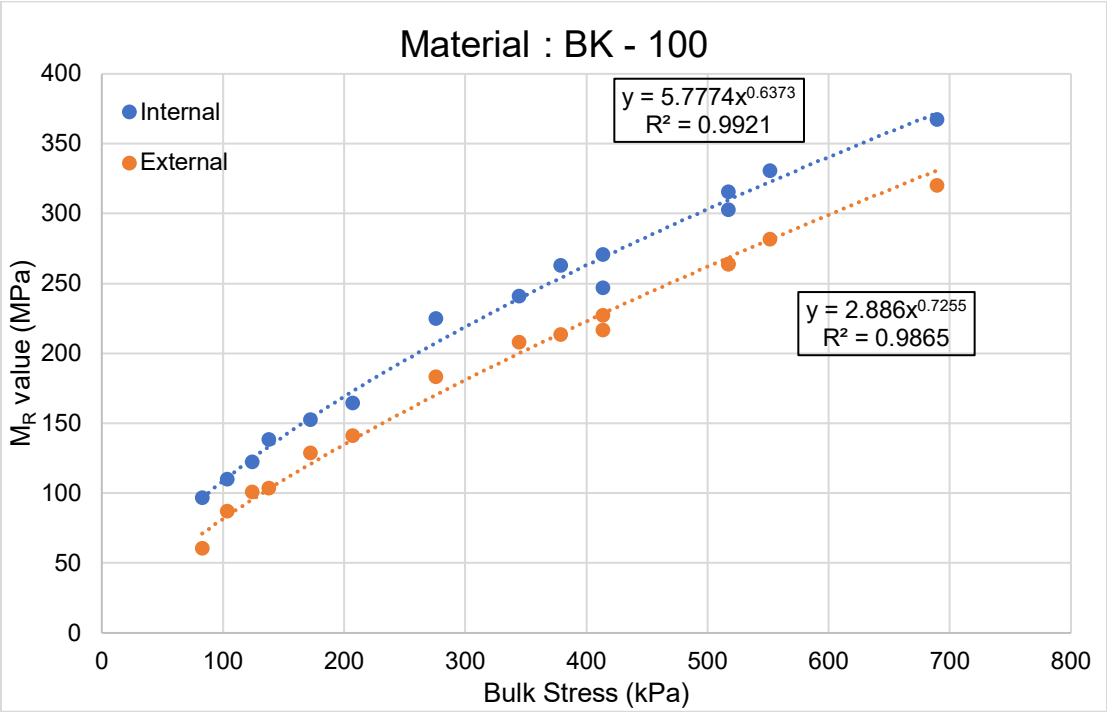
Material : BK - 100
Internal
External
y = 5.7774x^0.6373
R² = 0.9921
y = 2.886x^0.7255
R² = 0.9865
M_R value (MPa)
Bulk Stress (kPa)
0
50
100
150
200
250
300
350
400
0
100
200
300
400
500
600
700
800

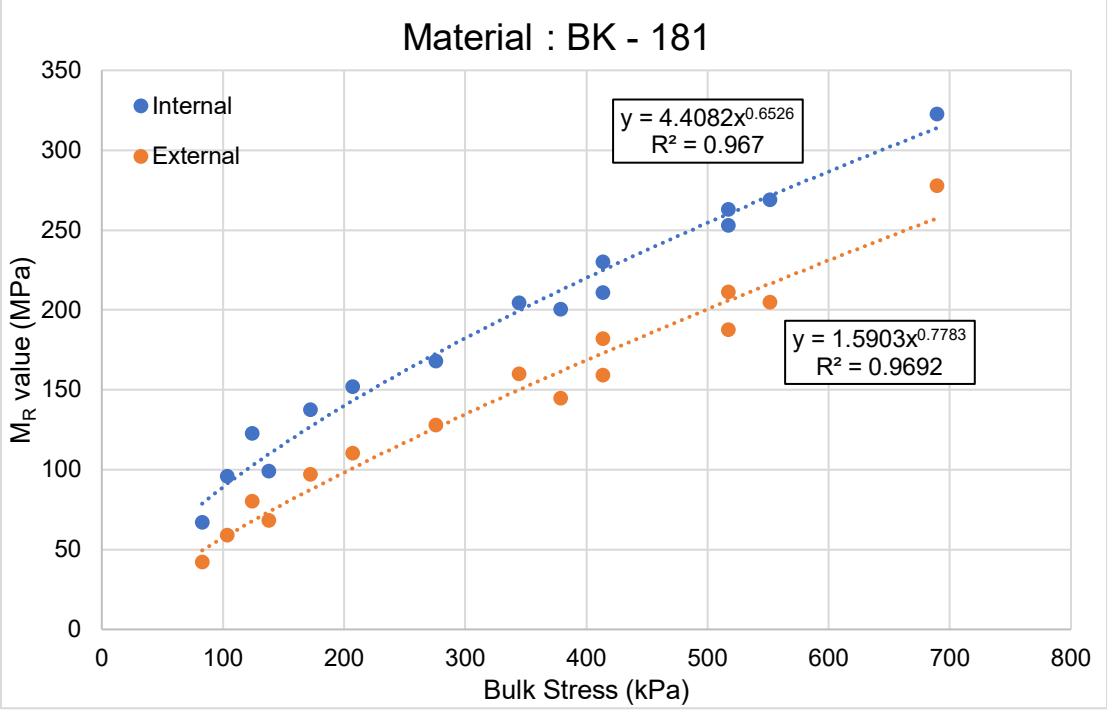
Material : BK - 181
Internal
External
y = 4.4082x^0.6526
R² = 0.967
y = 1.5903x^0.7783
R² = 0.9692
M_R value (MPa)
Bulk Stress (kPa)
0
50
100
150
200
250
300
350
0
100
200
300
400
500
600
700
800

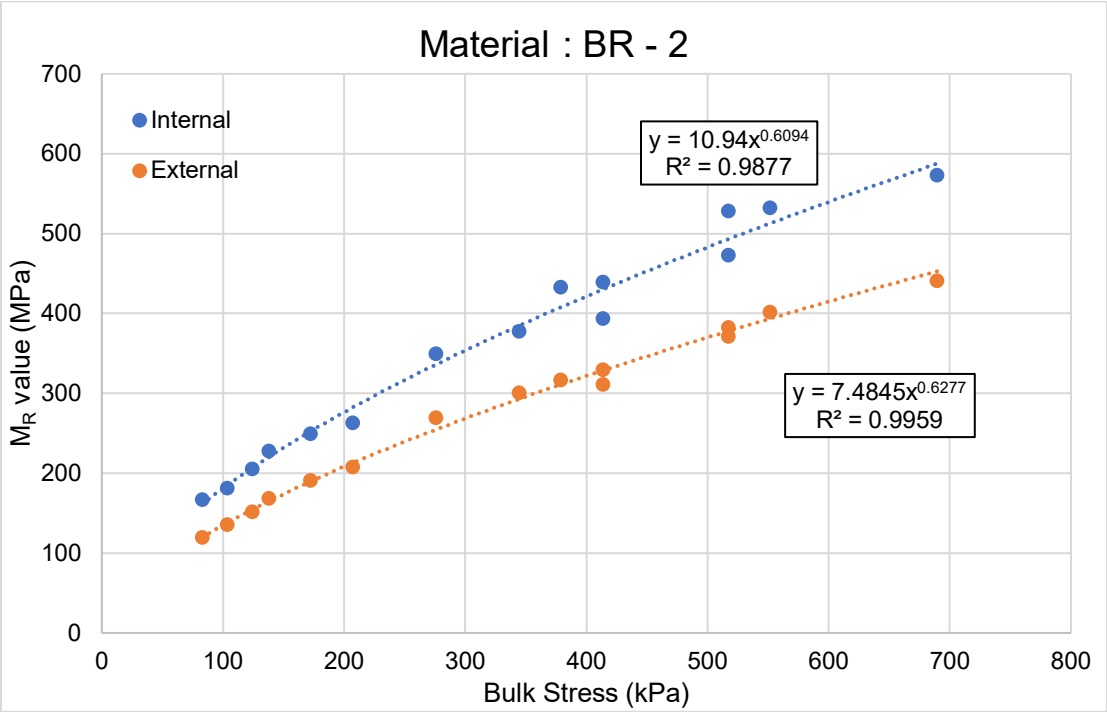
Material : BR - 2
Internal
External
y = 10.94x^0.6094
R² = 0.9877
y = 7.4845x^0.6277
R² = 0.9959
MR value (MPa)
Bulk Stress (kPa)
0
100
200
300
400
500
600
700
800

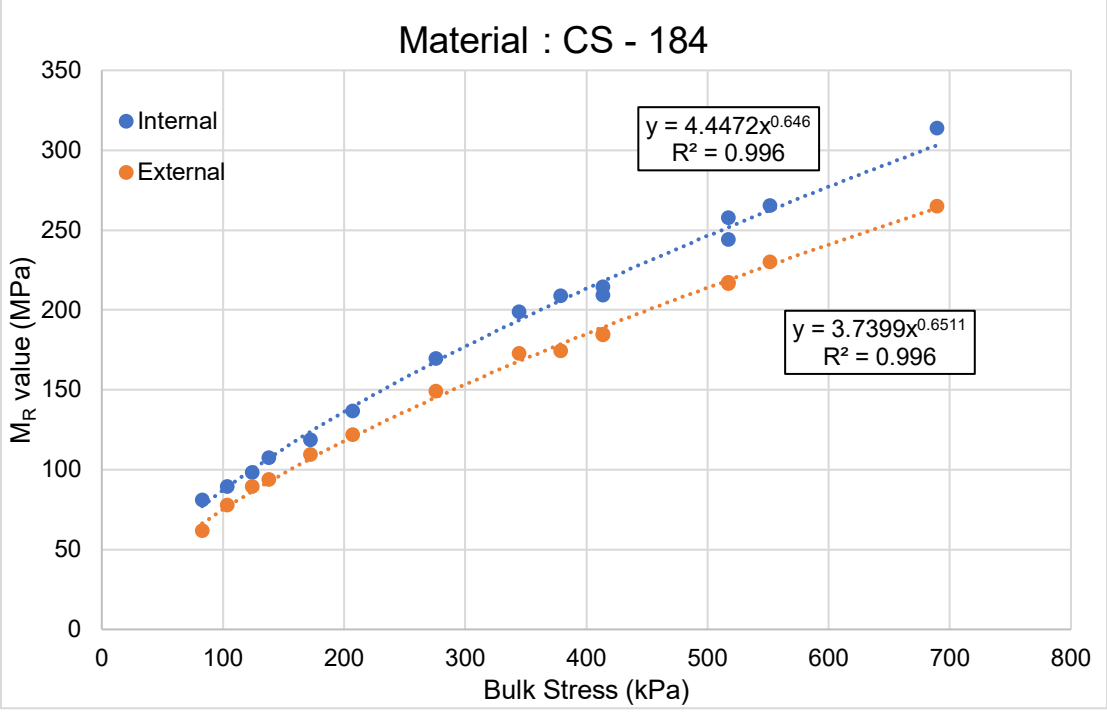
Material : CS - 184
Internal
External
y = 4.4472x^0.646
R² = 0.996
y = 3.7399x^0.6511
R² = 0.996
MR value (MPa)
Bulk Stress (kPa)
0
50
100
150
200
250
300
350
400
500
600
700
800

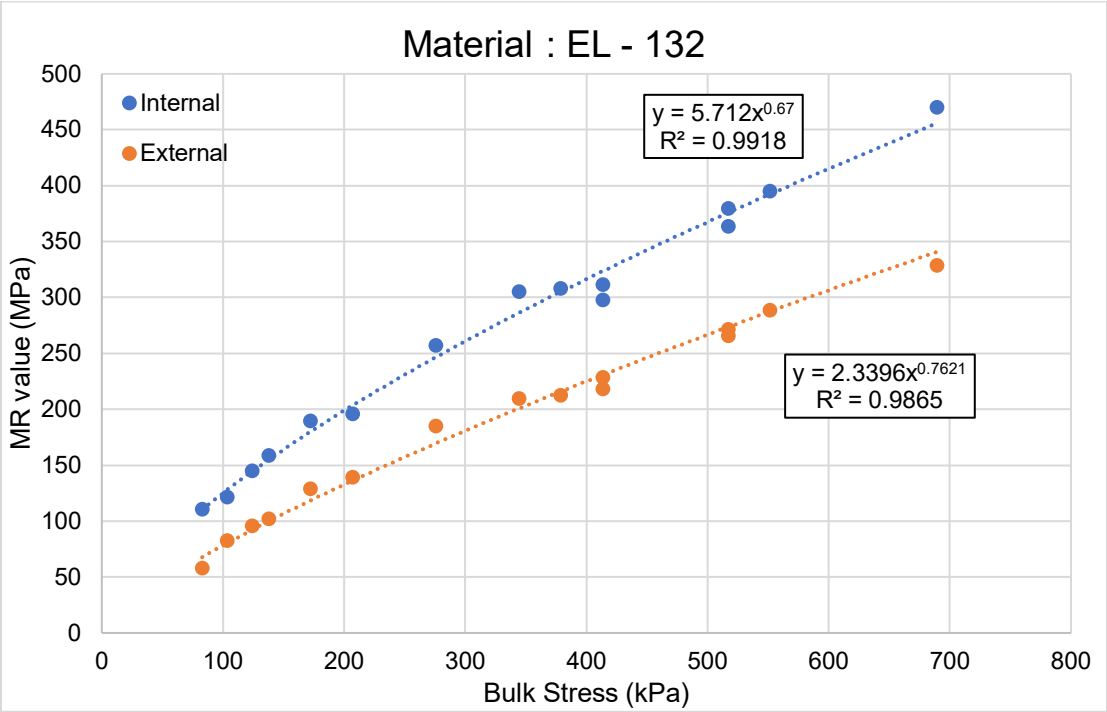
Material : EL - 132
Internal
External
y = 5.712x^0.67
R² = 0.9918
y = 2.3396x^0.7621
R² = 0.9865
MR value (MPa)
Bulk Stress (kPa)
0
50
100
150
200
250
300
350
400
450
500
0
100
200
300
400
500
600
700
800

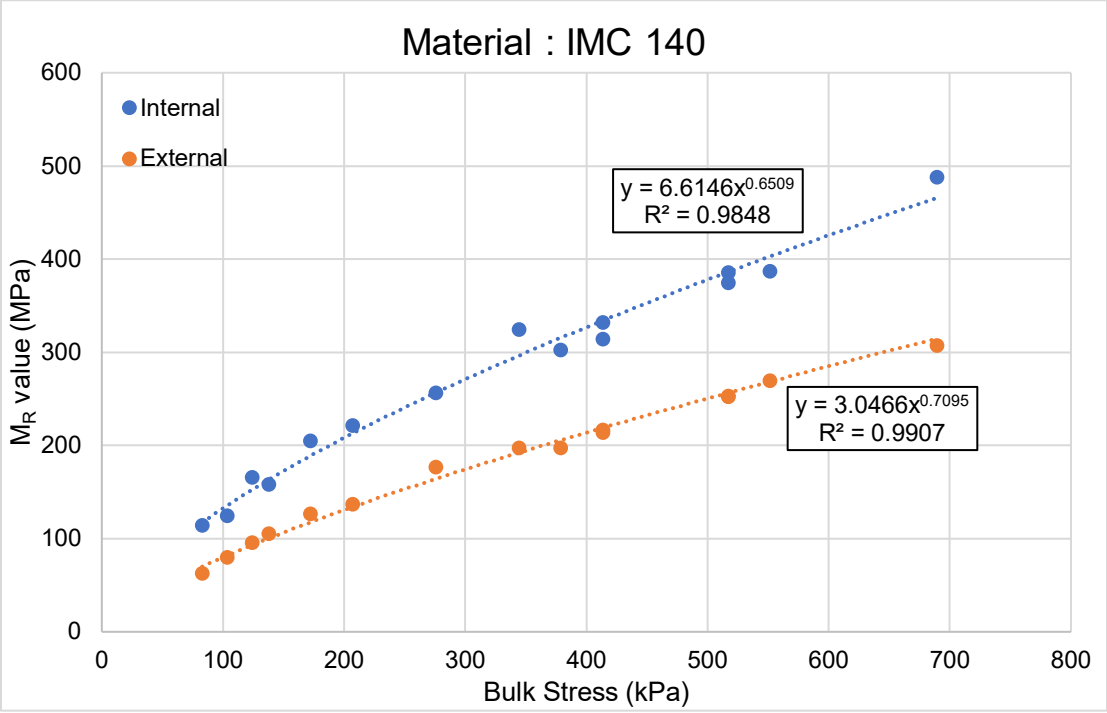
Material : IMC 140
Internal
External
y = 6.6146x^0.6509
R² = 0.9848
y = 3.0466x^0.7095
R² = 0.9907
MR value (MPa)
Bulk Stress (kPa)
0
100
200
300
400
500
600
0
100
200
300
400
500
600
700
800

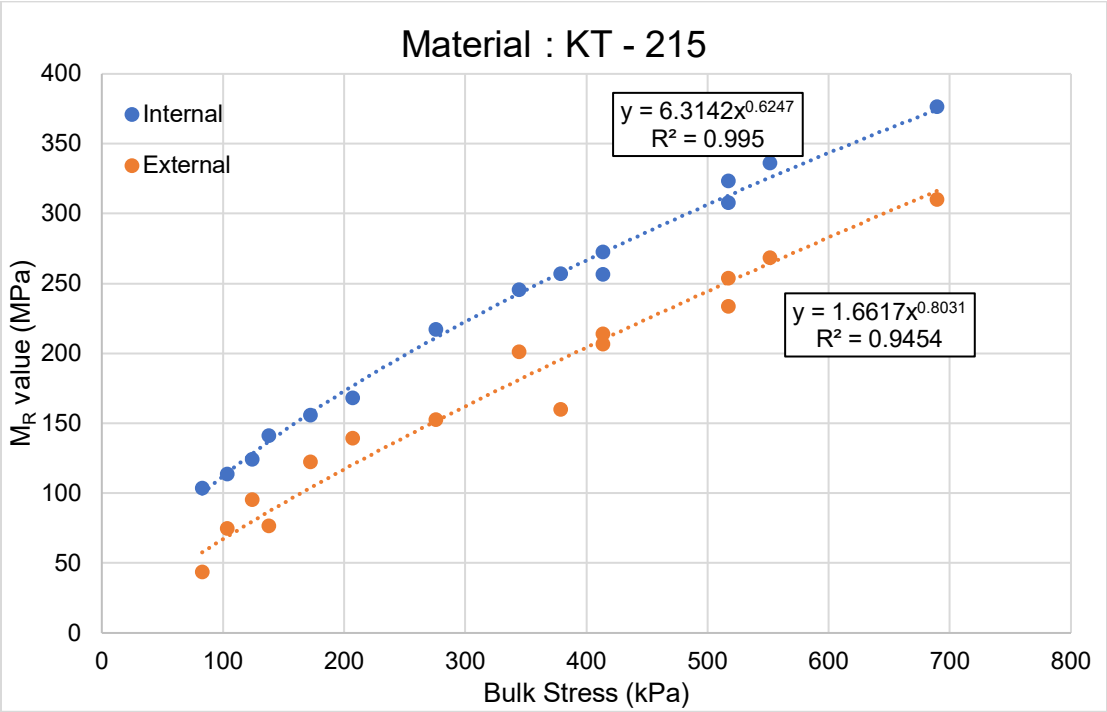
Material : KT - 215
Internal
External
y = 6.3142x^0.6247
R² = 0.995
y = 1.6617x^0.8031
R² = 0.9454
MR value (MPa)
Bulk Stress (kPa)
0
50
100
150
200
250
300
350
400
0
100
200
300
400
500
600
700
800

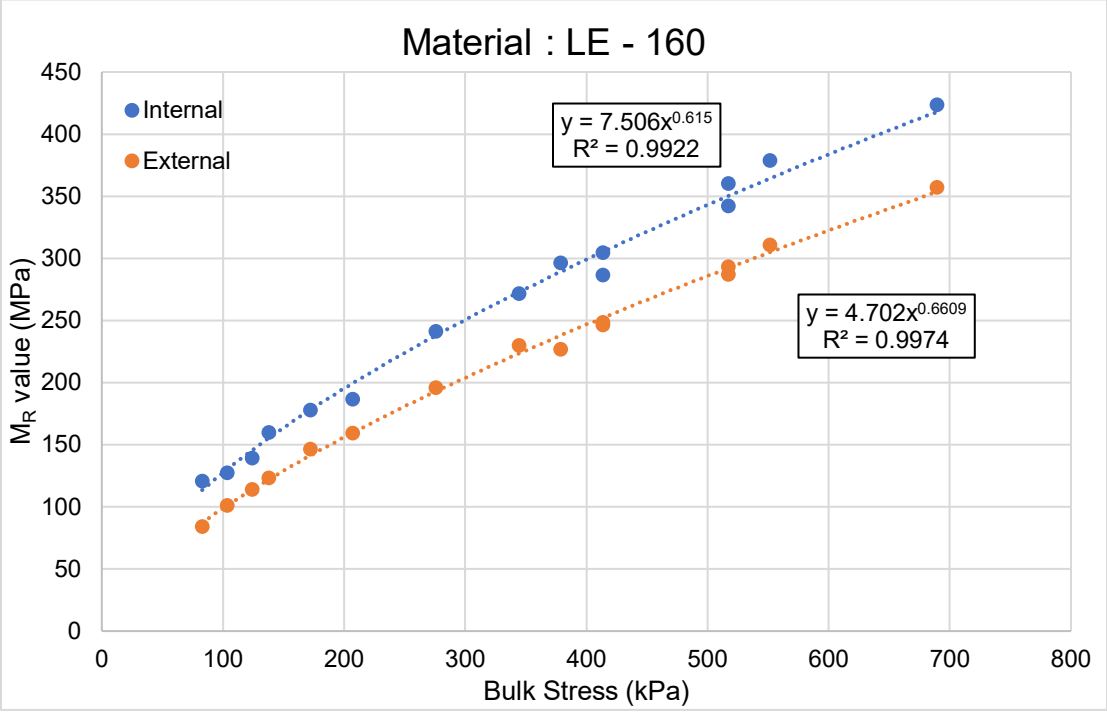
Material : LE - 160
Internal
External
y = 7.506x^0.615
R² = 0.9922
y = 4.702x^0.6609
R² = 0.9974
MR value (MPa)
Bulk Stress (kPa)
0
50
100
150
200
250
300
350
400
450
0
100
200
300
400
500
600
700
800

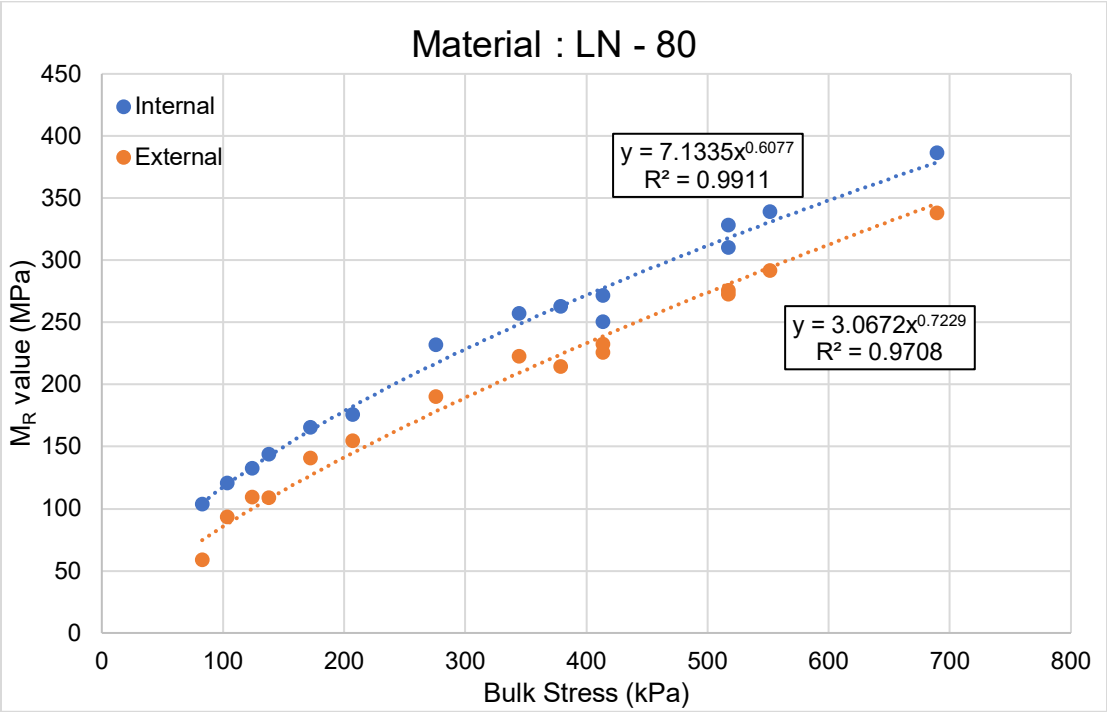
Material : LN - 80
Internal
External
y = 7.1335x^0.6077
R² = 0.9911
y = 3.0672x^0.7229
R² = 0.9708
MR value (MPa)
Bulk Stress (kPa)
0
50
100
150
200
250
300
350
400
450
0
100
200
300
400
500
600
700
800

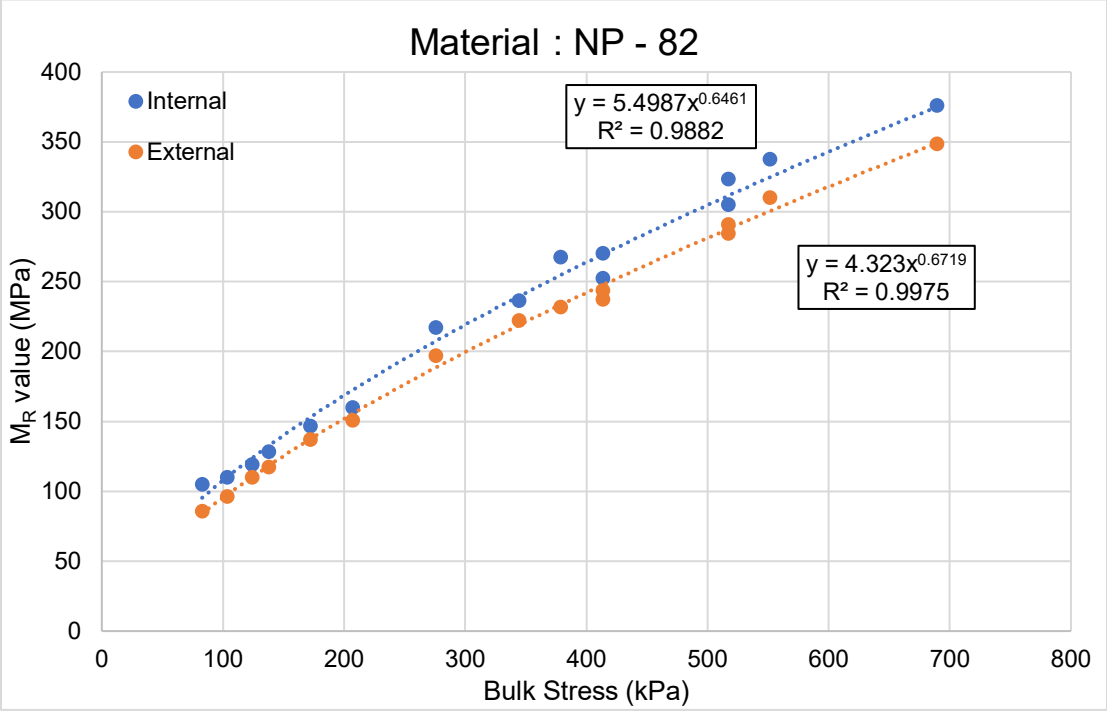
Material : NP - 82
Internal
External
y = 5.4987x^0.6461
R² = 0.9882
y = 4.323x^0.6719
R² = 0.9975
MR value (MPa)
Bulk Stress (kPa)
0
50
100
150
200
250
300
350
400
0
100
200
300
400
500
600
700
800

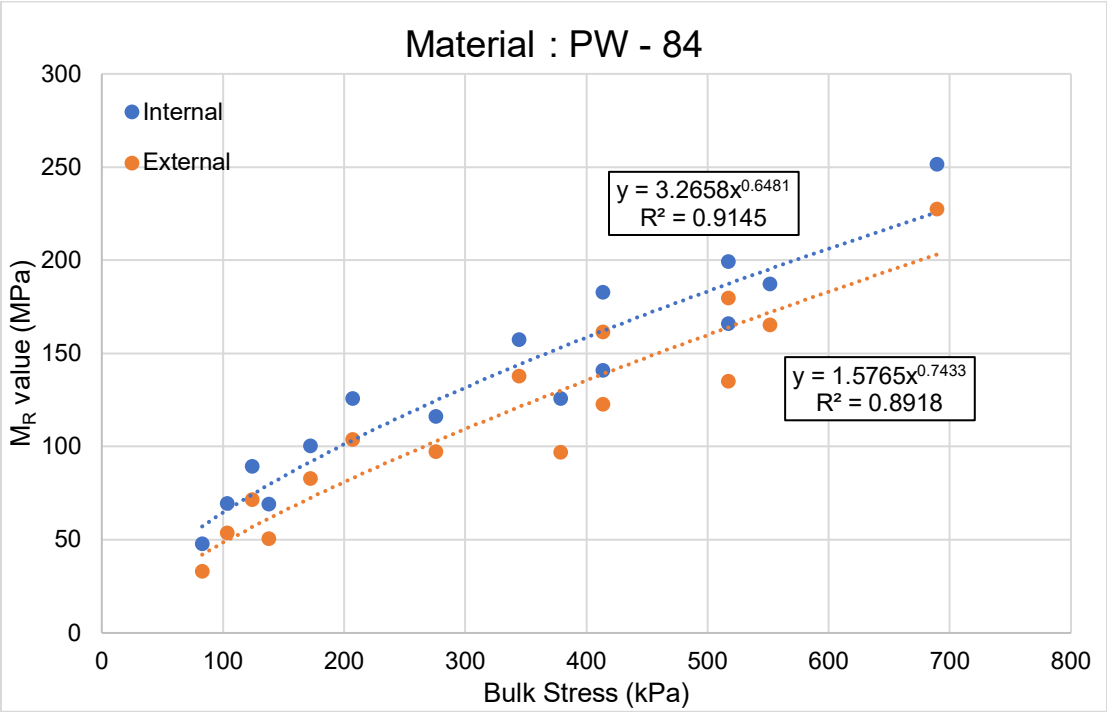
Material : PW - 84
Internal
External
y = 3.2658x^0.6481
R² = 0.9145
y = 1.5765x^0.7433
R² = 0.8918
M_R value (MPa)
Bulk Stress (kPa)
0
50
100
150
200
250
300
0
100
200
300
400
500
600
700
800

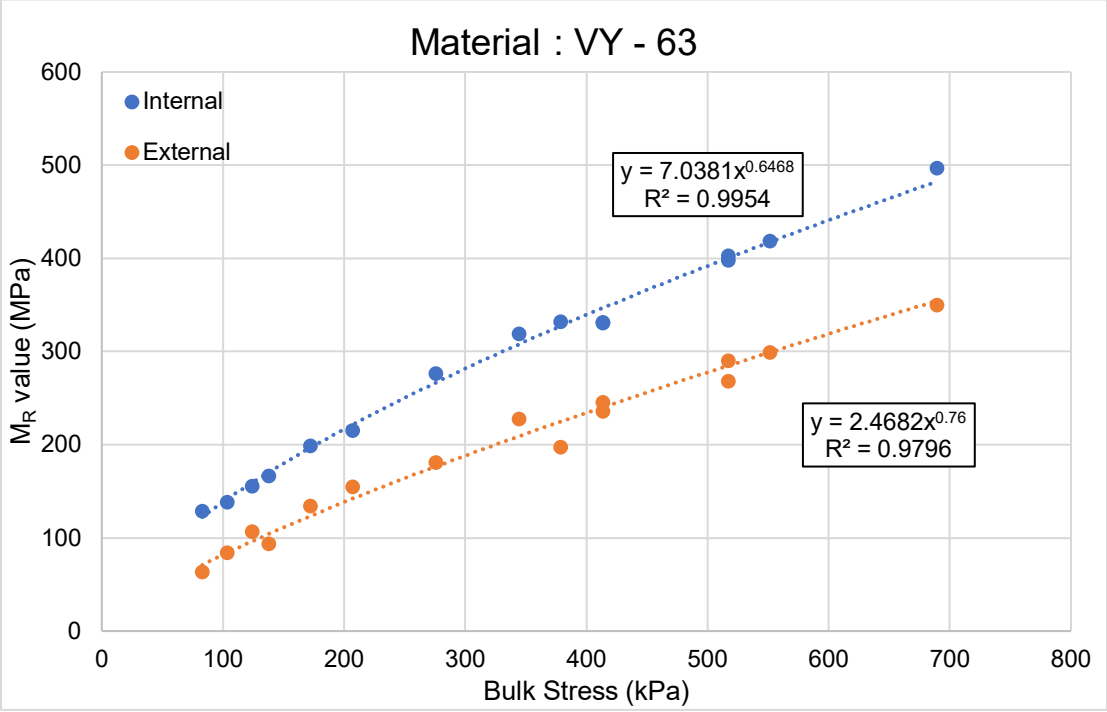
Material : VY - 63
Internal
External
y = 7.0381x^0.6468
R² = 0.9954
y = 2.4682x^0.76
R² = 0.9796
M_R value (MPa)
Bulk Stress (kPa)
0
100
200
300
400
500
600
0
100
200
300
400
500
600
700
800

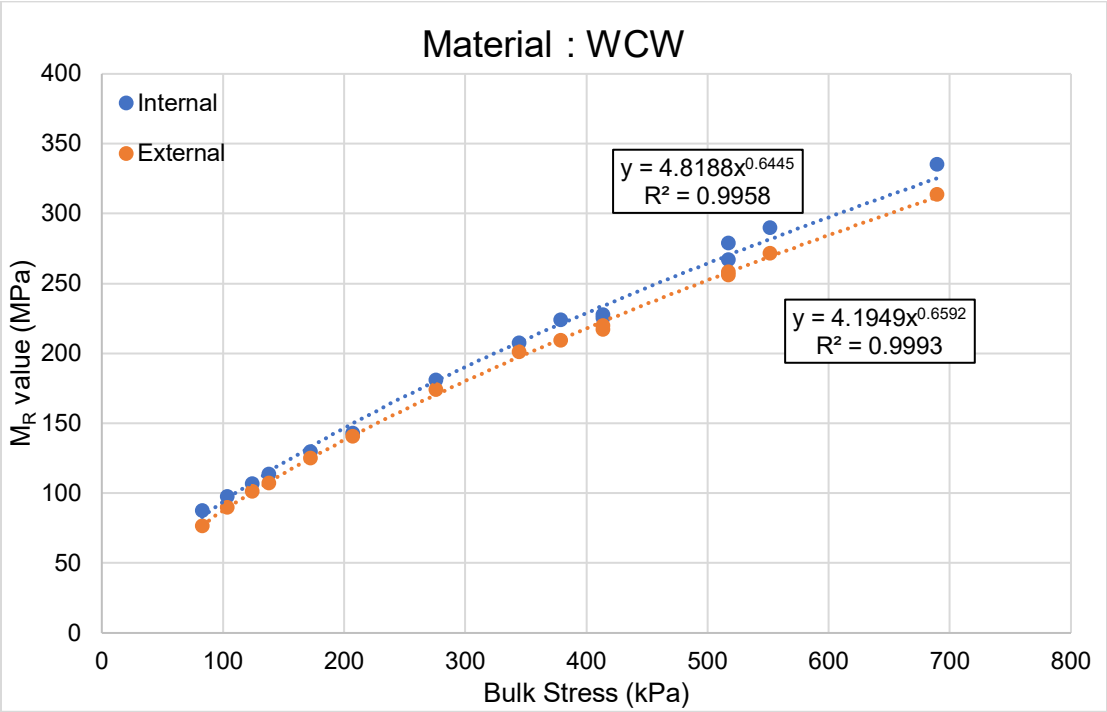
Material : WCW
Internal
External
y = 4.8188x^0.6445
R² = 0.9958
y = 4.1949x^0.6592
R² = 0.9993
M_R value (MPa)
Bulk Stress (kPa)
0
50
100
150
200
250
300
350
400
0
100
200
300
400
500
600
700
800

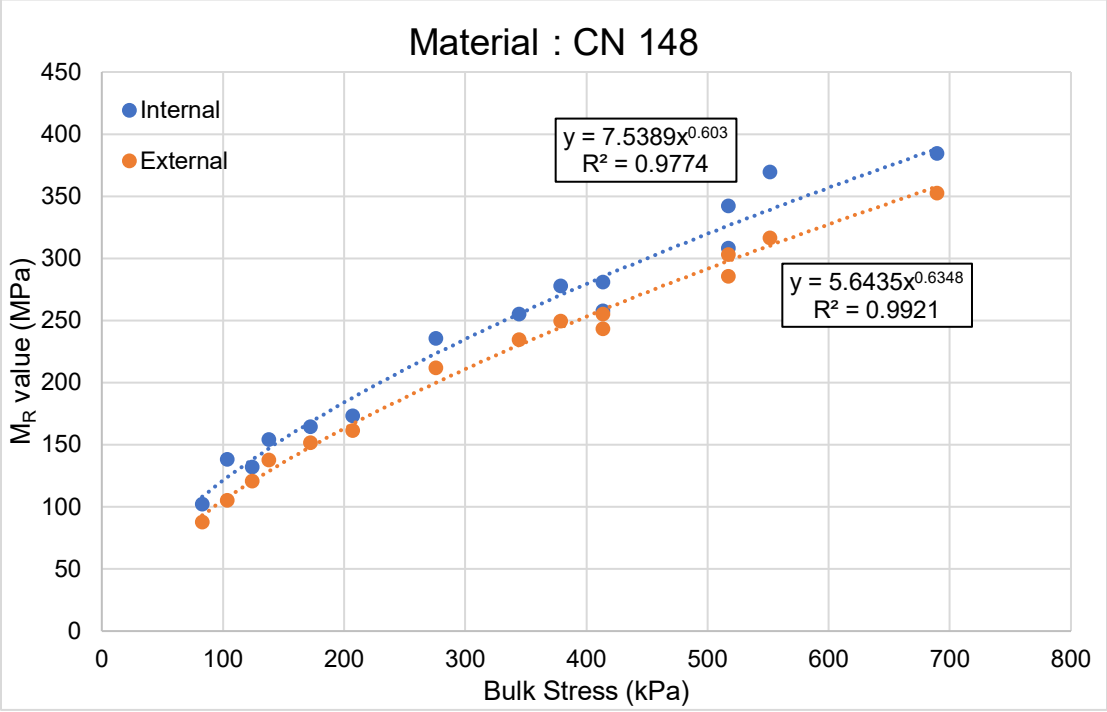
Material : CN 148
Internal
External
y = 7.5389x^0.603
R² = 0.9774
y = 5.6435x^0.6348
R² = 0.9921
M_R value (MPa)
Bulk Stress (kPa)
0
50
100
150
200
250
300
350
400
450
0
100
200
300
400
500
600
700
800

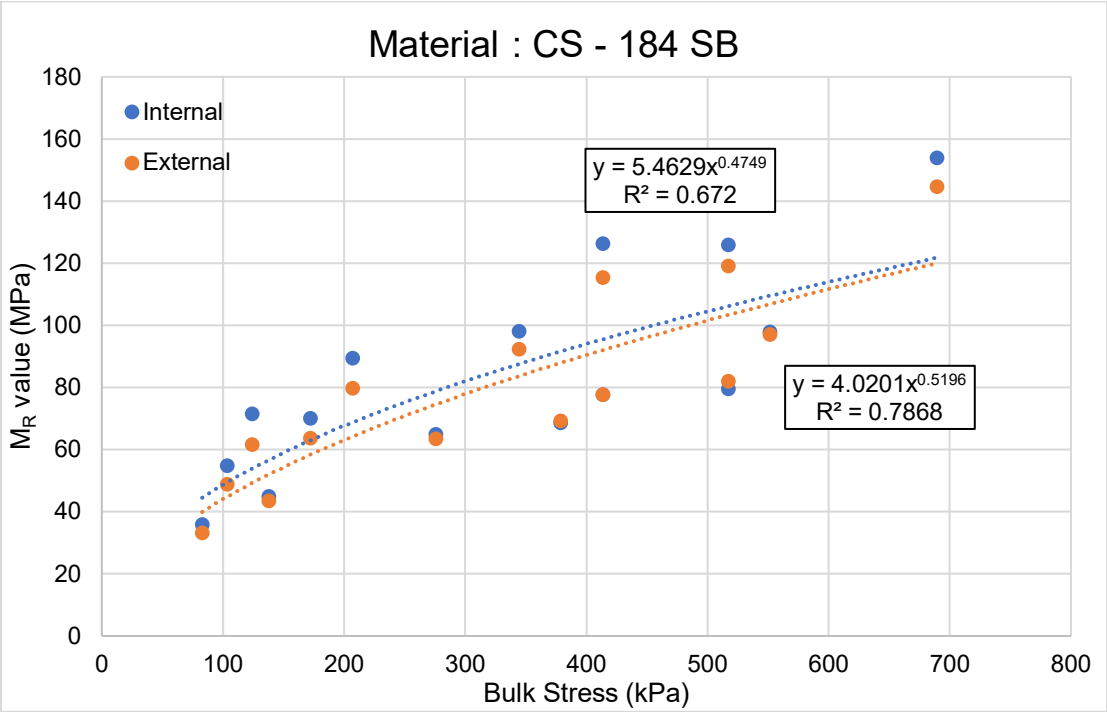
Material : CS - 184 SB
Internal
External
y = 5.4629x^0.4749
R² = 0.672
y = 4.0201x^0.5196
R² = 0.7868
M_R value (MPa)
Bulk Stress (kPa)
0
20
40
60
80
100
120
140
160
180
0
100
200
300
400
500
600
700
800

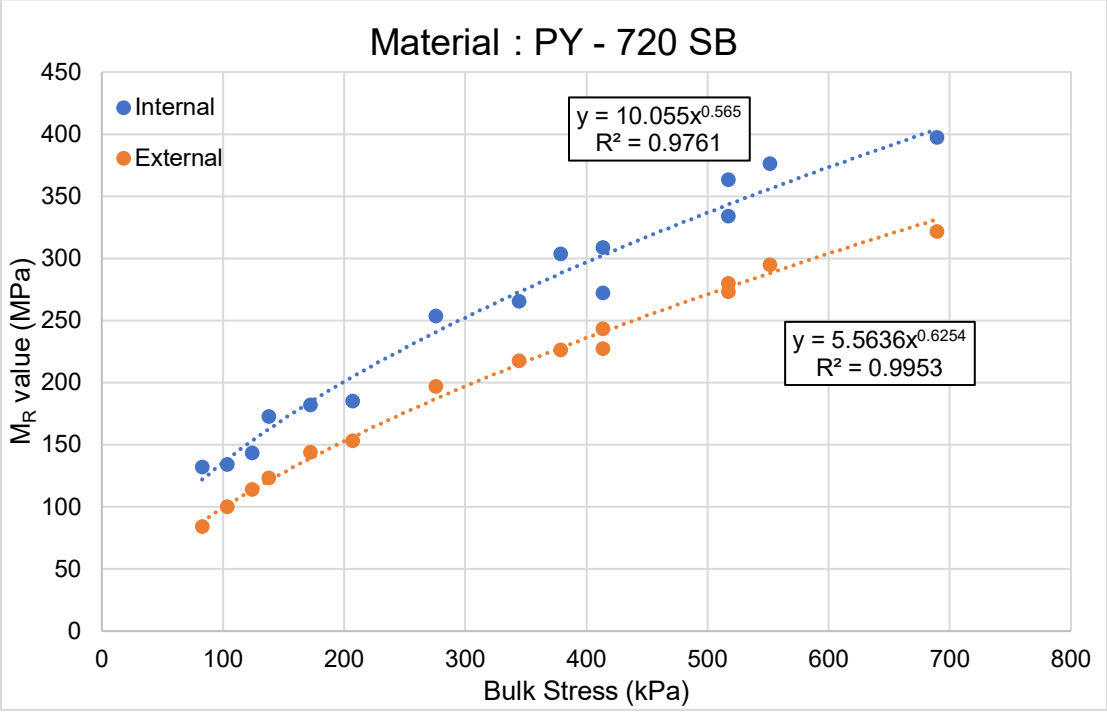
Material : PY - 720 SB
Internal
External
y = 10.055x^0.565
R² = 0.9761
y = 5.5636x^0.6254
R² = 0.9953
M_R value (MPa)
Bulk Stress (kPa)
0
50
100
150
200
250
300
350
400
450
0
100
200
300
400
500
600
700
800

Appendix B: Uzan Model fitting

Table B.1: Regression coefficients for *"Uzan Model"*

Material ID	External Measurement				Internal Measurement			
	k_1	k_2	k_3	R^2	k_1	k_2	k_3	R^2
A	912.750	0.709	-0.024	0.996	1063.110	0.705	-0.073	0.994
B	977.050	0.679	-0.020	0.994	1158.343	0.744	-0.104	0.996
BK - 100	834.520	0.705	-0.015	0.994	993.710	0.712	-0.085	0.996
BK - 181	719.290	0.577	0.205	0.994	1011.160	0.538	0.110	0.992
BR - 2	1275.000	0.673	-0.059	0.998	1552.980	0.739	-0.135	0.998
CS - 184	762.190	0.633	0.011	0.997	824.890	0.688	-0.028	0.996
EL - 132	798.139	0.745	-0.024	0.993	993.710	0.712	-0.085	0.996
IMC - 140	829.750	0.676	0.006	0.995	1469.020	0.558	0.093	0.991
KT - 215	852.450	0.600	0.157	0.981	993.710	0.712	-0.085	0.997
LE - 160	1007.830	0.638	0.024	0.997	1155.710	0.696	-0.069	0.997
LN - 80	929.620	0.651	0.030	0.989	1090.990	0.665	-0.055	0.990
NP - 82	911.880	0.707	-0.033	0.997	951.540	0.750	-0.093	0.997
PW -84	773.910	0.331	0.424	0.993	923.300	0.332	0.336	0.993
VY - 63	961.590	0.619	0.117	0.992	1357.760	0.659	-0.002	0.995
WCW	868.560	0.660	0.000	0.999	874.400	0.699	-0.034	0.997
CN - 148 SB	991.540	0.681	-0.063	0.995	1052.190	0.722	-0.117	0.987
CS - 184 SB	750.000	0.045	0.530	0.995	937.730	-0.107	0.650	0.991
PY -720 SB	951.220	0.658	-0.048	0.996	1145.220	0.708	-0.143	0.996

Graphical representation of *"Uzan Model"* fitting

Material : A (Internal)

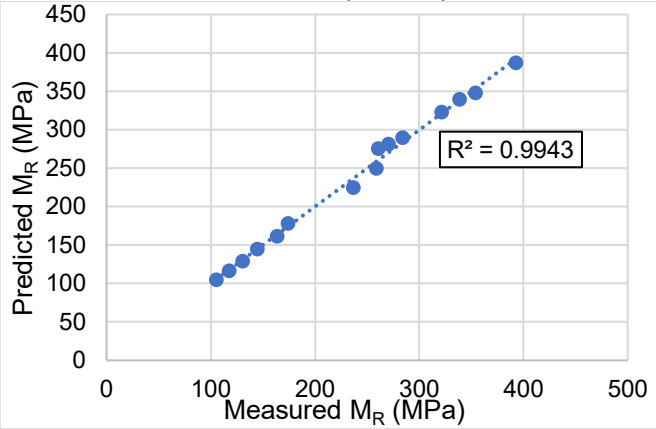

Material : A (External)

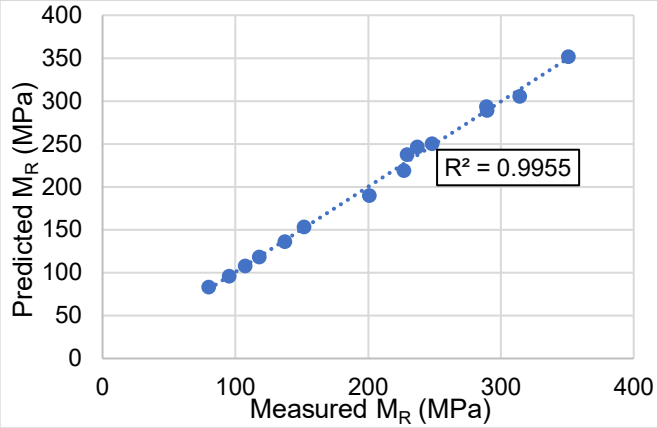

Material : B (Internal)

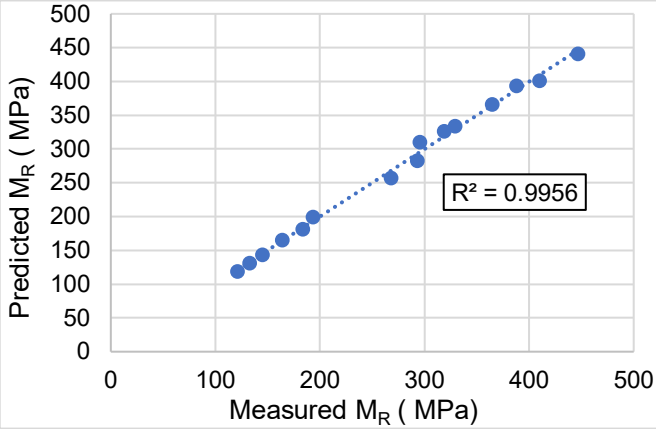

Material : B (External)

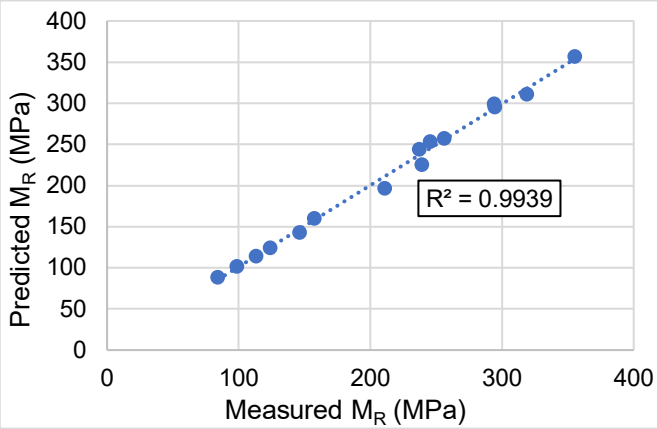

Material : BK - 100 (Internal)

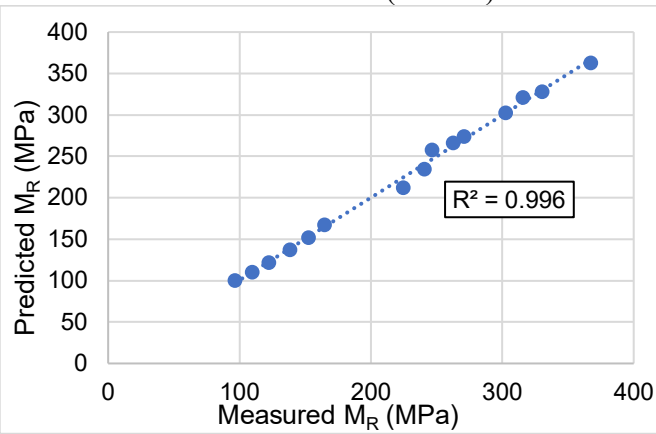

Material : BK - 100 (External)

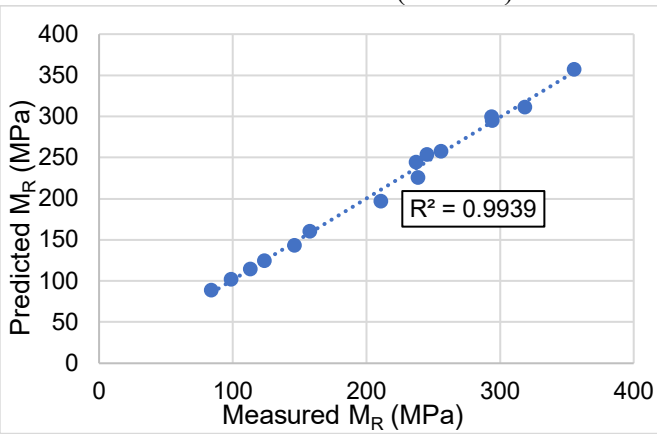

Material : BK - 181 (Internal)

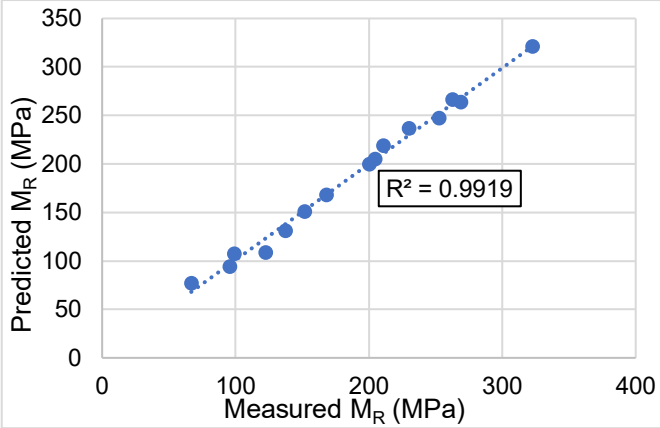

Material : BK - 181 (External)

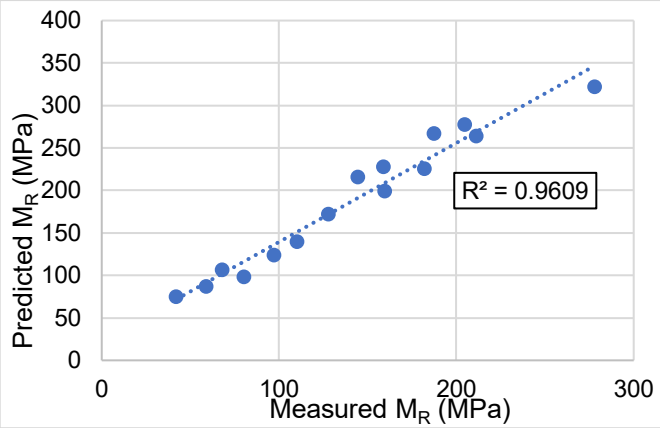

Material : BR - 2 (Internal)

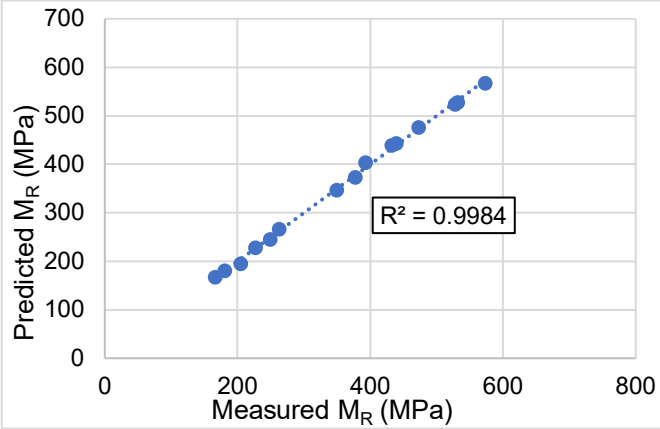

Material : BR - 2 (External)

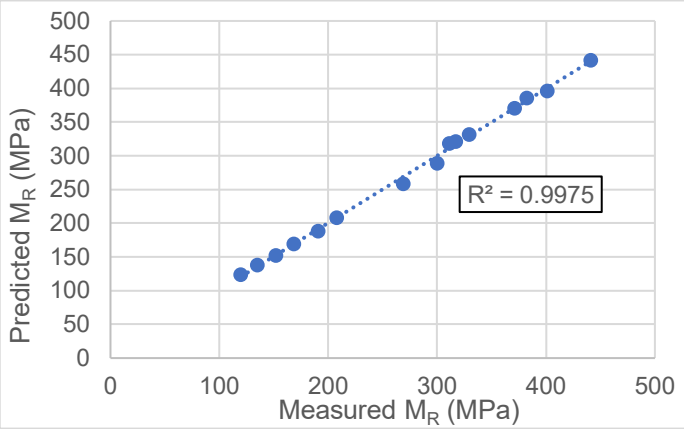

Material : CS - 184 (Internal)

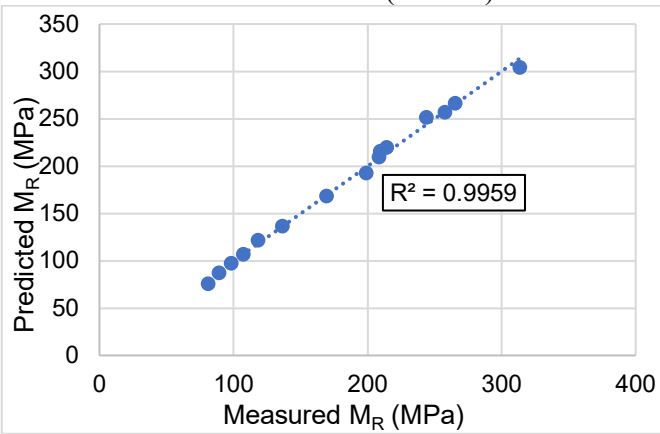

Material : CS - 184 (External)

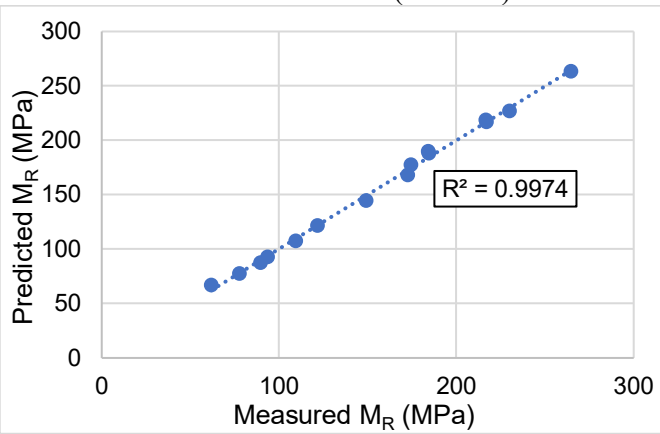

Material : EL - 132 (Internal)

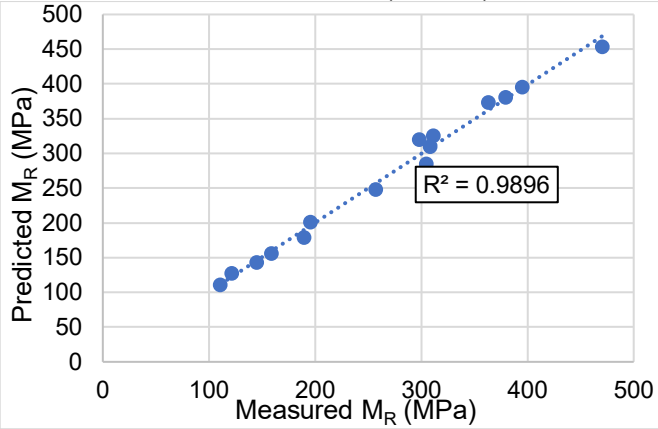

Material : EL - 132 (External)

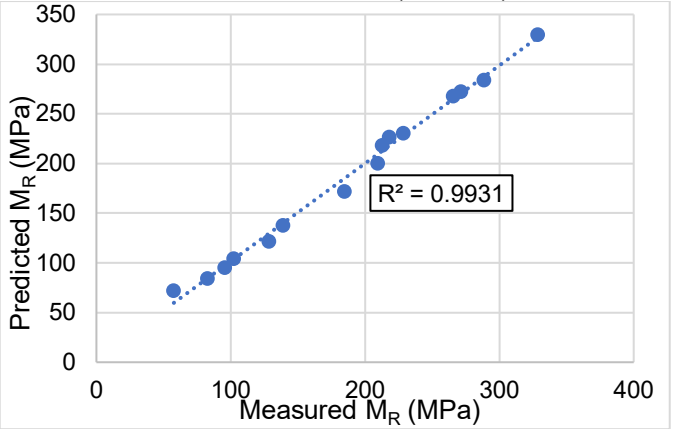

Material : IMC - 140 (Internal)

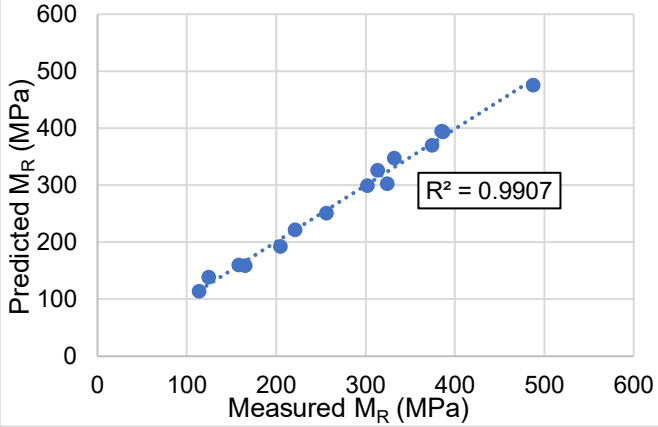

Material : IMC - 140 (External)

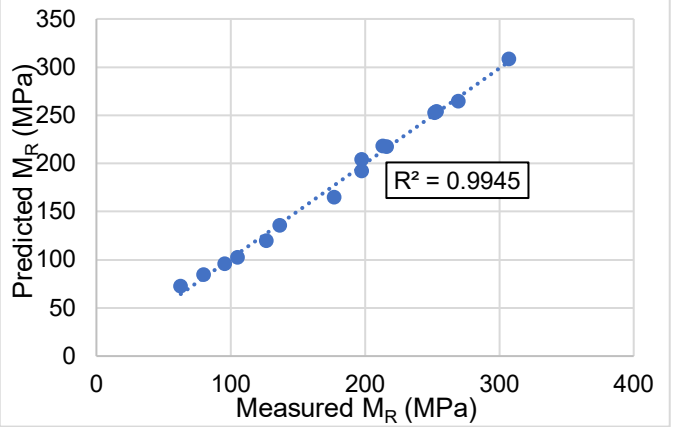

Material : KT - 215 (Internal)

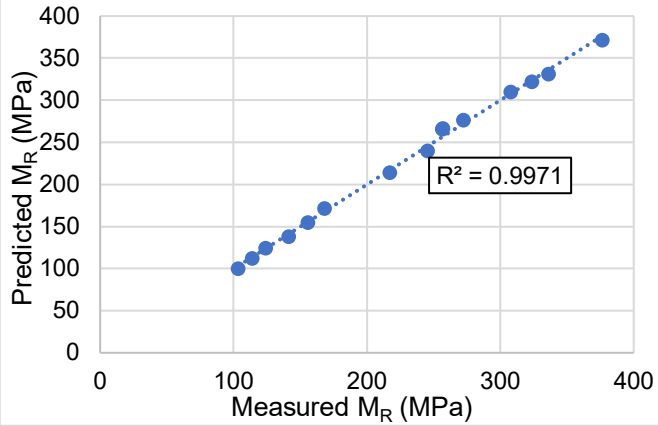

Material : KT - 215 (External)

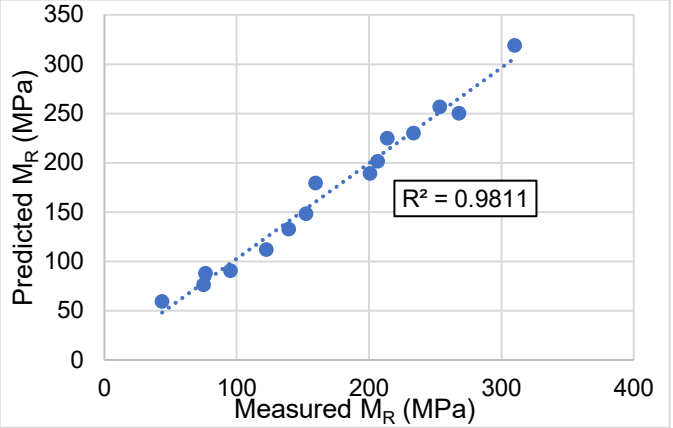

Material : LE - 160 (Internal)

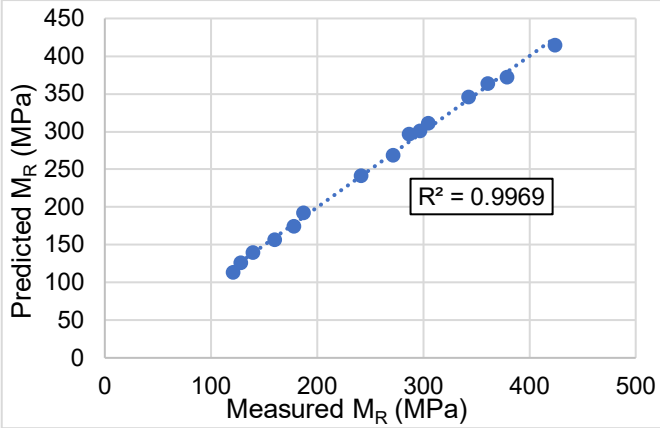

Material : LE - 160 (External)

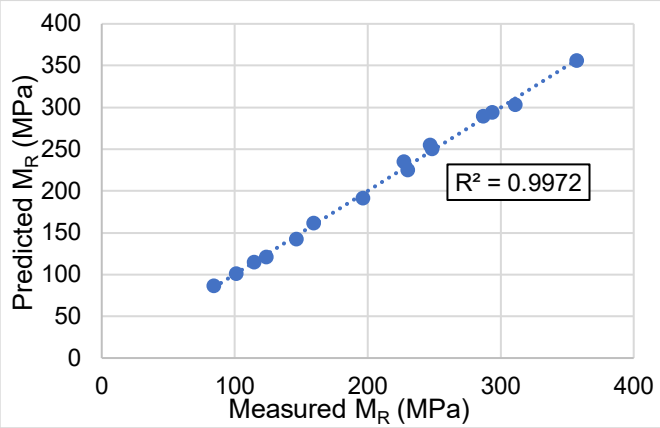

Material : LN - 80 (Internal)

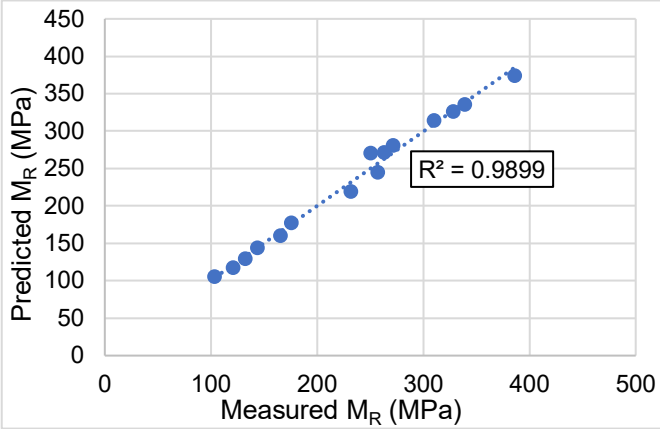

Material : LN - 80 (External)

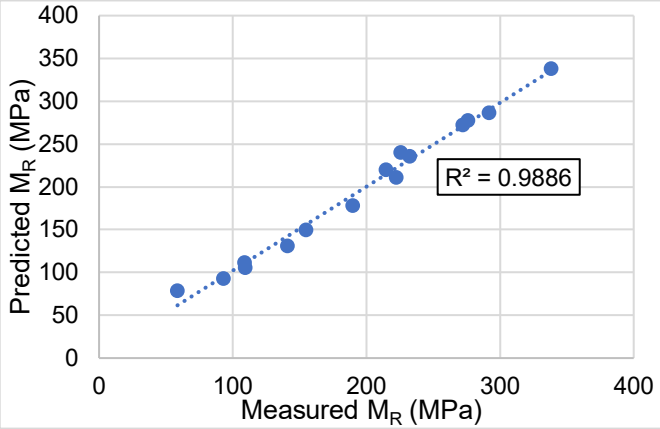

Material : NP - 82 (Internal)

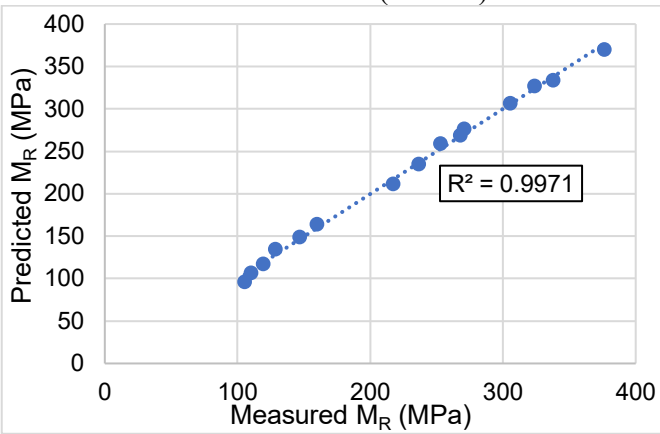

Material : NP - 82 (External)

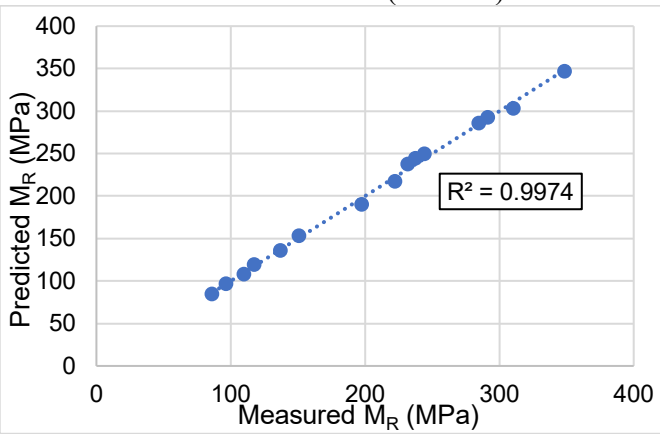

Material : PW - 84 (Internal)

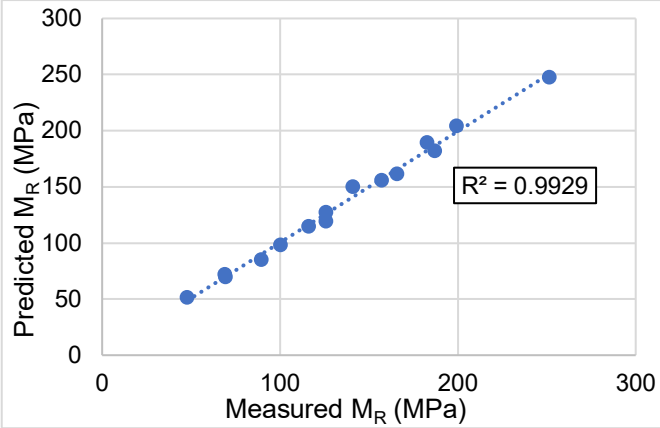

Material : PW - 84 (External)

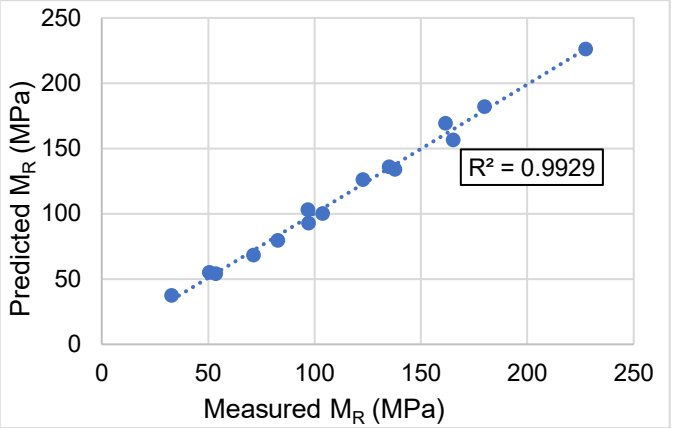

Material : VY - 63 (Internal)

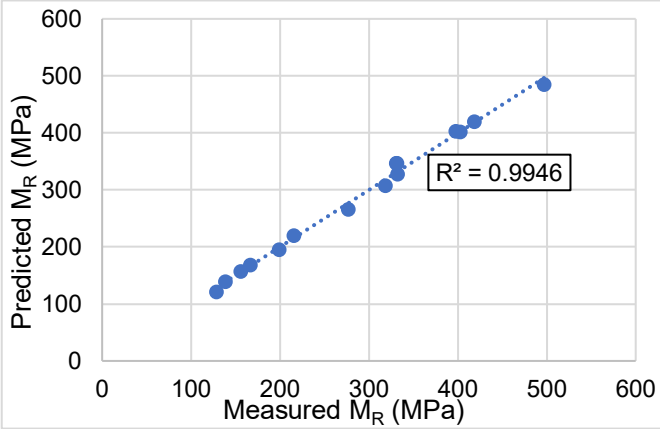

Material : VY - 63 (External)

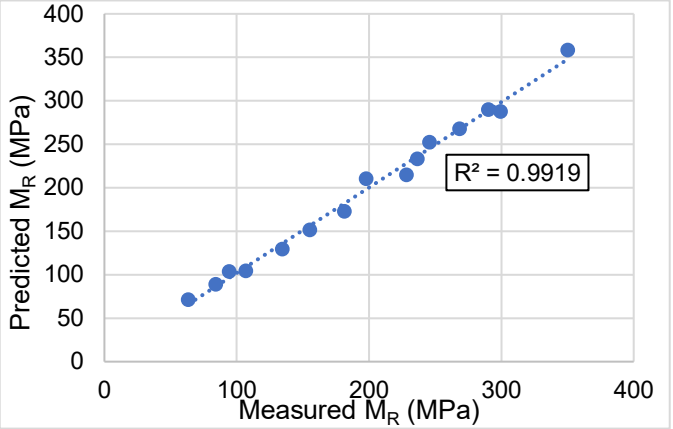

Material : WCW (Internal)

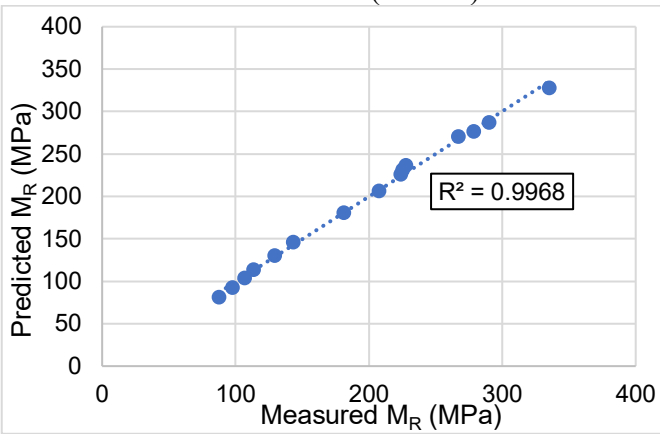

Material : WCW (External)

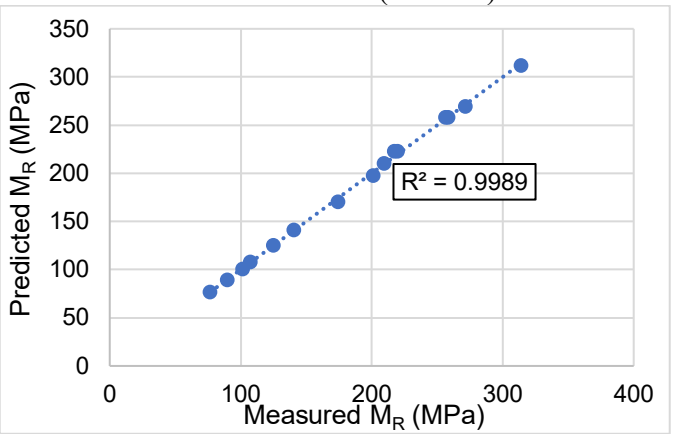

Material : CN – 148 SB (Internal)

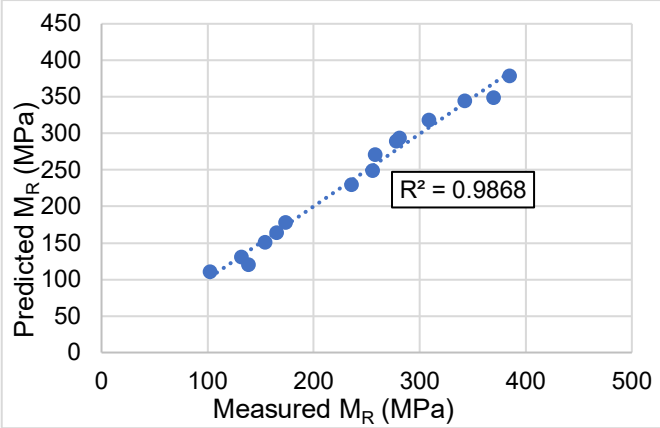

Material : CN – 148 SB (External)

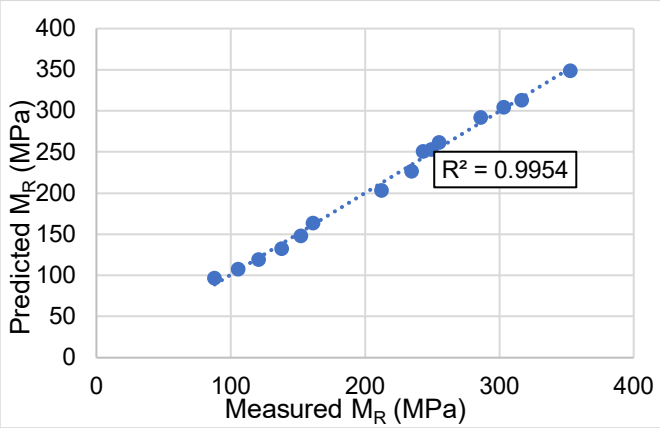

Material : CS – 184 SB (Internal)

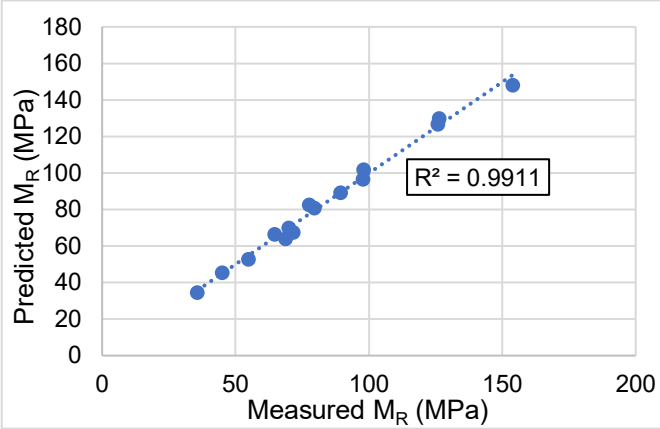

Material : CS – 184 SB (External)

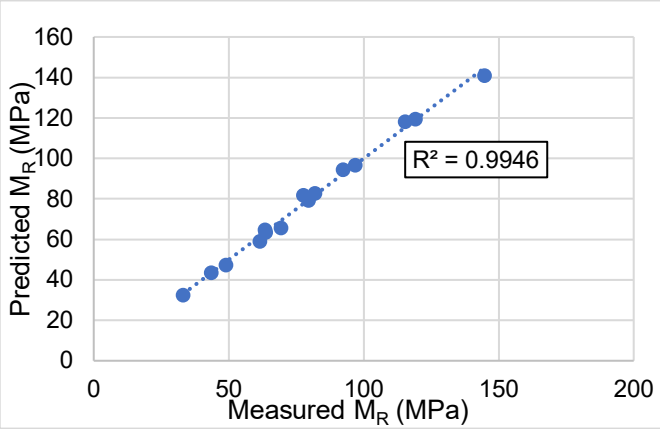

Material : PY – 720 SB (Internal)

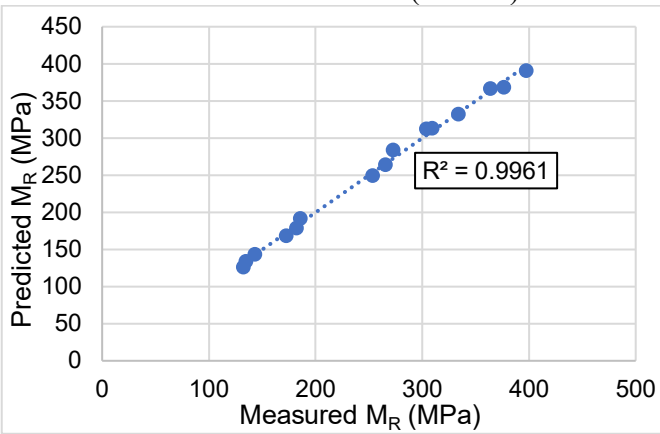

Material : PY – 720 SB (External)

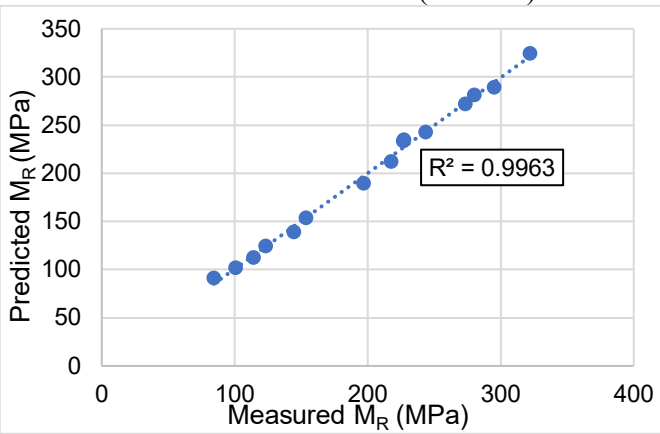

Appendix C: Modified Uzan Model fitting

Table C.1: Regression coefficients for *"Modified Uzan Model"*

Material ID	External Measurement				Internal Measurement			
	k_1	k_2	k_3	R^2	k_1	k_2	k_3	R^2
A	896.538	0.709	-0.024	0.996	1006.113	0.705	-0.073	0.994
B	962.555	0.679	-0.020	0.994	1070.870	0.744	-0.104	0.996
BK - 100	824.865	0.705	-0.016	0.994	932.323	0.712	-0.085	0.995
BK - 181	839.301	0.577	0.205	0.994	1098.583	0.538	0.110	0.992
BR - 2	1219.861	0.673	-0.059	0.998	1403.239	0.739	-0.135	0.998
CS - 184	751.953	0.639	0.017	0.994	807.756	0.688	-0.028	0.996
EL - 132	783.820	0.745	-0.024	0.993	1204.569	0.698	-0.027	0.990
IMC - 140	833.196	0.676	0.006	0.995	1575.466	0.558	0.093	0.991
KT - 215	959.413	0.600	0.157	0.981	993.290	0.688	-0.057	0.997
LE - 160	1026.458	0.638	0.024	0.997	1096.877	0.696	-0.070	0.997
LN - 80	950.596	0.651	0.030	0.989	1046.768	0.665	-0.055	0.990
NP - 82	889.707	0.707	-0.033	0.997	887.414	0.750	-0.093	0.997
PW -84	1064.573	0.331	0.424	0.993	1188.566	0.332	0.336	0.993
VY - 63	1049.872	0.619	0.117	0.992	1355.567	0.659	-0.002	0.995
WCW	868.646	0.660	0.000	0.999	852.493	0.699	-0.034	0.997
CN - 148 SB	945.984	0.681	-0.063	0.995	963.777	0.722	-0.117	0.987
CS - 184 SB	1116.874	0.045	0.530	0.995	1528.630	-0.107	0.650	0.991
PY -720 SB	917.675	0.658	-0.048	0.996	1028.468	0.708	-0.143	0.996

Graphical representation of *"Modified Uzan Model"* fitting

Material : A (Internal)

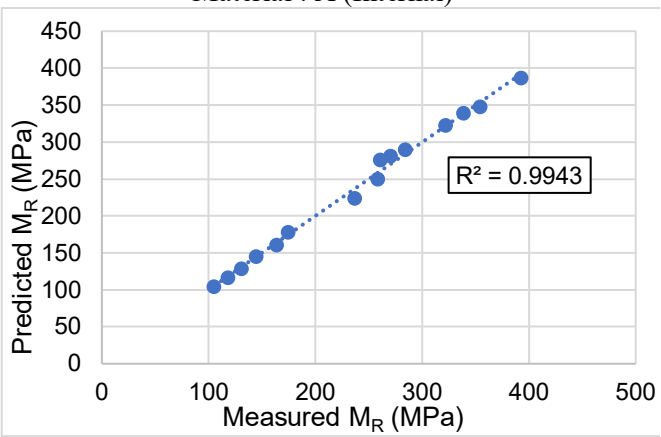

Material : A (External)

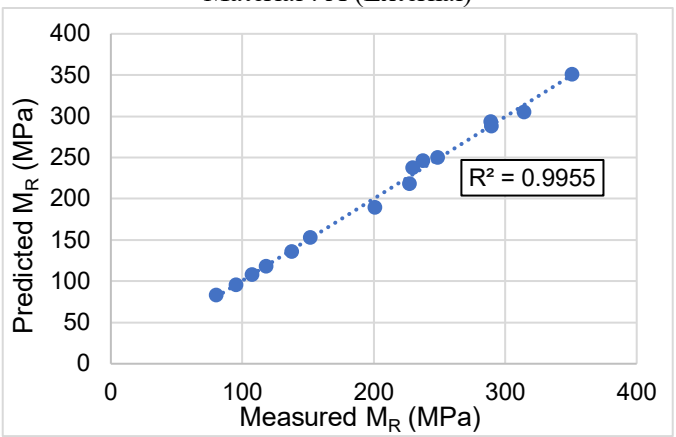

Material : B (Internal)

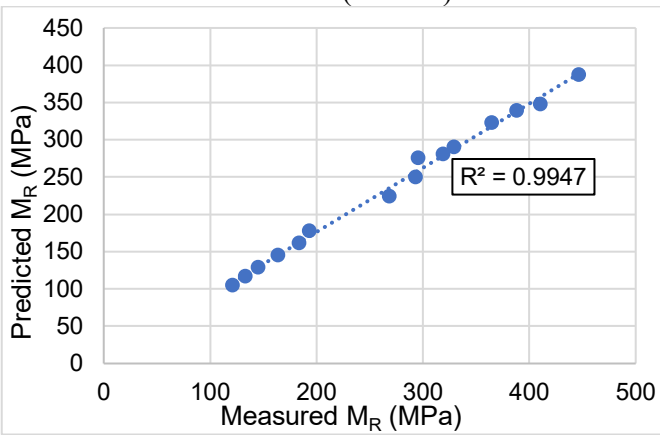

Material : B (External)

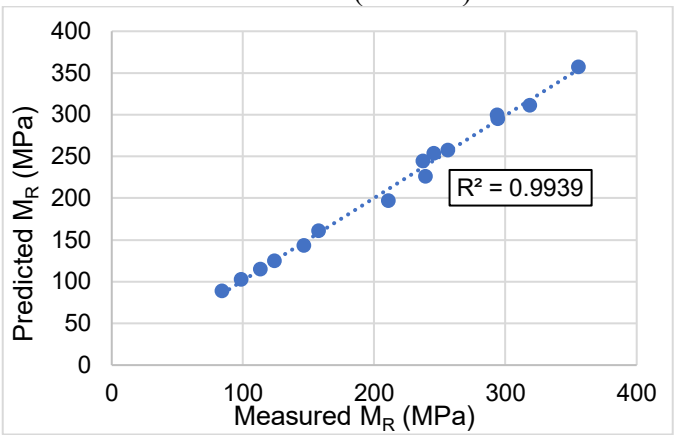

Material : BK - 100 (Internal)

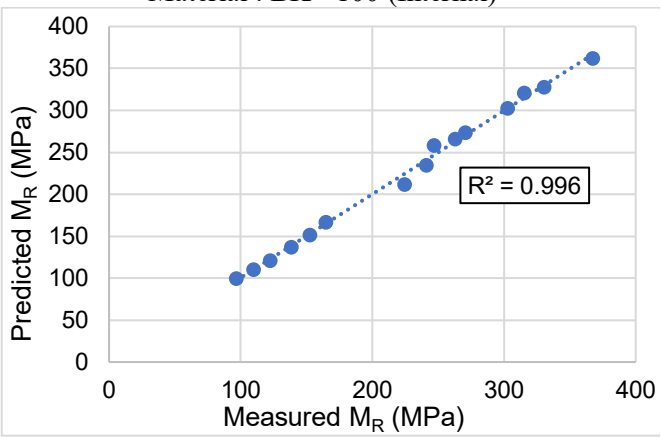

Material : BK - 100 (External)

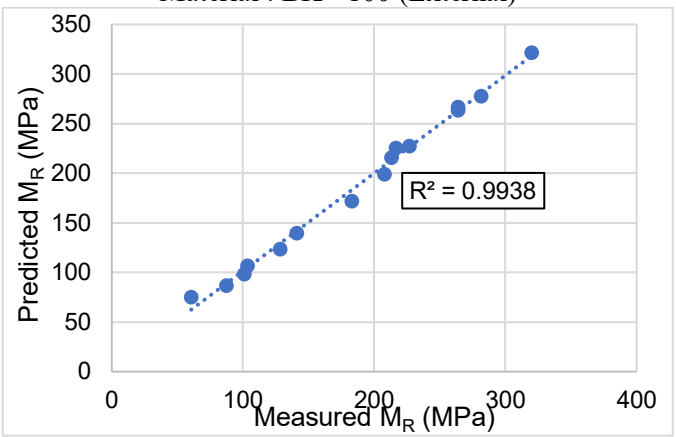

Material : BK - 181 (Internal)

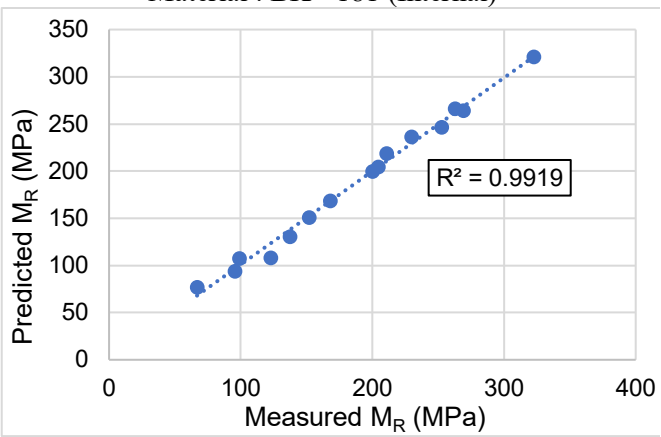

Material : BK – 181 (External)

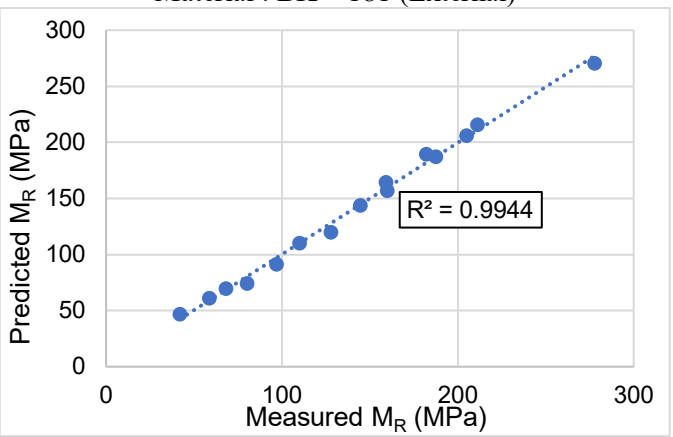

Material : BR - 2 (Internal)

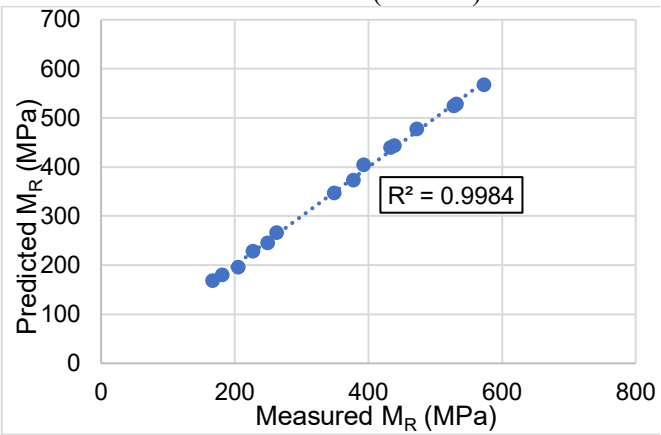

Material : BR - 2 (External)

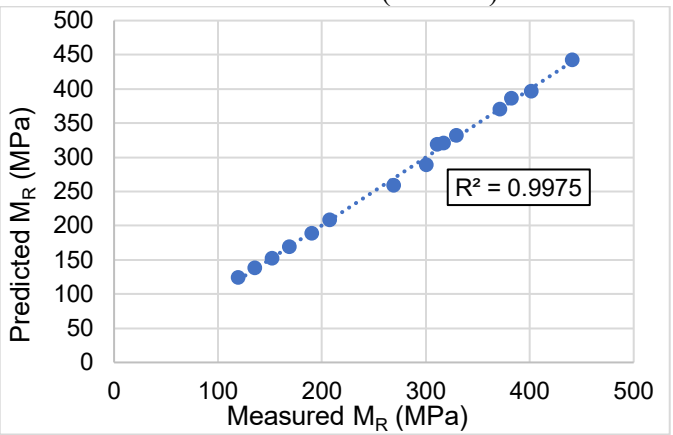

Material : CS – 184 (Internal)

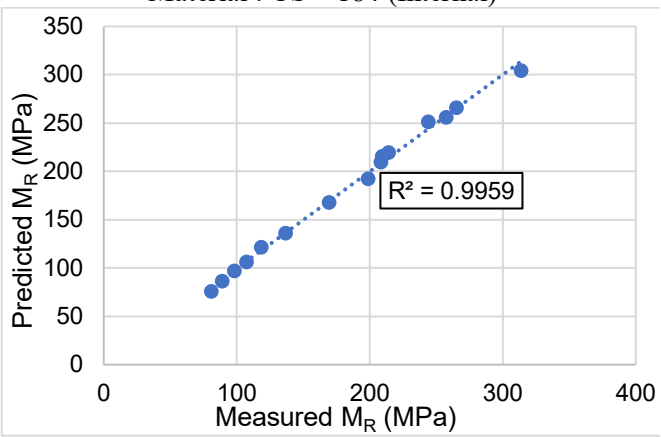

Material : CS – 184 (External)

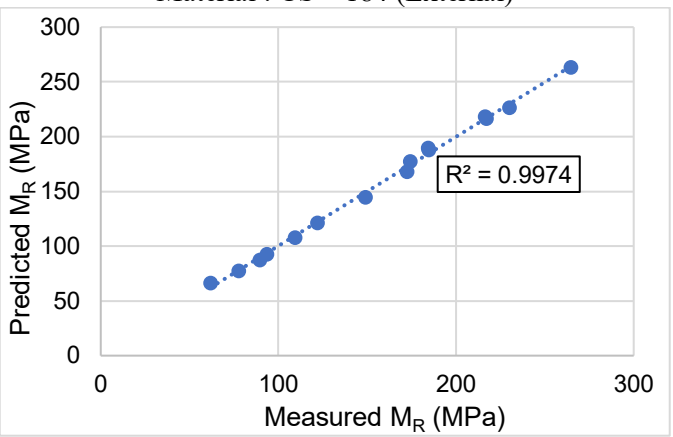

Material : EL - 132 (Internal)

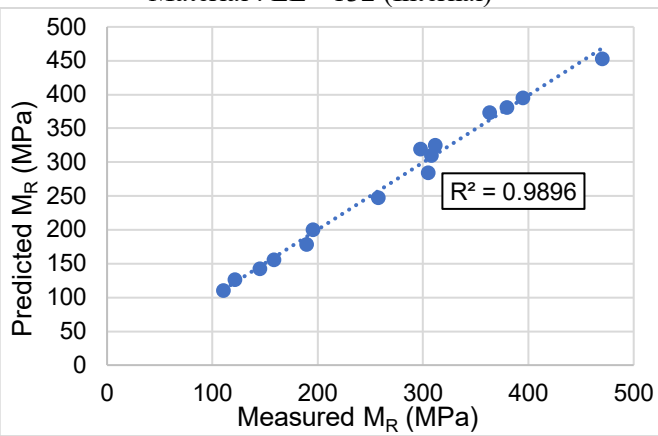

Material : EL – 132 (External)

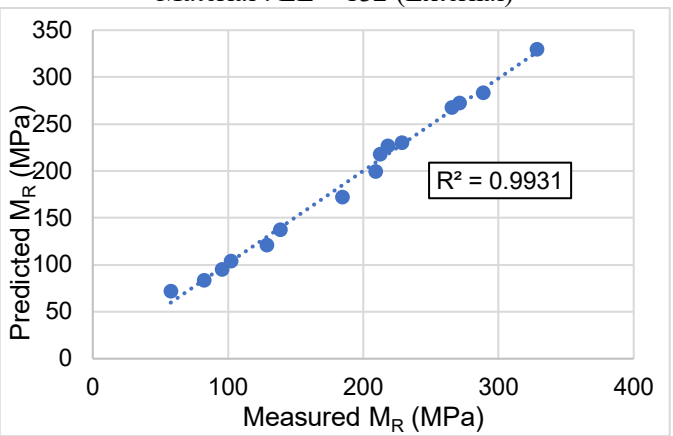

Material : IMC – 140 (Internal)

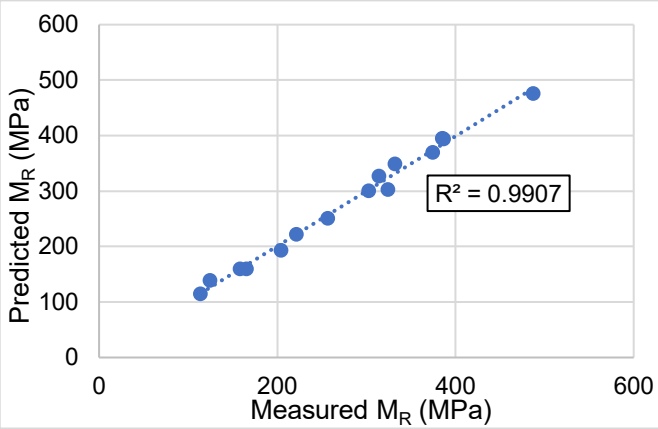

Material : IMC – 140 (External)

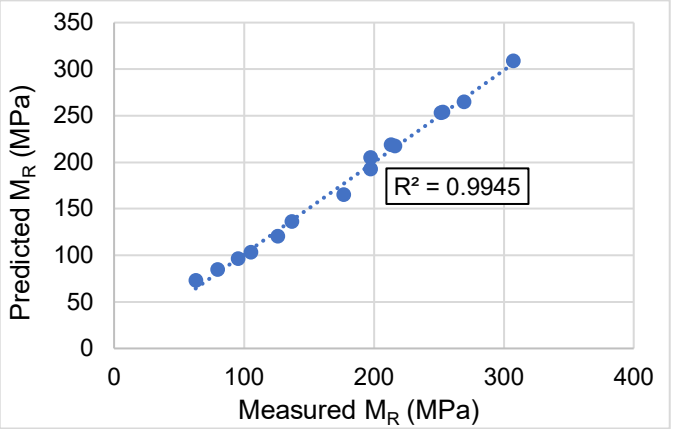

Material : KT - 215 (Internal)

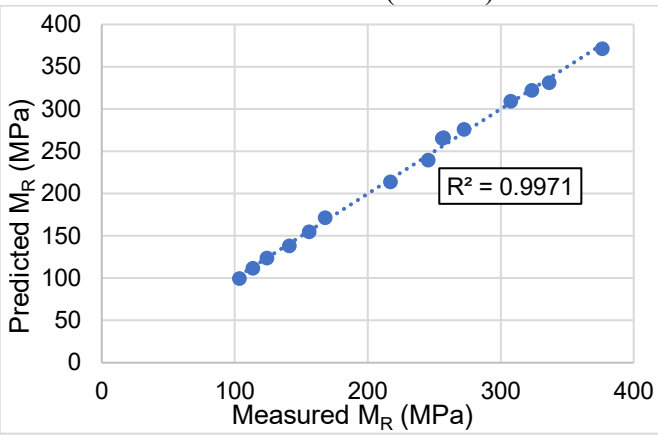

Material : KT - 215 (External)

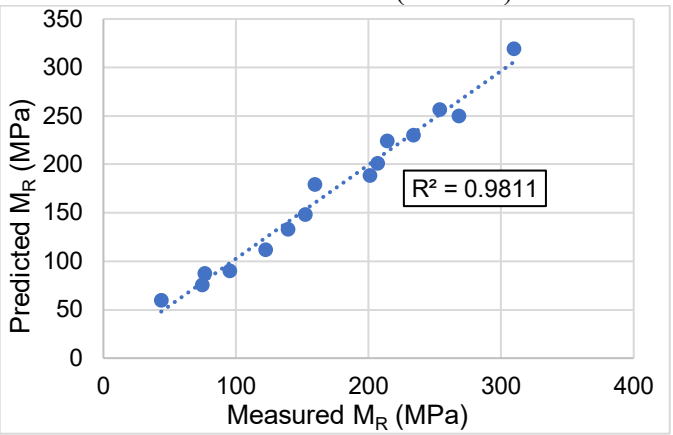

Material : LE - 160 (Internal)

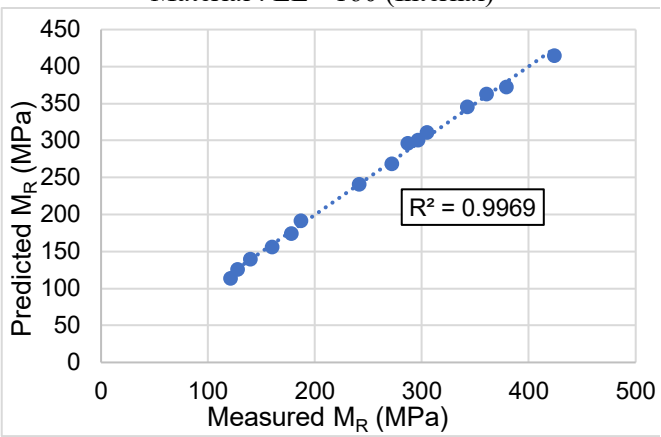

Material : LE - 160 (External)

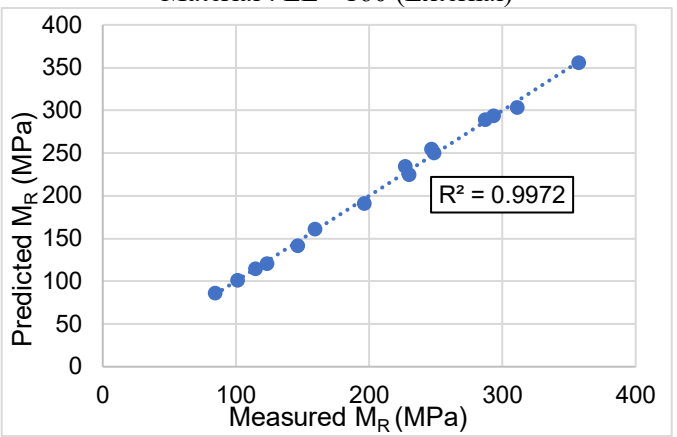

Material : LN - 80 (Internal)

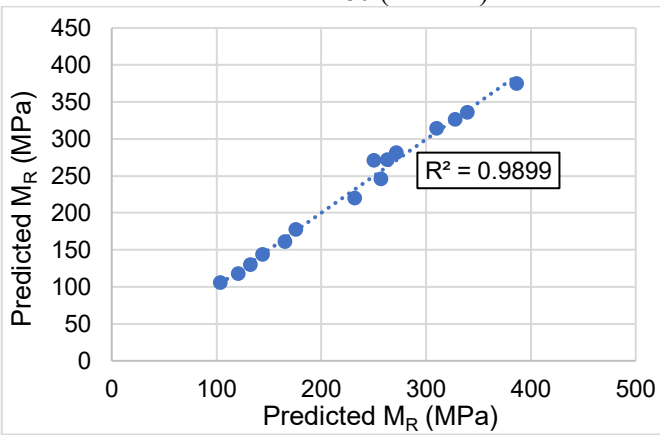

Material : LN - 80 (External)

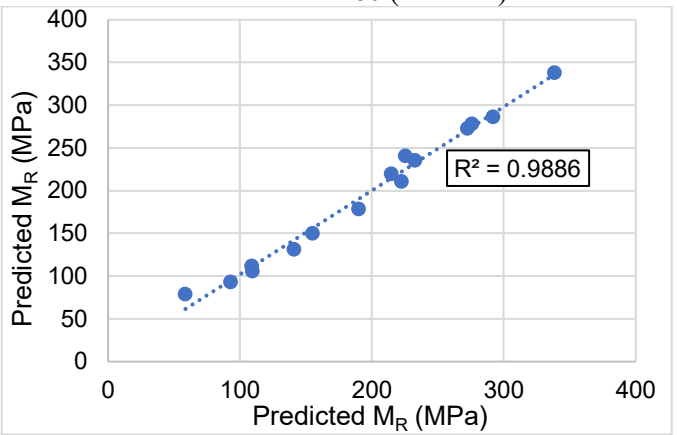

Material : NP - 82 (Internal)

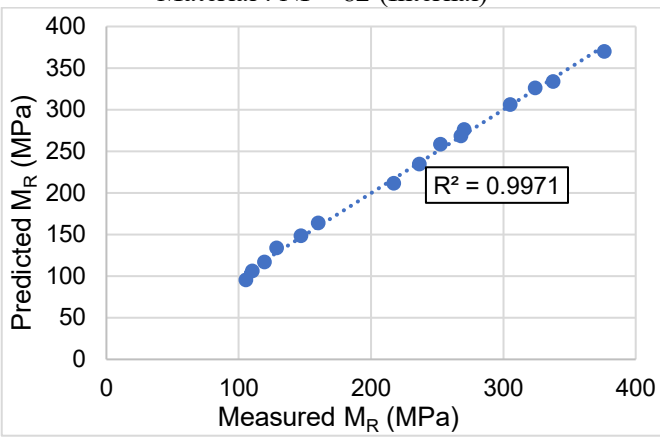

Material : NP - 82 (External)

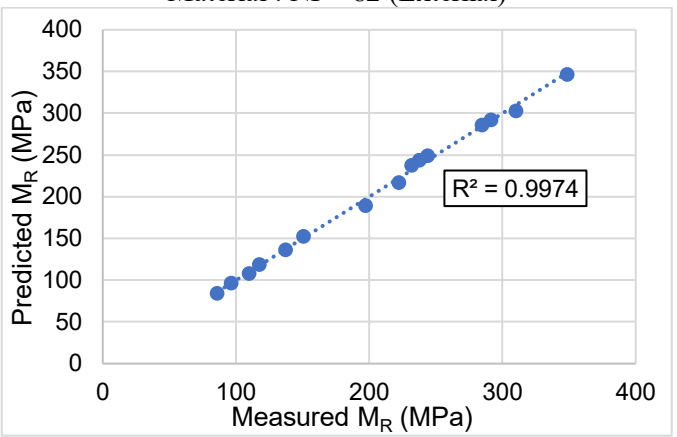

Material : PW – 84 (Internal)

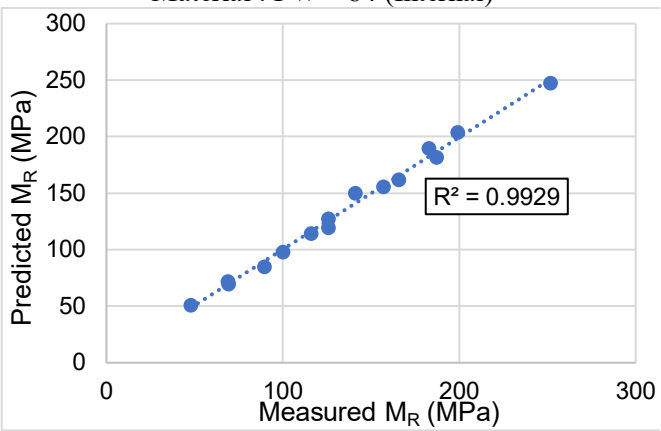

Material : PW – 84 (External)

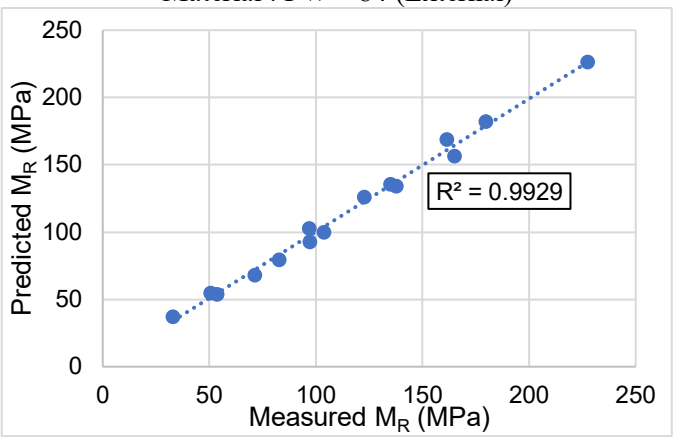

Material : VY – 63 (Internal)

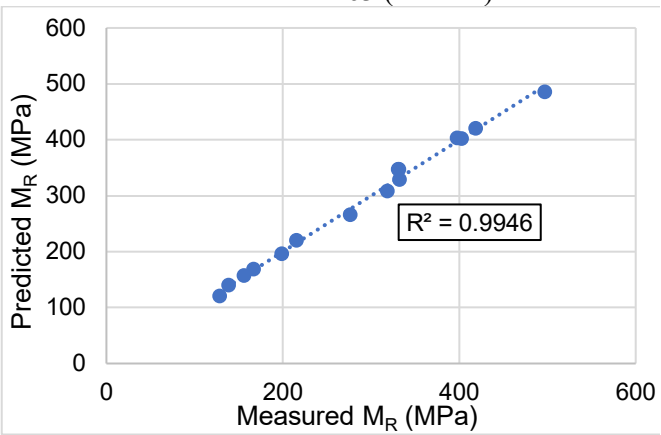

Material : VY – 63 (External)

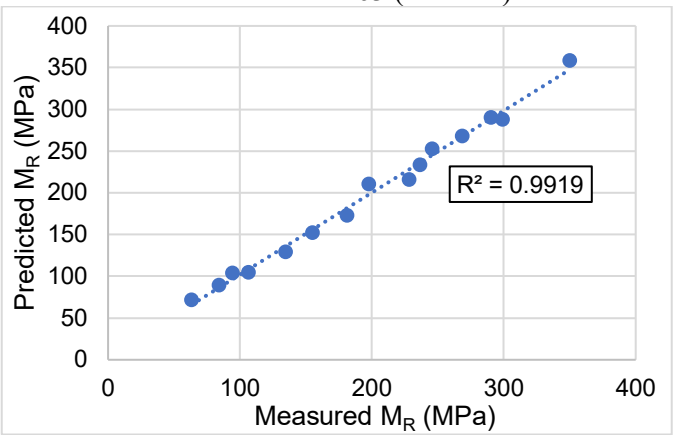

Material : WCW (Internal)

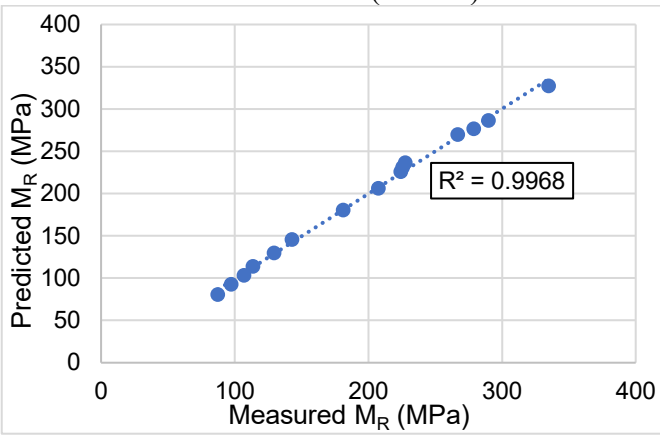

Material : WCW (External)

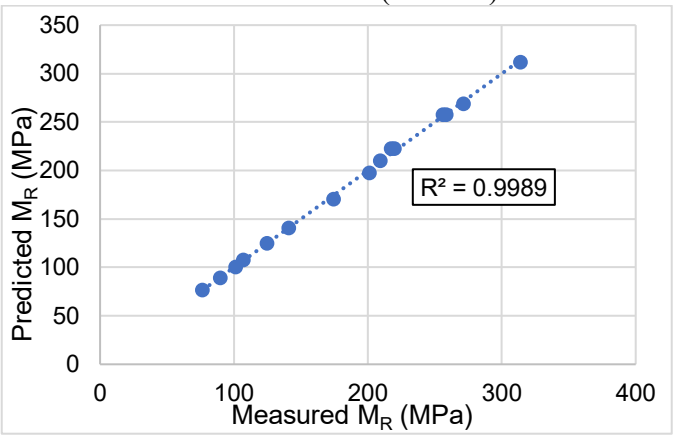

Material : CN – 148 SB (Internal)

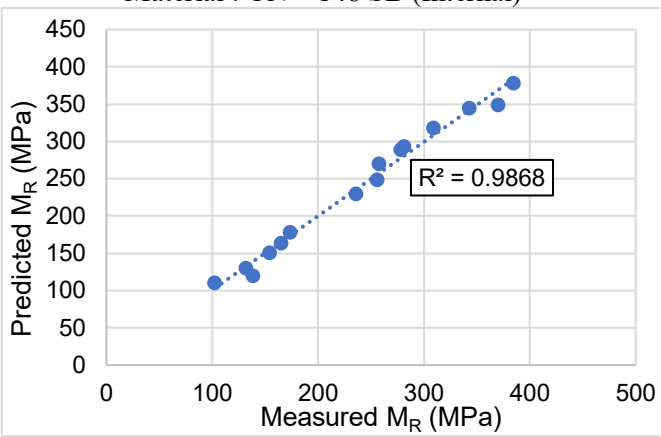

Material : CN – 148 SB (External)

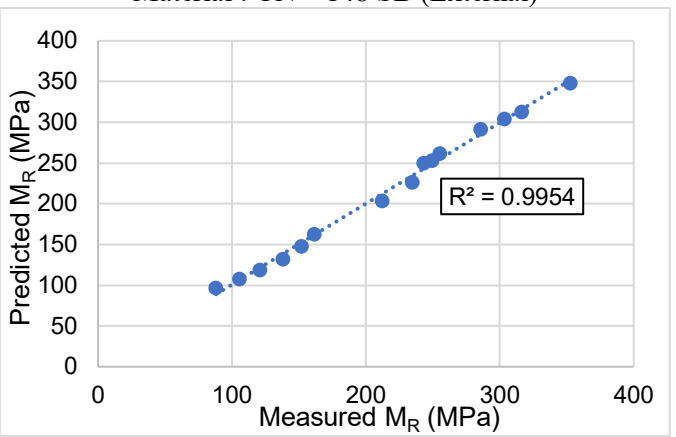

Material : CS – 184 SB (Internal)

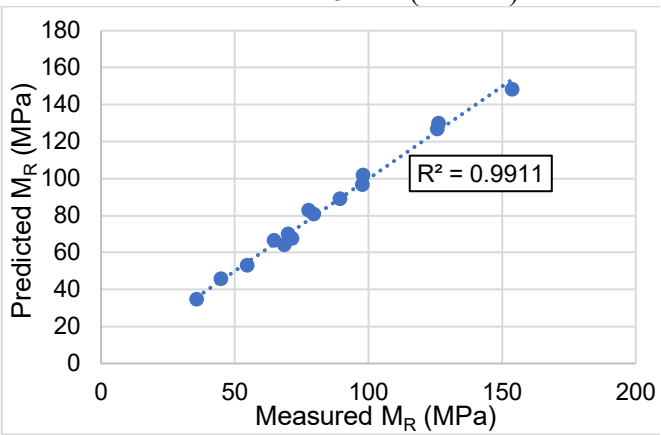

Material : CS – 184 SB (External)

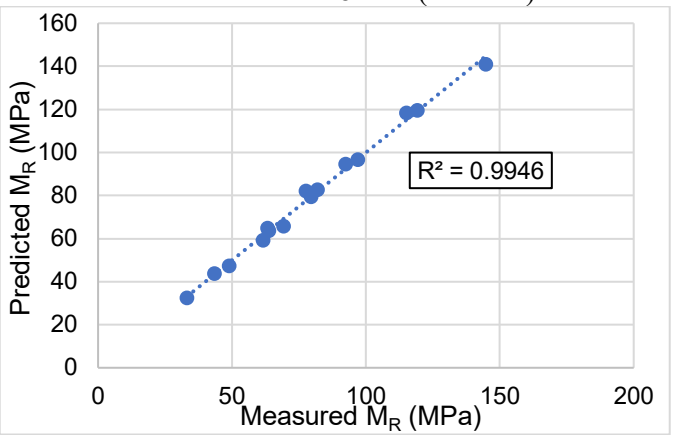

Material : PY – 720 SB (Internal)

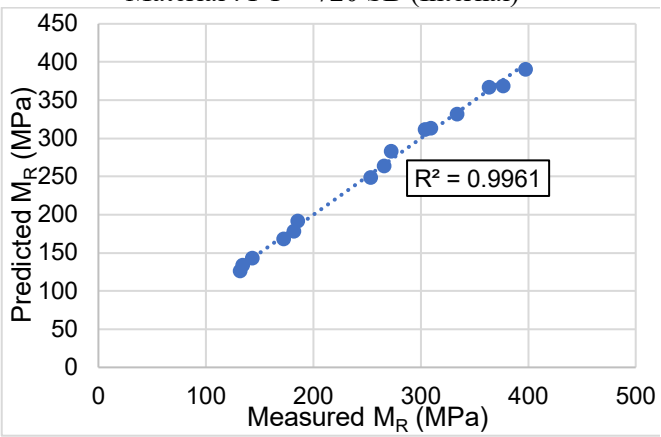

Material : PY – 720 SB (External)

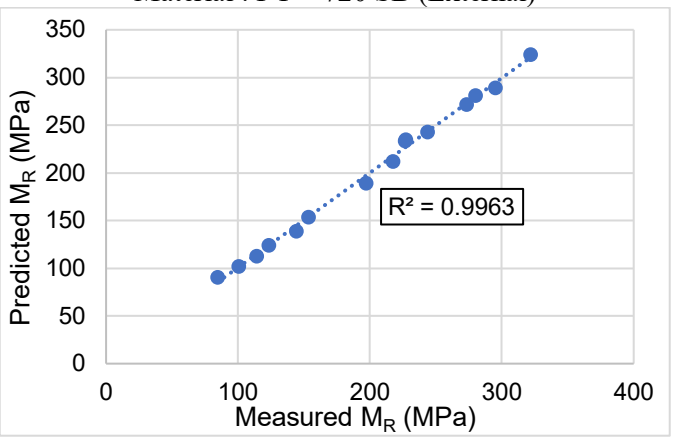

Appendix D: MEPDG Model fitting

Table D.1: Regression coefficients for *"MEPDG Model"*

Material ID	External Measurement				Internal Measurement			
	k_1	k_2	k_3	R^2	k_1	k_2	k_3	R^2
A	940.475	0.708	-0.069	0.996	1164.365	0.689	-0.171	0.994
B	1002.486	0.681	-0.066	0.994	1318.374	0.721	-0.242	0.994
BK - 100	852.193	0.713	-0.071	0.994	1104.398	0.694	-0.199	0.995
BK - 181	562.601	0.613	0.486	0.993	883.243	0.570	0.233	0.989
BR - 2	1373.348	0.664	-0.152	0.998	1839.625	0.711	-0.320	0.997
CS - 184	751.953	0.639	0.017	0.997	852.502	0.675	-0.042	0.996
EL - 132	823.403	0.752	-0.091	0.994	1243.790	0.688	-0.047	0.989
IMC - 140	825.294	0.685	-0.013	0.995	1309.718	0.576	0.220	0.990
KT - 215	705.926	0.659	0.284	0.974	1111.841	0.673	-0.124	0.996
LE - 160	978.308	0.645	0.053	0.997	1257.726	0.674	-0.141	0.996
LN - 80	898.157	0.672	0.026	0.988	1168.073	0.651	-0.122	0.989
NP - 82	949.280	0.701	-0.077	0.997	1065.595	0.725	-0.200	0.995
PW -84	467.246	0.420	0.960	0.978	613.667	0.402	0.775	0.983
VY - 63	836.145	0.660	0.220	0.988	1359.433	0.651	0.018	0.995
WCW	868.372	0.660	0.001	0.999	910.070	0.685	-0.054	0.996
CN - 148 SB	1072.674	0.670	-0.154	0.995	1218.380	0.697	-0.278	0.986
CS - 184 SB	391.217	0.142	1.276	0.978	420.916	0.010	1.573	0.966
PY -720 SB	1011.395	0.655	-0.136	0.997	1369.226	0.672	-0.321	0.992

Graphical representation of *"MEPDG Model"* fitting

Material : A (Internal)

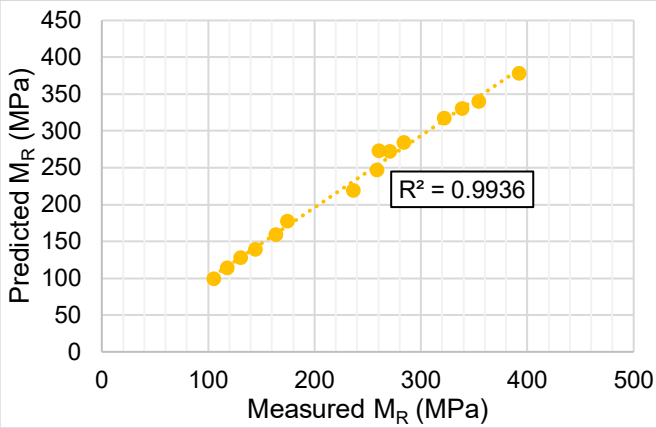

Material : A (External)

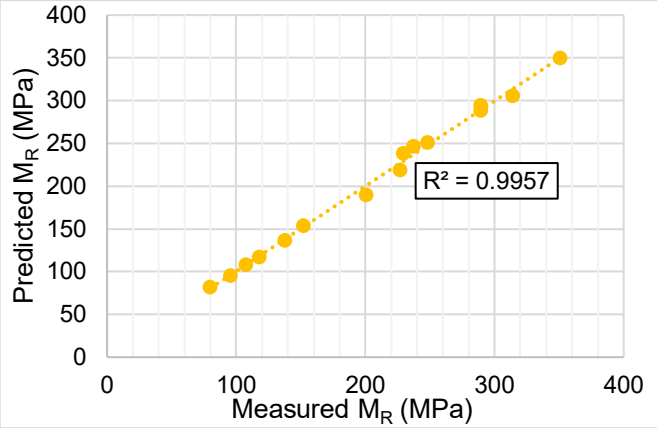

Material : B (Internal)

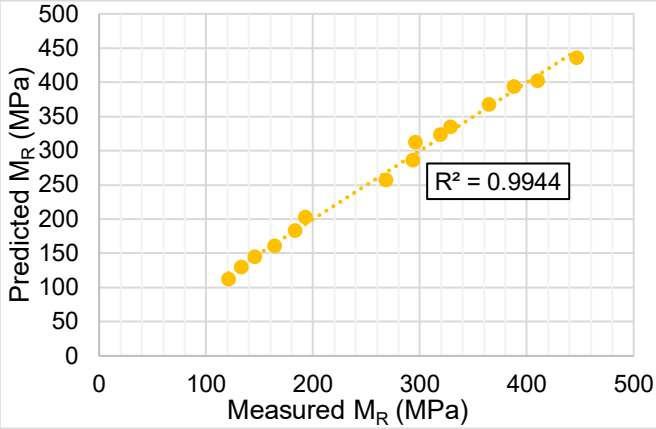

Material : B (External)

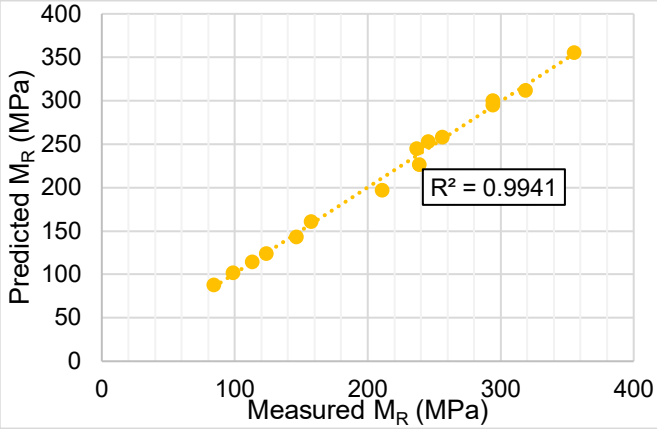

Material : BK - 100 (Internal)

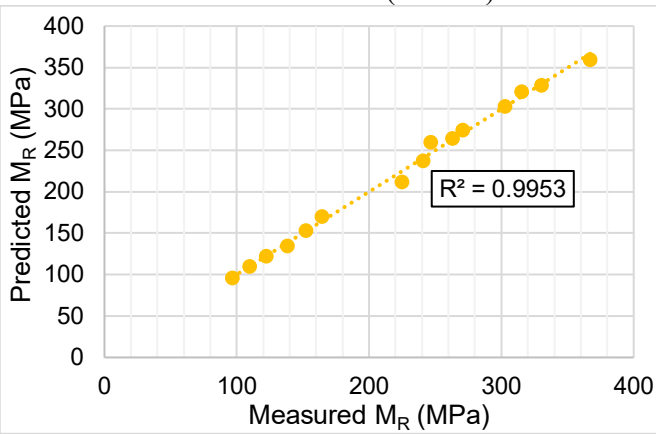

Material : BK - 100 (External)

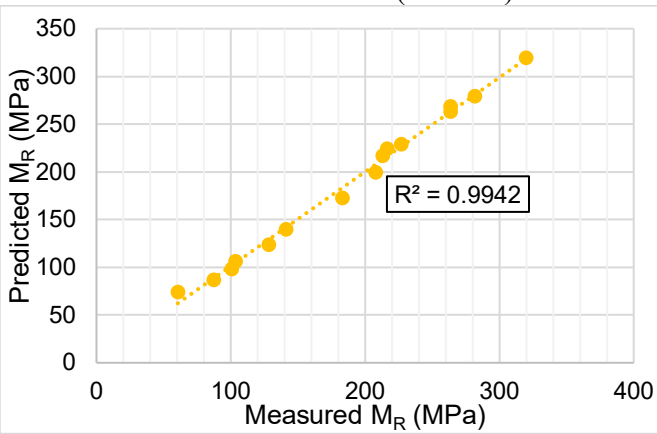

Material : BK – 181 (Internal)

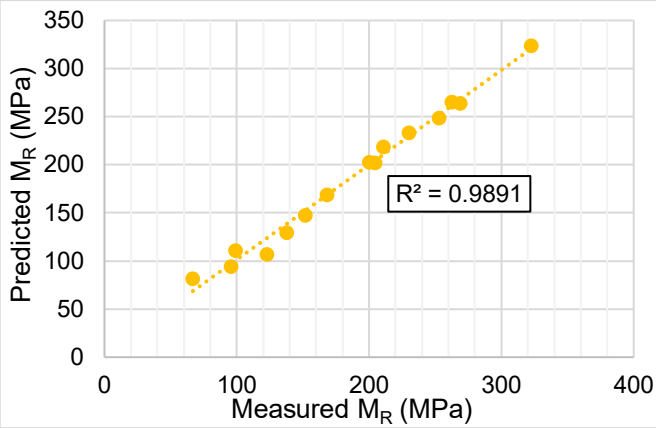

Material : BK - 181 (External)

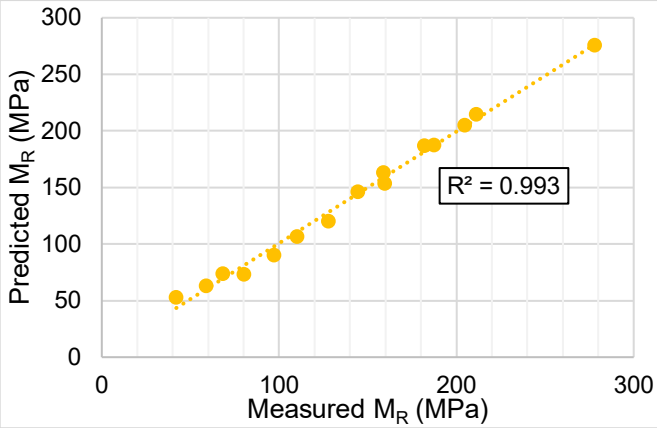

Material : BR - 2 (Internal)

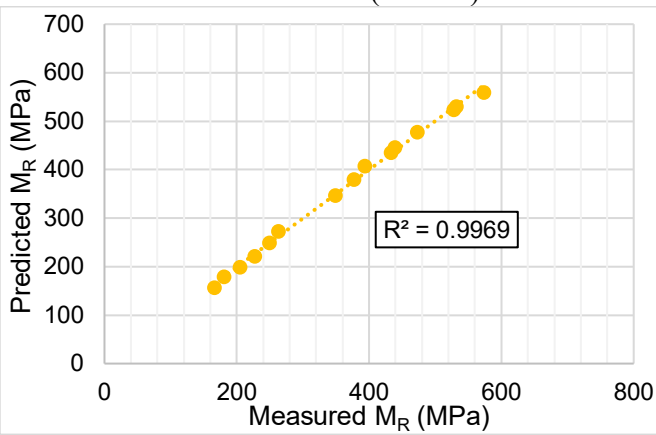

Material : BR - 2 (External)

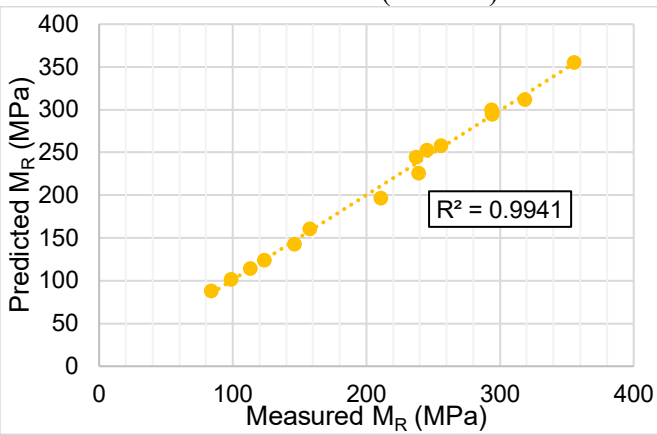

Material : CS - 184 (Internal)

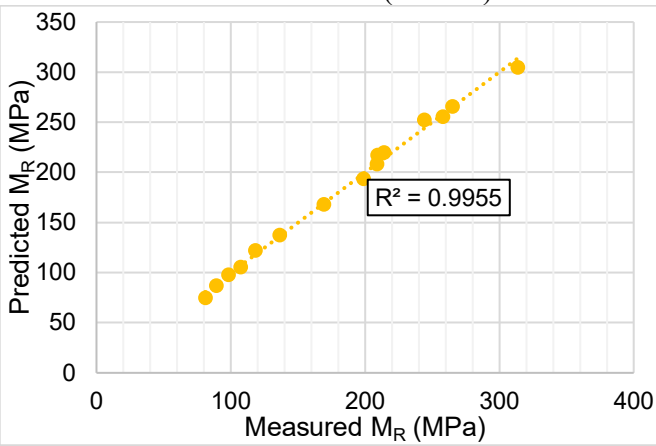

Material : CS - 184 (External)

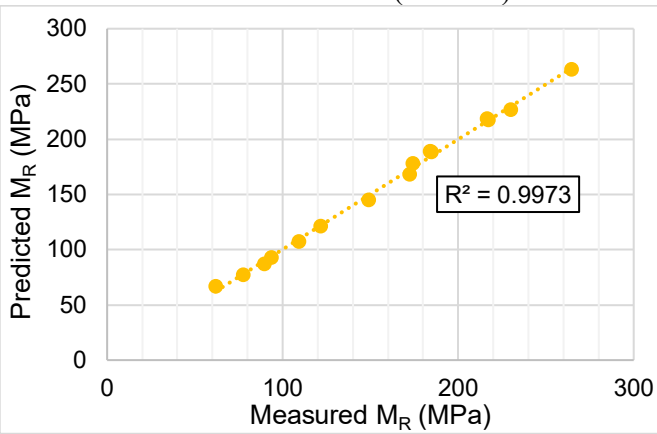

Material : EL - 132 (Internal)

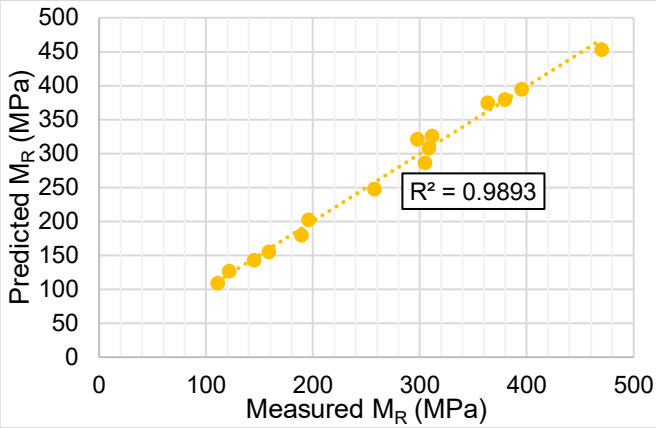

Material : EL - 132 (External)

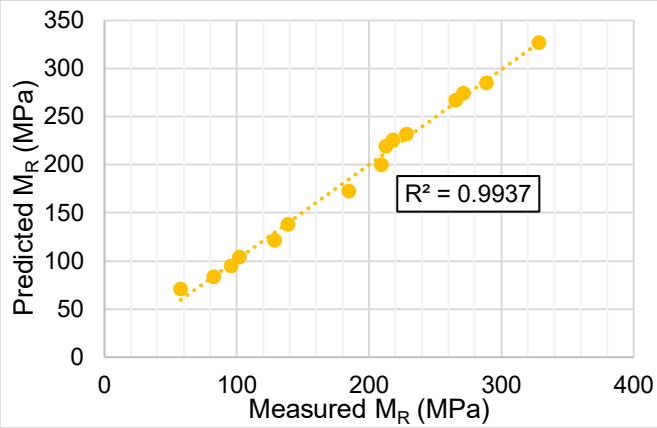

Material : IMC – 140 (Internal)

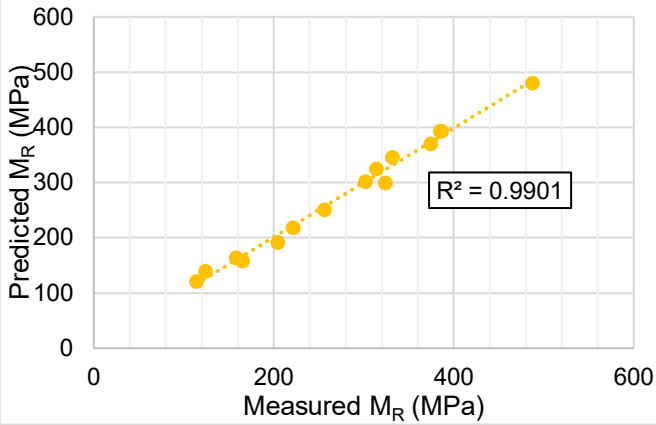

Material : IMC – 140 (External)

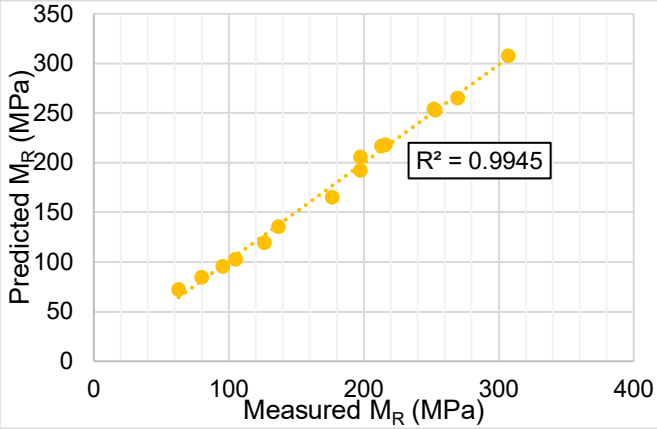

Material : KT - 215 (Internal)

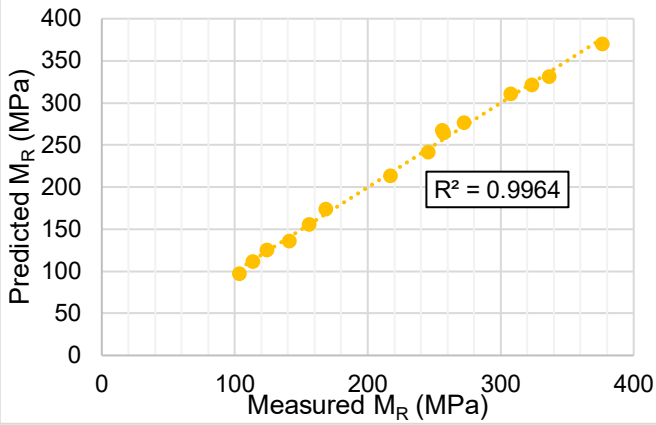

Material : KT - 215 (External)

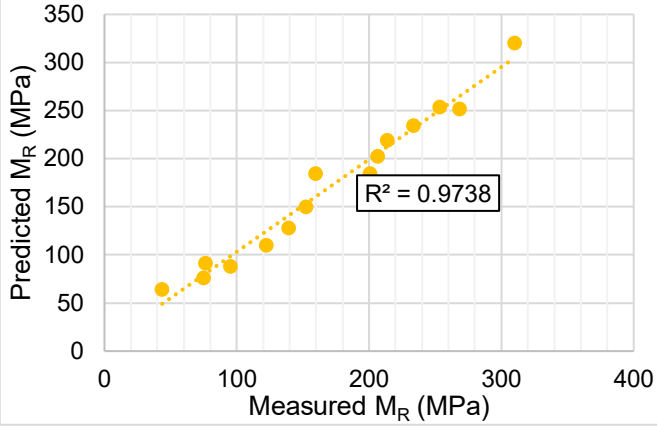

Material : LE - 160 (Internal)

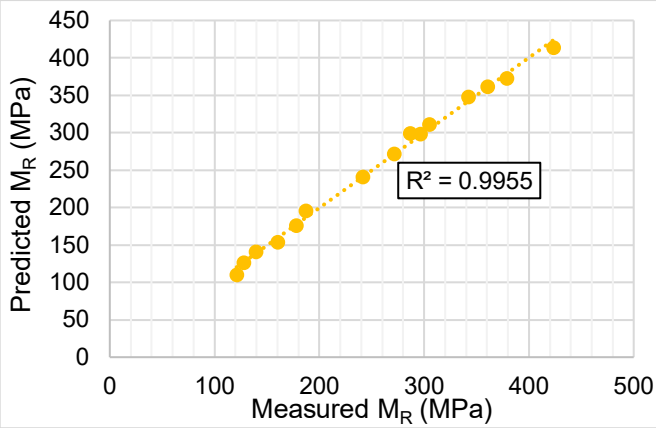

Material : LE - 160 (External)

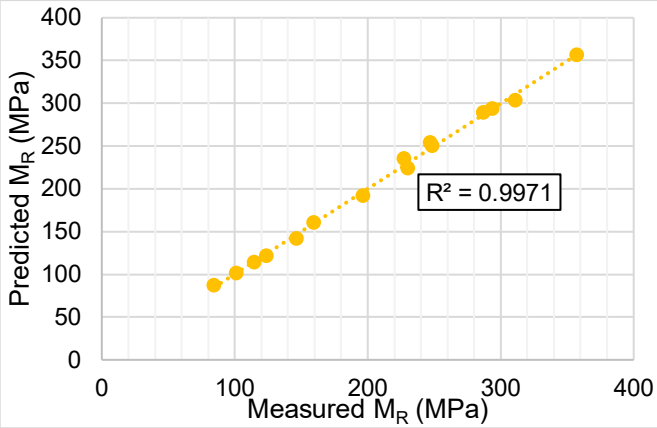

Material : LN – 80 (Internal)

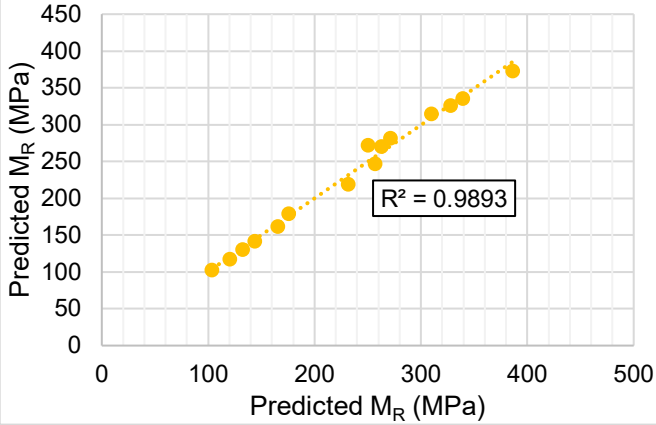

Material : LN – 80 (External)

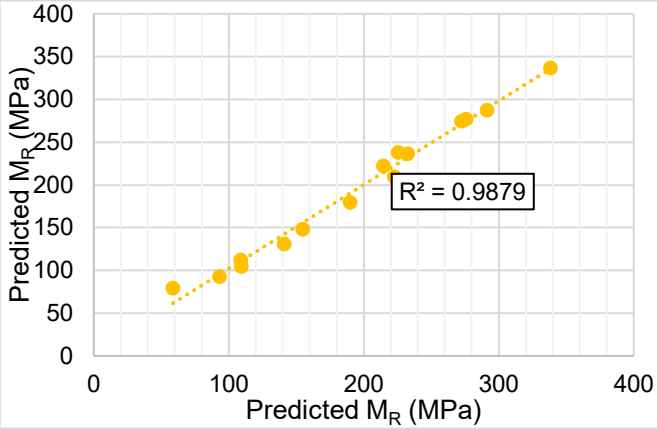

Material : NP – 82 (Internal)

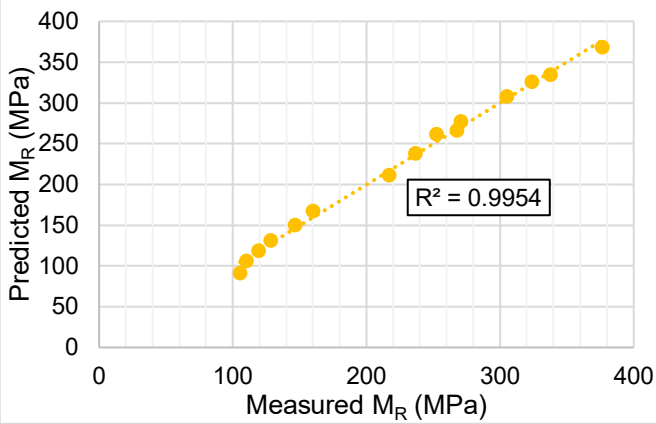

Material : NP – 82 (External)

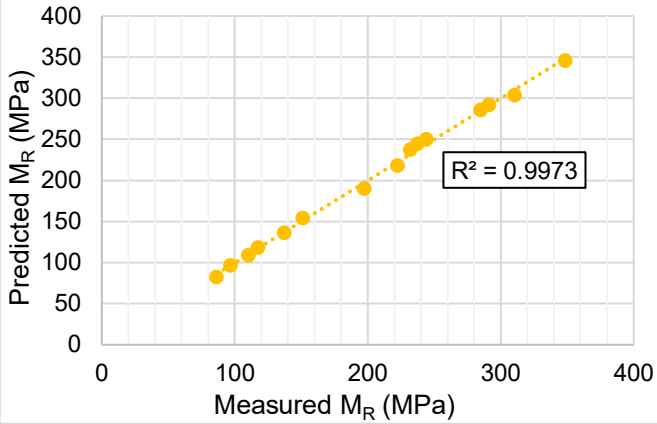

Material : PW – 84 (Internal)

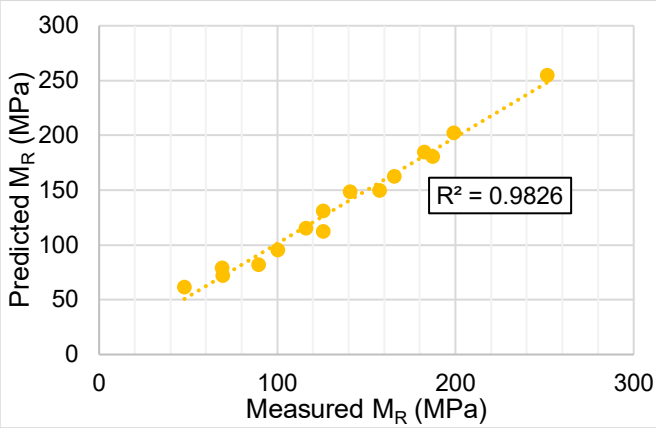

Material : PW – 84 (External)

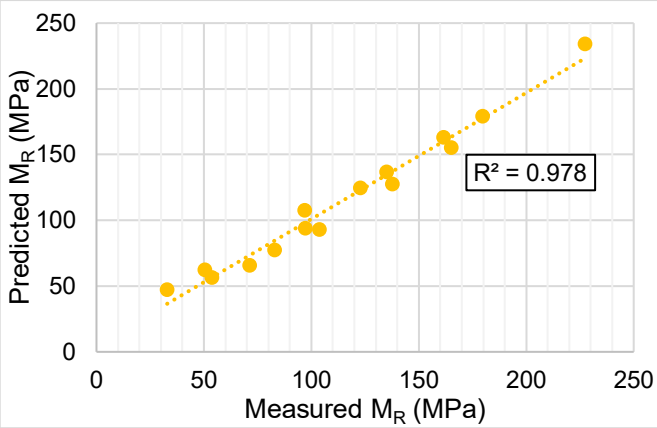

Material : VY – 63 (Internal)

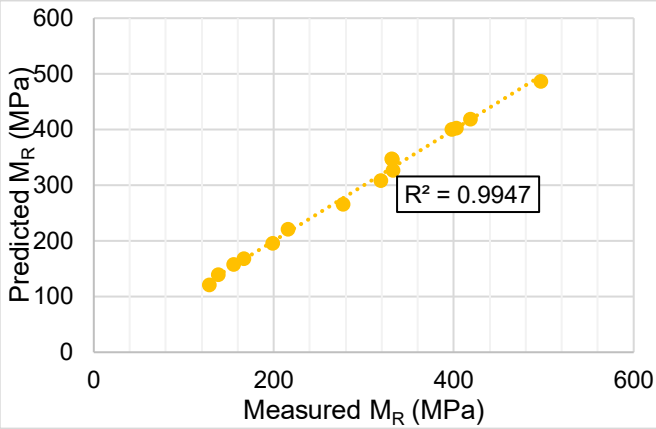

Material : VY - 63 (External)

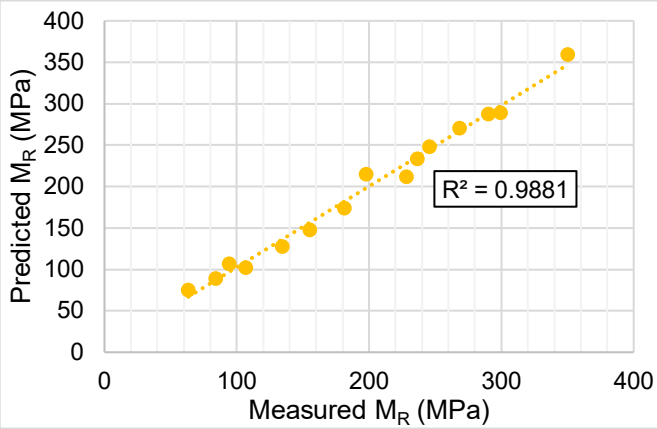

Material : WCW (Internal)

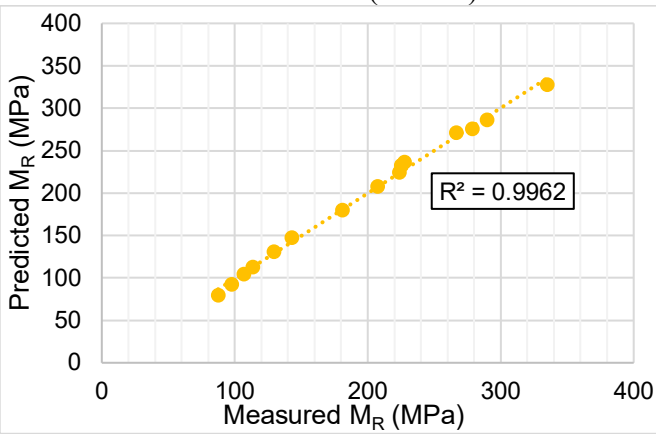

Material : WCW (External)

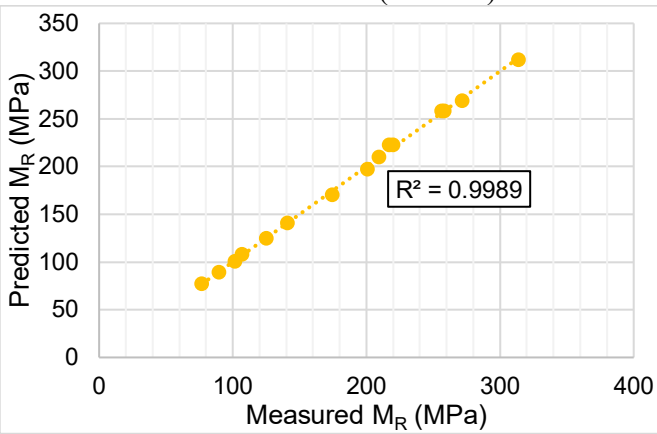

Material : CN – 148 SB (Internal)

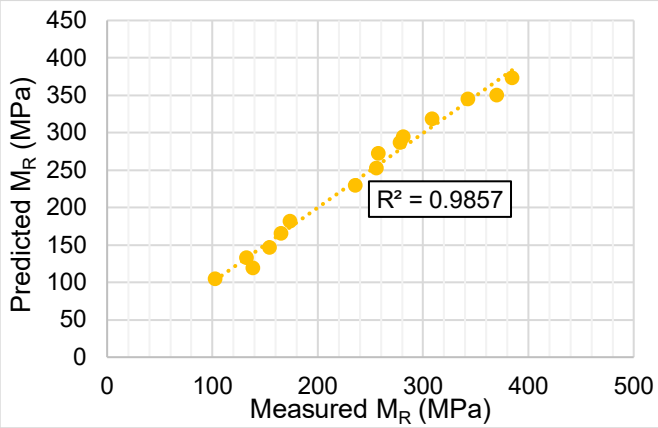

Material : CN – 148 SB (External)

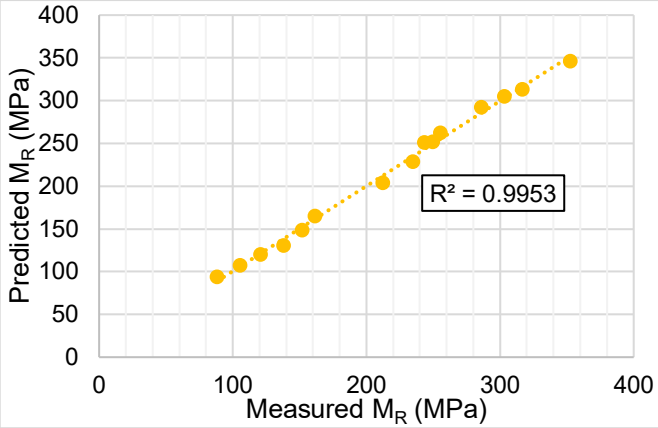

Material : CS – 184 SB (Internal)

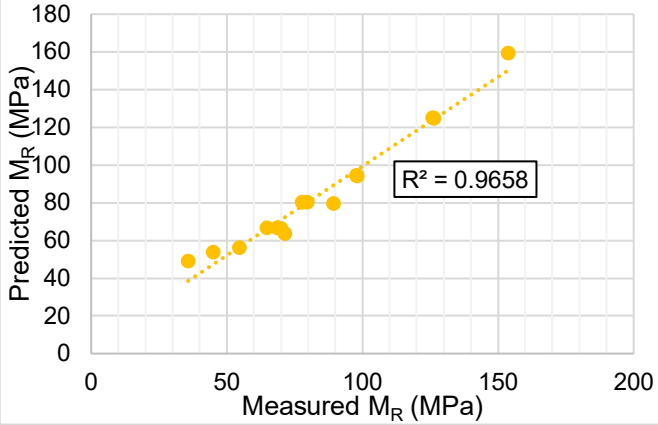

Material : CS – 184 SB (External)

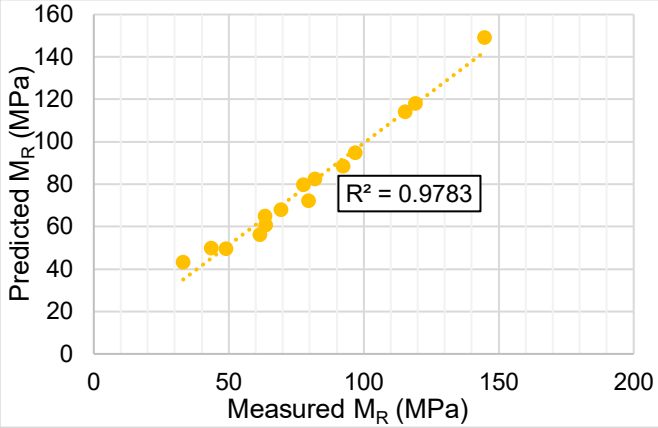

Material : PY – 720 SB (Internal)

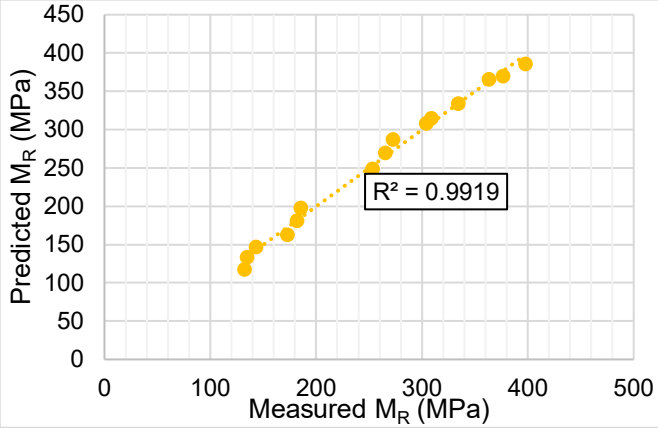

Material : PY – 720 SB (External)

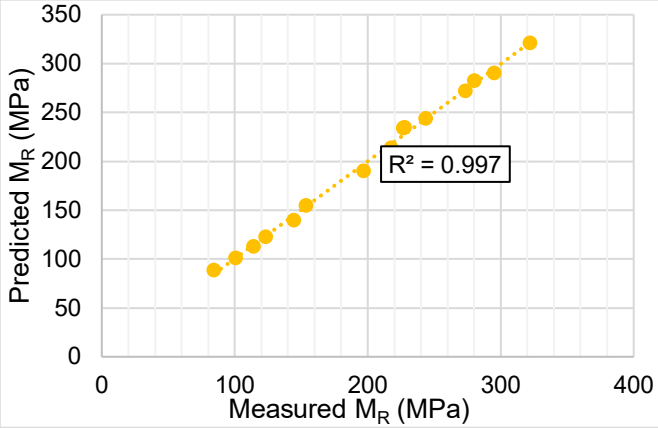

Appendix E: Statistical Analysis

Prediction model for summary resilient modulus

Table E.1 Summary of statistical analysis for SRM prediction model

Coefficients					
Term	**Coef.**	**SE Coef.**	**T-Value**	**P-Value**	**VIF**
Constant	198.2	27.3	7.26	0	
MDD^0.73/OMC^1.3863	1.405	0.319	4.4	0.003	1.73
(D_{10} + D_{30}) ^ 1.18	-16.82	2.58	-6.51	0	9.96
P_4	-1.081	0.429	-2.52	0.04	4.25
Large					
1	123	13.8	8.94	0	4.88
High					
1	-53.24	9.65	-5.52	0.001	1.31
Analysis of Variance					
Source	**DF**	**Adj SS**	**Adj MS**	**F-Value**	**P-Value**
Regression	5	10278.6	2055.73	31.29	0
MDD^0.73/OMC^1.3863	1	1271.3	1271.32	19.35	0.003
(D_{10} + D_{30}) ^ 1.18	1	2783.7	2783.69	42.36	0
P_4	1	418.4	418.37	6.37	0.04
Large	1	5253.1	5253.09	79.95	0
High	1	2000	2000.02	30.44	0.001
Error	7	694.3	99.18		
Total	12				

Prediction model for MEPDG model parameters

Table E.2 Summary of statistical analysis for "k_1" prediction model

Coefficients					
Term	**Coef.**	**SE Coef.**	**T-Value**	**P-Value**	**VIF**
Constant	1130.1	55.2	20.47	0	
D_{10}	-749	120	-6.23	0	6.33
MDD^0.719064/OMC^3.90237	188	56.6	3.32	0.007	1.62
Cc	-79	28.3	-2.79	0.018	1.45
L					
1	1109	155	7.17	0	6.04
H					
1	-486.2	95.5	-5.09	0	1.23
Analysis of Variance					
Source	**DF**	**Adj SS**	**Adj MS**	**F-Value**	**P-Value**
Regression	5	648915	129783	18.56	0
D_{10}	1	271615	271615	38.85	0
MDD^0.719064/OMC^3.90237	1	77053	77053	11.02	0.007
Cc	1	54292	54292	7.77	0.018
L	1	359015	359015	51.35	0
H	1	181046	181046	25.9	0
Error	11	76903	6991		
Total	16	725818			

Table E.3 Summary of statistical analysis for "k_2" prediction model

Coefficients					
Term	**Coef.**	**SE Coef.**	**T-Value**	**P-Value**	**VIF**
Constant	0.5901	0.0622	9.49	0	
$P_{3/8}$	0.001198	0.000886	1.35	0.198	1.05
H					
1	-0.5419	0.0342	-15.86	0	1.05
Analysis of Variance					
Source	**DF**	**Adj SS**	**Adj MS**	**F-Value**	**P-Value**
Regression	2	0.268132	0.134066	128.06	0
$P_{3/8}$	1	0.001913	0.001913	1.83	0.198
H	1	0.263322	0.263322	251.53	0
Error	14	0.014657	0.001047		
Total	16	0.282789			

Table E.4 Summary of statistical analysis for "k_3" prediction model

Coefficients					
Term	**Coef.**	**SE Coef.**	**T-Value**	**P-Value**	**VIF**
Constant	-4.22	1.24	-3.4	0.004	
MDD	0.001873	0.000549	3.41	0.004	1.21
H					
1	1.475	0.151	9.74	0	1.21
Analysis of Variance					
Source	**DF**	**Adj SS**	**Adj MS**	**F-Value**	**P-Value**
Regression	2	1.7028	0.85142	47.69	0
MDD	1	0.2081	0.20814	11.66	0.004
H	1	1.6941	1.69413	94.89	0
Error	14	0.25	0.01785		
Total	16	1.9528			

Appendix F: Permissions

Permission for Figure 2.1

American Society of Civil Engineers LICENSE TERMS AND CONDITIONS

Apr 09, 2019

This is a License Agreement between 1989 -- S M Robinur Chowdhury ("You") and American Society of Civil Engineers ("American Society of Civil Engineers") provided by Copyright Clearance Center ("CCC"). The license consists of your order details, the terms and conditions provided by American Society of Civil Engineers, and the payment terms and conditions.

All payments must be made in full to CCC. For payment instructions, please see information listed at the bottom of this form.

License Number	4564800462865
License date	Apr 08, 2019
Licensed content publisher	American Society of Civil Engineers
Licensed content title	Journal of Transportation Engineering
Licensed content date	Jan 1, 1983
Type of Use	Thesis/Dissertation
Requestor type	Not-for-profit entity
Format	Print, Electronic
Portion	image/photo
Number of images/photos requested	1
The requesting person/organization is:	S M Robinur Mohshin Chowdhury
Title or numeric reference of the portion(s)	Figure 1: Stresses beneath Rolling Wheel Load
Title of the article or chapter the portion is from	State of the Art. I: Resilient Response of Unbound Aggregates
Editor of portion(s)	N/A
Author of portion(s)	Fredrick Lekarp, Ulf Isacsson, and Andrew Dawson
Volume of serial or monograph.	126
Issue, if republishing an article from a serial	1
Page range of the portion	1
Publication date of portion	2000
Rights for	Main product
Duration of use	Life of current edition
Creation of copies for the disabled	no
With minor editing privileges	no
For distribution to	Worldwide
In the following language(s)	Original language of publication
With incidental promotional use	no
The lifetime unit quantity of new product	Up to 499
Title	Evaluation of Resilient Modulus of Unbound Coarse Materials in Idaho

Permission for Figure 2.4

AMERICAN ASSOCIATION
OF STATE HIGHWAY AND
TRANSPORTATION OFFICIALS
AASHTO

CARLOS BRACERAS, P.E., PRESIDENT
EXECUTIVE DIRECTOR, UTAH DEPARTMENT OF TRANSPORTATION

JIM TYMON, EXECUTIVE DIRECTOR

444 NORTH CAPITOL STREET NW, SUITE 249, WASHINGTON, DC 20001
(202) 624-5800 • FAX: (202) 624-5806 • WWW.TRANSPORTATION.ORG

March 25, 2019

S.M. Robinur Mohshin Chowdhury
Graduate Student
Department of Civil Engineering
University of Idaho
Moscow, ID 83844

Dear Mr. Chowdhury:

This is in response to your request to reproduce Figure 2 of T 307 (Determining the Resilient Modulus of Soils and Aggregate Materials) in the AASHTO publication *Standard Specifications for Transportation Materials and Methods of Sampling and Testing* and include that figure in your master's thesis.

You have AASHTO's permission to use the above-cited excerpt. Please note that this authorization applies only to your master's thesis. In addition, please insert the following language or something similar with the figure:

From T 307 (Determining the Resilient Modulus of Soils and Aggregate Materials) in *Standard Specifications for Transportation Materials and Methods of Sampling and Testing*, by the American Association of State Highway and Transportation Officials, Washington, D.C. Used with permission.

If you have any questions about this authorization, please feel free to contact me at bcullen@aashto.org or 202-624-8918. Thank you for your interest in AASHTO's work.

Sincerely,

Robert Cullen

Robert Cullen
Information Resource Manager